Shear Thinning Biopolymers Fluids in a Taylor-Couette Flow

by

Muaadh Ali Baessa

A thesis submitted in partial fulfillment of the requirements for the degree of

Master of Science

Department of Mechanical Engineering

University of Alberta

Abstract

The current study investigates the effect of shear thinning rheology characteristics of high viscosity non-Newtonian biopolymers on the flow regime characterizations in Taylor Couette flow. The rheology measurements were carried out to investigate the viscoelastic properties of the biopolymers prior to the flow visualization experiments.

Both concentrated xanthan gum (XG) and guar gum (GG) solutions were used in this study to investigate their pseudoplastic rheology properties in aqueous solutions over various ranges of concentrations from 0.1%wt to 4%wt. The flow curve and viscoelastic frequency sweep experiments were used to study the rheology of the concentrated biopolymers. The flow curve was performed over the shear rate range of 0.1 s^{-1} to 100 s^{-1} whereas the frequency sweep was performed over the frequency of 0.1 to 300 rad/s**.** The rheology experiments were performed using a cylindrical head rheometer manufactured by Anton Paar model number NCR-302.

The effect of storage time on the solution viscosity and yield stress of both solutions for the concentration of 1%wt was also investigated, with successive viscosity and yield stress stability progress obtained after performing the experiments at the end of each week and after up to 4 weeks of storage period. Additionally, an extra agitation time was applied for the solutions, and it was evaluated three different times 8 h, 24 h, and 48 h of continuous agitation time.

After the rheology analysis, the flow visualization investigations experiments using a Taylor Couette system were performed, aiming to study the flow transition characteristics in the Taylor Couette system with a fixed outer cylinder and a rotating inner cylinder. The experiments focused on the flow mapping structure at the onset of each bifurcation for non-Newtonian solutions. We link the flow characterization transition of the shear thinning solutions in the Taylor Couette flow to the viscoelastic and yield stress properties obtained from the rheology analysis for each concentrated solution. Additionally, the flow mapping experiment aims to investigate the effect of the rheology viscoelastic properties such as the shear thinning flow index (n) on the flow mapping main parameters such as critical Reynolds number Re, and the azimuthal variations in the vortex wavelength and vortex count.

The Taylor Couette (TC) flow system has numerous applications which depend on the concept of a rotating inner cylinder, including science, engineering, industrial, and fluid processes applications. The TC system is of great interest in the oil field where understanding in needed of

the viscoelastic properties of the non-Newtonian fluids that are used as drilling. Additives may contribute to the transport of sediments outside the well, by using inducing high viscous muds. The Taylor Couette system is a proper prototype to conduct experiments similar to the downhole walls and rotating string by considering the borehole wall as the outer cylinder and the rotating string as the inner cylinder. Additionally, the Taylor Couette system is also observed in various types of engineering applications, including journal-bearing lubrication, cooling of rotating machinery among others, and purification of industrial wastewater.

Preface

The work done in this thesis is an original work carried out by Muaadh Ali Baessa under the Supervision of Prof. Brian Fleck from the Department of Mechanical Engineering, University of Alberta; and co-supervision of Dr. Tim Weis from the Department of Mechanical Engineering, University of Alberta. The Taylor Couette setup was designed by Pallavi Bhambri. Currently, the Taylor Couette design is modified by myself and the continuous assistance of Prof. Brian Fleck prior to the flow visualization experiments.

The biopolymers solutions were prepared in DR. Fleck's laboratory. Also, all experiments for rheology and flow visualization characterizations were conducted by myself. The rheology raw data were obtained at Dr. Prashant Waghmare's Lab for Chapter 3, whereas the data in Chapter 4 were collected in Dr. Amy Tsai's lab. Furthermore, the flow visualization experiments were carried out in Dr. David Nobes's laboratory.

Three chapters are in preparation for publishing as follows:

- Chapter 2 is submitted to be published in the Canadian Journal of Chemical Engineering as Baessa M., Fleck B., Weis T., "Rheology Investigations and Yield stress Characterizations of Concentrated Shear-Thinning Biopolymer Solutions".
- Chapter 3 also is Submitted to be published in Multidisciplinary Digital Publishing Institute (MDPI) -Polymers as Baessa M., Fleck B., Weis T., "Viscoelastic Rheology Characterization of Concentrated Shear-Thinning Xanthan and Guar Gum Solutions".
- Chapter 4 is final base work of the flow characterization is also under revision before submitting it this by Fall 2022 as Baessa M., Fleck B., Weis T., Bessa G., Nobes ., *"The influence of concentrated shear-thinning guar and xanthan gum solutions on flow patterns in Taylor Couette flow"*

I was responsible for performing the experiments, collecting, and analyzing the raw data. Also, I was preparing the manuscript for publishing. B. A. Fleck was the supervisory author and was involved with the manuscript edits. T. Weis was involved with the concept formation, assisted with the data collection and contributed to manuscript edits and composition.

Acknowledgments

First of all, I would like to express my sincere gratitude to my supervisors Professor Brian Fleck and Dr. Tim Weis for their continuous support during my graduate studies, their patience and immense knowledge in every walk of life. I am thankful to them for always motivating me and giving me the insight to solve research problems. They have been wonderful mentors, I will always be indebted for their kindness and further, their academic experience has been invaluable for my project. I am confident that working under their supervision, not only made me a better scientist but a better & stronger individual as well.

I am also grateful to Dr. David Nobes, and Dr. Amy Tsai. and Dr. Prashant Waghmare for letting me use their research facilities and equipment to conduct my experiments. Also, I am grateful to Dr. *Guilherme Bessa* for his support in designing and fabrication of the Taylor Couette system as well as his continuous assistance during performing the flow visualization experiments. I am thankful to *Ahmed Al Dhaleai* from Dr. Amy Tsai's lab, and *Ryan Baily* from Dr. Waghmare's lab for training me in using the rheometer for the rheology characterization experiments.

My sincere thanks to Leslie Wang and Hoazhe (Andrew) Li, my colleagues and friends from our research group (Dr. Fleck's lab), for their enormous support throughout the project and for making the research lab an enjoyable workspace. I would like to wish them all the very best in their future endeavors.

In the end, I would like to thank my loving and caring family for always standing beside me and trusting me in my decisions. Without you all, this work would never have been possible. Thanks **Family**, **Mom, Dad, beloved Wife, Brother, and Sister** for always believing in me.

Muaadh Baessa

Table of Content

List of Tables

List of Figures

Nomenclature and Abbreviations

TC	Taylor Couette
ppm	Weight parts per million
% wt.	weight percentage
τ	Shear stress
γ	Shear rate (s^{-1})
μ	Dynamic viscosity (Pa.s)
μ_0	Viscosity when the shear rates appraoch to zero ($kg{\cdot}m^{-1}{\cdot}s^{-1}$)
μ_{inf}	Constant viscosity based on Carreau Model
v	Kinematic viscosity (m^2/s)
τ_y	Yield shear stress (N/m^2)
n	Flow index
k	Index of consistency
L	Inner cylinder length
R_i	Inner cylinder radius (m)
R_o	Outer cylinder radius (m)
d	Annular gap (R_o-R_i)
Ω	Inner cylinder speed
RPM	Revolutions per minute
η	Radius ratio
Γ	Aspect Ratio
Re	Reynolds number
Re_{c1}	Reynolds number at the first flow instability

Re_{c2}	Reynolds number at the second flow instability
Rec3	Reynolds number at the third flow instability
Ta	Taylor number
∇	The gradient,
P	Pressure
CCF	Circular Couette flow
TVF	Taylor Vortex flow
WVF	Wavy Vortex flow
MWVF	Modulated Wavy Vortex flow
TTF	Taylor Turbulent flow
SVF	Spiral Vortex flow
CVF	Coiled Vortex flow

CHAPTER 1

Introduction and Background

1.1) Introduction

1.1.1) Biopolymers Introduction and Background

Biopolymers are widely used in several industrial and food applications. Over the last decades, biopolymers are involved in the oil field drilling applications [7], where they are used as thickening additives in drilling mud preparation and play a key role in enhancing drilling processes due to their stable shear thinning nature.[1]–[3]. The biopolymers were selected in this study are xanthan gum (XG) and guar gum (GG). Xanthan gum has been involved in a wide range of applications including food, and fluid mechanics, because of its stable shear thinning viscosity at different flow and temperature conditions [4]. Moreover, XG and GG solutions can be used in mixing and dispersion processes in the pharmaceutical industries and agricultural production, due to their ability to create viscous emulsion solutions [5]. In addition, XG and GG have also played a role in the petroleum production, specifically in drilling, enhanced oil recovery (EOR) and polymer flooding processes through their ability to dissolve in the aqueous solutions that have been required in oil recovery enhancement processes [6]. One of the main reasons that make experts and researchers interested in using biopolymers solutions in industrial applications is to reduce adverse environmental impact. They are considered environmentally friendly additives and they cause no apparent harm to surrounding areas. Furthermore, biopolymers are also used in the hydraulic fracturing process underground due to their gelling properties to transport viscous solutions in the well [7].

The literature is rich [8] with rheological studies focused on structured biopolymer fluids and yield stress analyses. Yield stress analysis of biopolymers has several applications, including in food productions [8]&[9] that contain a variety of products such as paint [8], foam, grease [11], and pastes[10]. When it comes to shear thinning fluids flowability, yield stress analysis is vital to characterize fluid behavior, indicating that lower yield stress means small resistance to flow; thus, the fluid will easily go to the flowing phase. In some applications [8]–[11], it is important to prevent solutions from aggregation and separation. The overall fluid flowability performance can be evaluated by characterizing yield stress points under specific shear conditions. To understand the entire rheology flow curves behavior under shear rate load, several rheological models fit the shear

stress vs. strain rate curves, such as the power law, the Herschel-Bulkley, and the Bingham models [8]–[11].

In this study, we have characterized the rheology, viscoelastic, and flow properties of the biopolymers XG and GG solutions by conducting rheology measurements using a rheometer and flow visualization investigation in the Taylor Couette system. The main reasons for selecting both biopolymer solutions are due to their unique shear thinning properties to remove drilling cuttings out of the downhole, preventing wells from being damaged by circulating drilling fluids, and to provide annulus sealing [12]. Most drilling fluids have thixotropic characteristics with yield stress values that vary based on the fluids' nature and rheology properties [13]&[14].

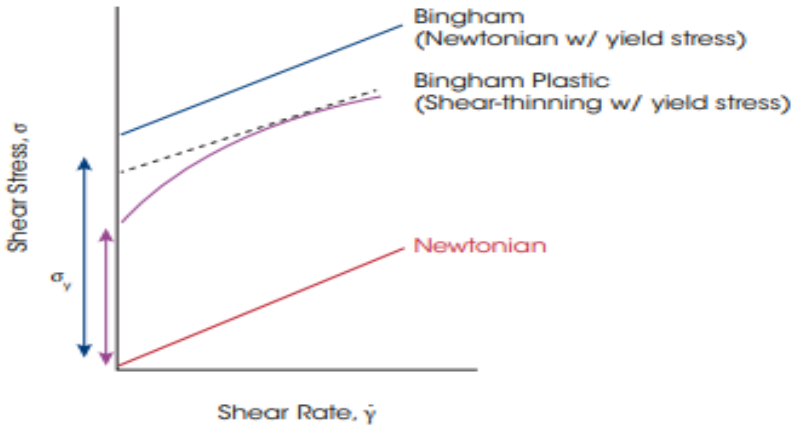

Figure 1-1. The rheology models for different fluid types [15]

1.1.2) Biopolymer Structure:

Xanthan Gum (XG) is one of the most common polysaccharide biopolymers that can be produced by the fermentation of simple sugars. XG was discovered in the United State in mid of twentieth century [16]. In the last decade, xanthan gum has attracted numerous scholars and industrial experts due to its variety and unique applications. It has unique properties, including adding a high viscosity and a gelling ability to solutions [17]. Also, XG has a unique structure that consists of two mannose units, glucose units, glucuronic acid and two repeated pentasaccharide units. There are about five rings connected to the XG structure, two-rings at the backbone with three side chains. The xanthan structure enables the solution to react with water, resulting in the XG solution behaving like a gel at the rest condition when there is no shear load, and like a liquid at applied shear load. These properties are associated with the hydrogen bonds connected to its chains. The XG becomes more viscous increase of the number of hydrogen bonds connecting to its chains. The

XG molecular structure has pyruvate and acetyl substituents in the mannose units at the side chains. The amount of the pyruvate and acetyl substituents associated with the Xanthomonas strain and fermentation condition [4]. The main function of the pyruvate and acetyl substituents is as follows: the acetyl group is to impose a control between xanthan gum and other biopolymers. While the removal of the pyruvate substituents group causes a significant rise in midpoint temperature associated with the ordered-disordered transition as a result of the electrostatic repulsion [18].

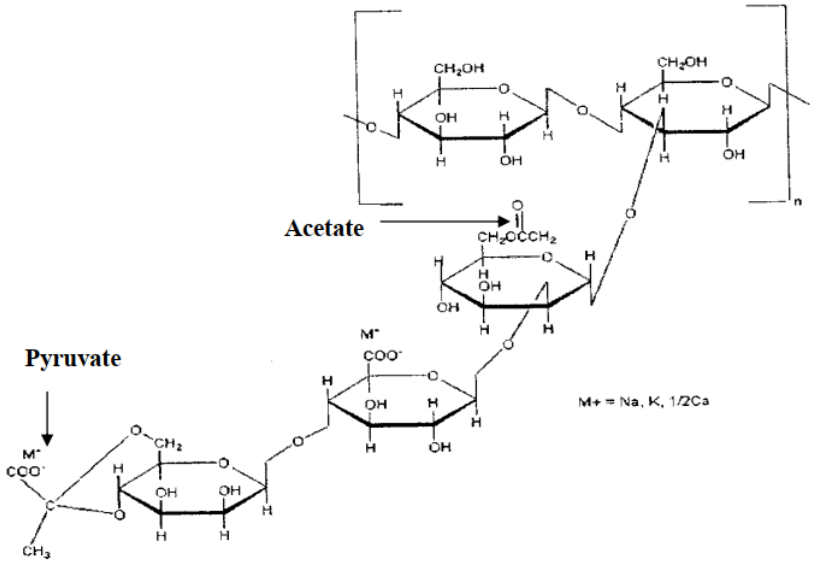

Figure 1-2. Xanthan gum molecular structure [19]

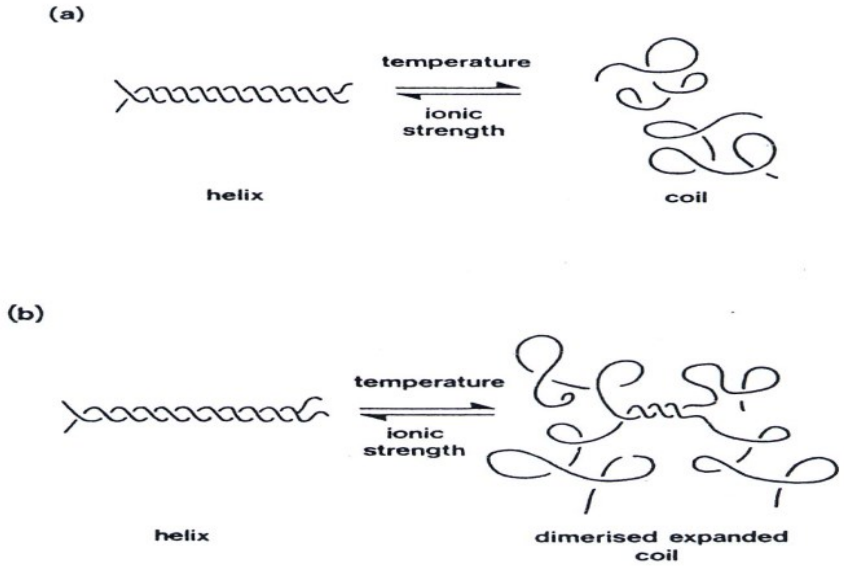

Figure 1-3. Xanthan gum molecular ordered-disordered confirmations [20].

On the other side, Guar Gum is a Leguminosae biopolymer that is produced as a crop of Cyamopsis tetragonolobus, containing about 40% dry seeds [21]. It grows in many countries around the world, including the US, Pakistan and India [21]. Like XG, GG has unique pseudoplastic properties making it compatible with many applications, including food and cosmetic products as well as oil industries. Its primary property is its ability to make solutions thickener and as an emulsifier.

Guar Gum is employed extensively in the oil field process with a total consumption of more than 35% in drilling mud preparation and fracturing fluids due to its unique merits and affordable price compared to the other drilling fluids [22]. The molecular structure of the GG contains chains and a backbone. The chains contain up to (1–4)-β-d-mannopyranosyl units, whereas there are about (1– 6) branch points connecting to the backbone as can be seen in Figure1-2. The GG exhibits strong non-Newtonian shear thinning behavior with high viscosity as a result of the molecular entanglements between the backbone and the guar chains [23]. The non-Newtonian behavior of the GG is affected by key parameters such as temperature, salinity, and pH [24]. The viscosity of GG drops as the solution shear deformation increase, resulting in a decrease in the interaction between the guar molecules and solvent. In addition, the thickening ability gives the GG a high capacity for gelation that can be required to be utilized in the oil industry, especially in preparation of drilling fluids. The GG molecules have a loop shape appearance, and it has a crosslinker structure

that easily attracts other molecules that contain hydroxyl chains. It also attracts water molecules and forms a solution [25]. Pure guar gum is required to use in the hydrofracturing process [25].

1.2) Rheology of Biopolymers

1.2.1) Fundamental of Rheology:

The word "rheology" is related to materials flow and deformation [26]. It comes from the ancient Greek language where the word "rheos" denotes the flow of materials. When the word rheology mentioning, this means that we are going to describe the flow and response of materials experiencing a shear rate load. Materials differ in their rheology response; solid materials deformation is usually described by an elastic behavior. While liquids show more flowability "viscous behavior". Also, for a long-time condition, even the solid materials might exhibit both viscous and elastic behavior. Thus, they are known as "viscoelastic materials". The rheology properties show three different phases including, elastic, viscous, and viscoelastic. The correlation between shear stress and the shear rate of fluids denotes the viscous phase [26]. Furthermore, the main parameter that plays a crucial role in rheology characterization is viscosity and yield stress.

1.2.2) Viscosity:

Viscosity is defined as liquids resistance to deform over known shear rate load. In physics, the force applied over the unit area is known as stress (its unit is Pascal, "*Pa*"). The deformation leads to a noticeable variation of the height of material layers as a result of the applied force is known as a strain which is a dimensionless parameter as illustrated in Figure 1-4. Whereas the rate of change of the material deformations due to the force is known as strain rate or shear rate (with unit s^{-1}). The viscosity can be mathematically expressed through the following relationship between stress and strain rate, as Newton's law where shear stress is proportional to the shear rate:

$$\mu = \frac{\tau}{\frac{\Omega r_i}{d}} = \frac{\tau}{\gamma} \qquad [11]$$

where (γ) denotes the shear rate, and (μ) to the viscosity.

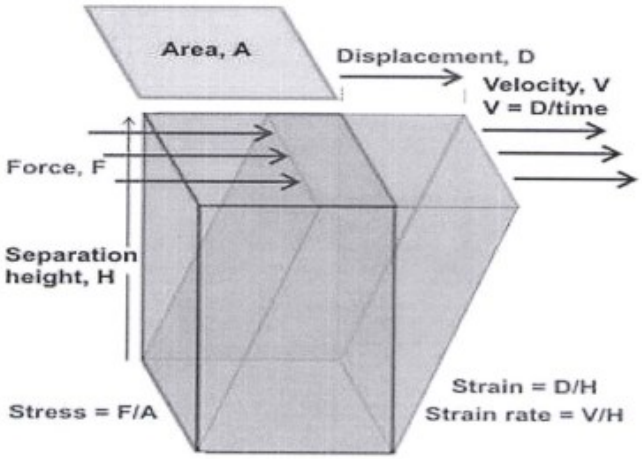

Figure1-4. Material deformation due to shear loads [27].

Generally, the rheological properties are demonstrated by characterizing solutions' viscosity behavior due to the shear rate. The flow behavior also can be illustrated either by experimental curve plots obtained from advanced rheology devices such as rheometers. In terms of graphical illustrations, the following parameters, including shear rate, shear stress, and apparent viscosity, can be examined to give us a clear insight into flow behaviour [28].

Additionally, viscosity is also known as the friction between a fluid's internal layers as well. Hence, the correlation of shear stress vs. rate is one of the most important tools to characterize solutions' rheological properties. This correlation can be schematically expressed as the slope line between the stress and strain rate, depending on the properties of fluids whether they are Newtonian or non-Newtonian. In many actual applications that depend on mixing materials such as adding or mixing polymers in a Newtonian fluid to divert the Newtonian behavior to non-Newtonian behavior, when the apparent viscosity drops as the shear rate increases, is known as shear thinning behavior, or pseudoplasticity and it is commonly in many products in our life such as polymers, gels, ink etc. Whereas the increase in solutions viscosity as the shear rate increases is known as shear thickening behavior. The biopolymer solutions in this study have a quite high molecular weight and are prepared over various ranges of concentrations, exhibiting a shear shear-thinning behavior [28].

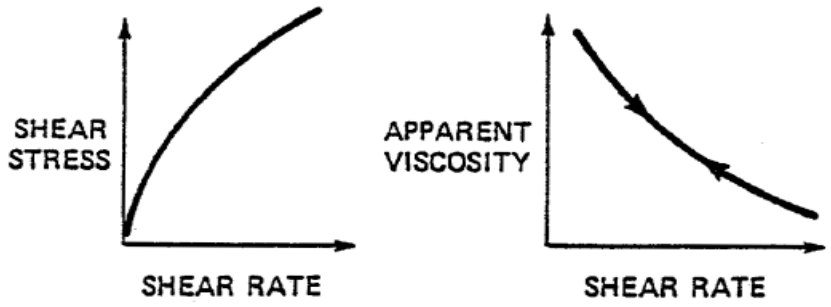

Figure 1-5. The rheological behaviour of shear thinning fluids Adapted [28].

1.2.3) Viscoelastic Materials:

Viscoelastic fluids are fluids that exhibit both elastic and viscous behaviors. Their overall behavior depends on which component is dominant; some materials show a viscous behavior, while others seem to have an elastic behavior [29]. A model example that has the most common viscoelastic properties is water. Several methods were well-documented in the literature [28]& [29] and were used to characterize the linear viscoelasticity including dynamic and static methods. The elastic method focuses on measuring the stress relaxation measurements (creeping); whereas the dynamic method focuses on measuring the oscillatory shear stress [29].

The main parameters such as storage and loss modulus that give us a clear insight into which the degree of viscoelasticity of materials, indicating if the viscous or elastic properties are more pronounced and dominant [29]. The loss modulus is also known as the viscous modulus, and it characterizes the viscous behavior of biopolymers in our study. It describes the energy dissipation due to fluid deformation. On the other hand, the storage modulus describes fluid elasticity and its ability to recover to the initial state. The difference between them is that elastic fluids usually store energy without dissipation during fluid deformation. Hence, the viscoelasticity of fluids is an important parameter to classify polymers as strong or weak gels [28]& [29].

1.2.4) Yield Stress:

Yield stress denotes a certain value of shear stress where the fluid starts showing a first flow response as it exceeded the critical shear rate value. It is a fluid plastic deformation behavior and it is denoted as τ_y as shown in Figure 1-6. The apparent yield stress is important when we measure the yield stress experimentally. In this thesis, we are going to investigate the yield stress response

of biopolymers solutions over various concentration ranges by performing a steady shear rate range starting from 0.1 s^{-1} to 100 s^{-1} [27].

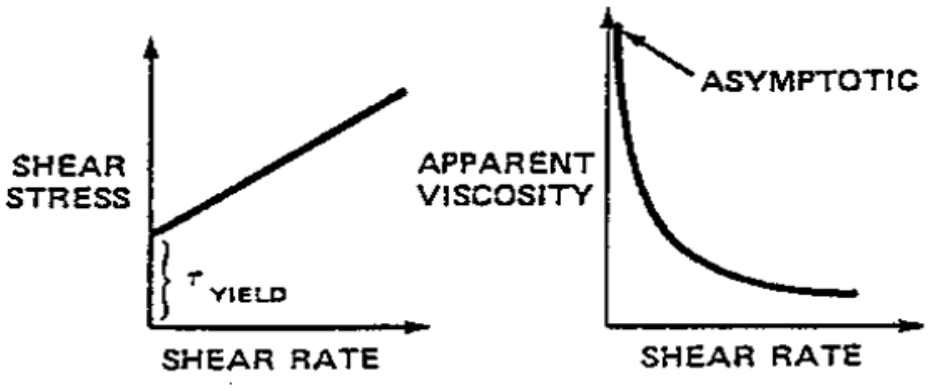

Figure 1-6. The rheological behavior of Bingham fluids [28].

1.3) Introduction to Taylor-Couette Flow:

Fluid circular flow motion is a part of fluid mechanics motion that demonstrates the flow around an object or axis. This type of flow could be easily observed in nature like a hurricane and storm on ocean currents. Indeed, the field of engineering and industry is full of applications of this flow including the separation processes and centrifugal applications. One of the special fluid rotational flows is known as the Taylor-Couette flow [30] when fluid is moving between two concentric cylinders. Numerous studies depended on the Taylor-Couette flow in order to investigate the flow regimes mapping [108]&[109] in the transition between laminar to turbulent flow as well as to characterize the flow instabilities in each flow mode. Different flow regimes can be observed when the angular speed of one of the cylinders varies and increases such as Circular Couette flow [30], and Taylor Vortex Flow [30]. As an illustration in Figure 1-7, the basic geometry of the Taylor Couette system contains two concentric cylinders, allowing a well-defined energy balance by measuring the torque in the rig, and the viscosity of the fluid between the cylinders can be inferred [30].

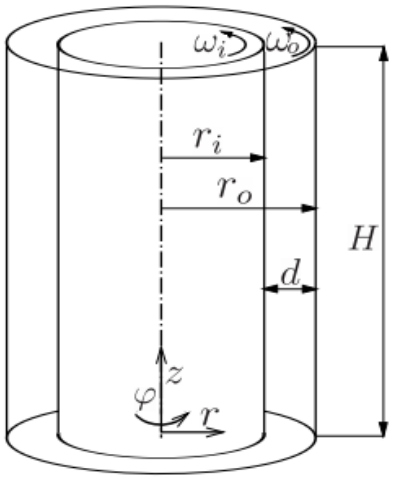

Figure 1-7.the geometry of the Taylor-Couette system.

1.3.1) Historical Background of Taylor-Couette Flow :

To begin with, the fluid circular flow motion between rotating coaxial cylinders was discovered and investigated in 1923 by Geoffrey I. Taylor [30]. Early in 1890, Maurice Couette [30] was the first scientist who performed his experiments using a device which was similar to the Taylor Couette system, which was called a viscometer with only the outer cylinder rotated. The early days of the Taylor Couette flow referred back to the most influential pioneers and scientists including Newton, Stoke, Margules, Mallock, Couette, Taylor, and Chandrasekhar [30]. They discovered the basic concepts and manifestations of this flow behavior. One of the reasons that make the Taylor Couette system common in fluid rotational flow experiments is the astonishing flow patterns in the transition regimes where instabilities occur. These characteristics are relatively complex to capture and explain based on fluid behavior, the flow is complex in the case of using non-Newtonian fluids. To bridge the gap, researchers still are conducting experiments on complex fluids under various conditions, then confirming the results with the theoretical and numerical solutions [30].

Correspondingly, the literature is full of studies focused on the Newtonian fluids flow characterizations in the Taylor-Couette flow; the circular motion of fluids was studied by Isaac Newton [30] at the end of Sixteen century. Along with Newton's experiments, George Stokes [31] has studied and solved fluid velocity equations in the TC system. He found the motion of the inner cylinder produces less flow stability, where eddies will be produced as a result of the centrifugal force creating fluid motion outward the inner cylinder. In 1881, the initial design scheme of the viscometer has been proposed by the famous instrumentalist Margules [32]. A few years later,

Mallock and Couette [33] constructed the viscometer and started their experiments. Hence, Mallock concluded that there was a nonlinear correlation between the angular velocity and the torque, causing unstable flow when the velocity exceeded the critical value. As a result of the first instability, vortices appeared, which were called Taylor Vortices [34]. Mallock's experimental work was observed by Kelvin [35] who was interested in the concept of flow stability. The stability was studied by Rayleigh [36] who was the first scientist concentrated his effort to explain the flow stability. He demonstrated that the stable flow was more pronounced when the only outer cylinder rotates, and unstable flow was obvious with the inner cylinder rotates. Eight years after Margules' proposal to construct the viscometer, Couette [37] finished his first experiment by using the viscometer focusing on both Newtonian. In 1890, Couette [38] conducted torque characterization experiments by studying the effect of fluids viscosity in Taylor Couette flow. A noticeable attempt to investigate the linear stability of viscous fluids flow was reported by Taylor [39]. Additionally, Chandrasekhar [30] published his book about hydrodynamic stability, focusing on different experimental and theoretical aspects of Taylor-Couette flow.

1.3.2) Flow visualization and mapping:

The flow transition from laminar to turbulent contains several flow regimes when the outer cylinder is fixed, and the inner cylinder rotates. These flow regimes are associated with the rotation of the inner and outer cylinder as can be seen in Figure 1-8. The laminar azimuthal flow in the Taylor Couette flow is known as Circular Couette Flow (CCF) where the gap between the cylinders has a direct impact on the tangential velocity. When the rotational speed increases the flow becomes quite unstable at the first instability occurs when the boundary turns to be curvy and takes a convex shape. This flow instability is known as Görtler instability [59].

When the inner cylinder speed increases further, the second instability occurs with the waviness characteristic, the flow, in this case, is known as Wavy Vortex Flow (WVF) [40]. The wavenumber increases with the speed leading to the third instability when the waviness becomes modulated with a higher wavenumber; this flow called a Modulated Wavy Vortex Flow (MWVF) [40] with the axial phase between vortices is not axisymmetric and not locked with each other. The flow is still laminar at this stage. As the inner cylinder speed evolves, the vortex flow becomes turbulent and the vortex flow looks like the TVF but without the flow stability as well as waviness characteristics it is known as Turbulent Taylor Vortices (TTV). The vortex flows in Figure 1-8 follow a broad vortex flow route as follows: CCF à TVF à WVF à MWVF à TTV [40].

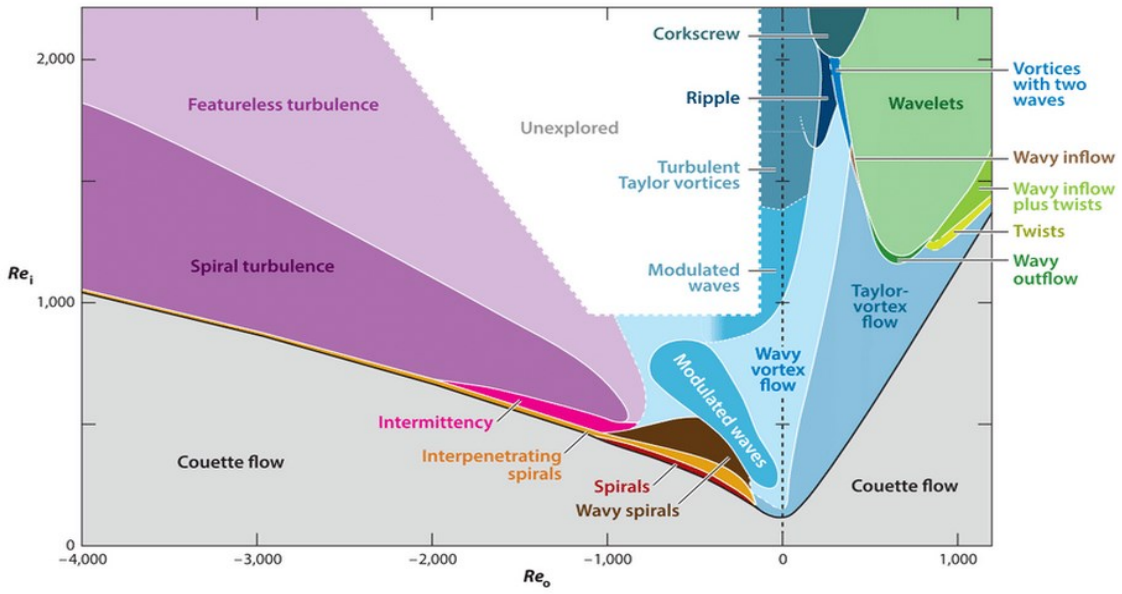

Figure 1-8 The Taylor-Couette flow regimes map depending on the rotation of setup cylinders as observed by Andereck et al. [40].

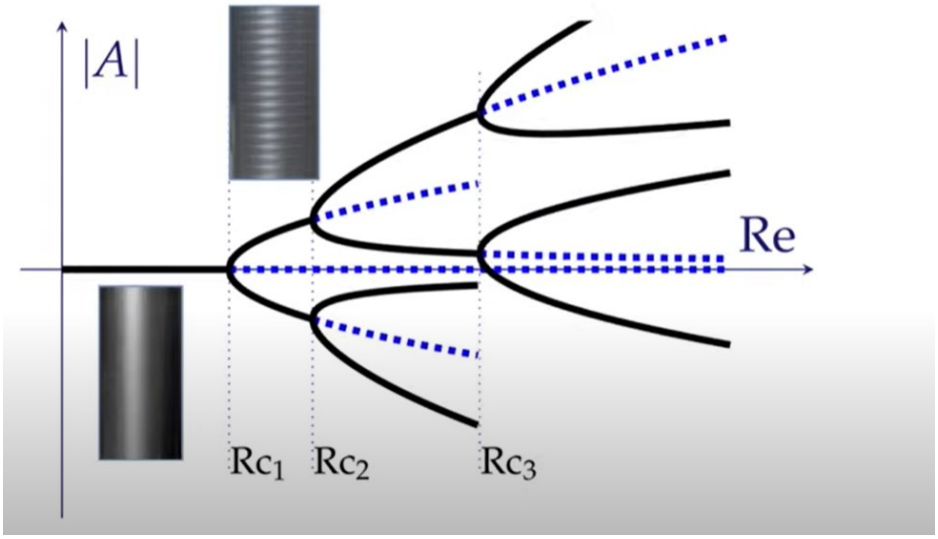

Figure 1-9. The bifurcations vortex map in the Taylor Couette flow

Most early studies as well as current investigations in the modern era have been full of significant attempts to make a valuable contribution in studying the onset of instability where turbulence, chaos, and bifurcations appear. In fact, the flow behavior beyond the stability stage is unpredictable and not easy to observe. One approach to handle this problem is by using visualization techniques through modern ways and devices, enabling researchers to observe the flow patterns and structure

in the TC system. For instance, Taylor [36] depended on ink to visualize the flow patterns by injecting ink into the system. Whereas Liao et al. [41] & [42] used visualization experiments to observe the spatial and temporal flow patterns. Recently, Wereley & Lueptow [43], [44] took a step in their experiments depending on particle tracking in order to observe and measure the velocity field in Taylor-Couette flow. Also, Henderson & Gwynllyw [45] used the same technique to observe steady Taylor vortices by depending on gravity force in the cylinder axis.

1.3.3) Aspect and Radius Ratios:

A series of recent experiments have been focusing on the main parameters associated with the Taylor Couette flow geometry [30], including the aspect ratio, which is the ratio of the length of the inner cylinder to the gap between the cylinders, and radius ratio which is the ratio of the inner cylinder radius to the outer cylinder radius[40]. The turbulent flow is more pronounced in a higher aspect ratio due to the effect of shear flow at a higher centrifugal force, resulting in a significant variation in the flow stability and vortex flow [40]. There have been numerous studies that investigated the effect of aspect ratio and radius ratio on the flow instabilities. For instance, Andereck et al. [40] performed his experiment in the Taylor Couette system with a radius ratio of 0.883 and an aspect ratio of 30; his results showed that the flow was characterized by analyzing the behavior of dimensionless parameters such as Reynolds number and normalized wavelength. Also, Burkhalter and Koschmieder [46] used radius ratios of 0.727 and 0.505 to investigate the effect of the vortices' wavelength due to using different radius ratios. They found that there is no correlation between the wavelength and Taylor number (Ta) of axisymmetric vortices in a large radius ratio. Several studies are reported in the literature to address the impact of the aspect ratio on the flow patterns behavior in Taylor Couette flow [39]. Correspondingly, a significant impact was achieved by using a wide range of aspect ratios =100 to 380 [39]. Whereas, Coles [47] conducted his experiments with lower aspect ratios were 14.4 and 27.9. Also, the aspect ratio of our study (AR= 31) is close to that one in Andereck et al. [40]. Then, Lueptow et al. [48] studied the flow behavior and transitions which occurred by using flow visualization experiments on TC setup with large aspect ratios = 41. They reported the impact of aspect ratio in the spiral vortex flow at a turbulent regime, while Coles [47] reported the flow behavior at intermediate transition regimes. Burkhalter and Koschmieder [46] evaluated vortex wavelength. Whereas, Andereck et al. [40] showed the intermediate regimes. Lueptow et al. [48] illustrated the flow mapping of the relationship between Taylor and Reynolds numbers.

1.3.4) Flow Instability and Vortex Flow:

The Taylor-Couette flow instability between coaxial cylinders occurs in the transition from laminar to turbulent regimes as the only inner cylinder rotates, creating massive inertia force required to overcome the viscous force that is reflected in higher Reynolds number. Accordingly, the flow instabilities in Taylor-Couette flow appear as toroidal vortices form, Taylor vortices (TVF). These vortices are influenced by main parameters such as fluids viscosity and Reynolds number (Re). The Reynolds number can be represented by the followed equation below:

$$Re = \frac{\Omega\, r_i\, (r_o - r_i)}{v} \qquad [1]$$

where ρ is the fluid density, μ is the viscosity, is the rotational speed of the inner cylinder, r_i is the inner cylinder radius, and $d = r_o - r_i$ is the gap between the cylinders. The Taylor-Couette system can be geometrically characterized by the radius ratio, $\eta = \frac{r_i}{r_o}$ where r_o is outer cylinder radius, and the aspect ratio, $\Gamma = \frac{d}{L}$, where L is the length of the cylinder.

Since we used non-Newtonian viscous fluids that exhibit shear thinning nature, when the viscosity of these fluids depends on the shear rate load; it changes its behavior as the shear rate evolves. Thus, to quantify the Re values for the shear thinning fluids, different definitions of Re have been used in the literature[49]–[51]. We define the Re values in our study based on viscosity values observed at the average nominal shear rate value as

$$\gamma = \frac{\Omega\, R_i}{d} \qquad [2]$$

Earlier at the beginning of the twentieth century, Taylor [39] studied laminar flow and illustrated that the fluid was becoming linearly unstable as the Taylor vortices appeared. These experiments focused on characterizing the flow regimes and torque of turbulent Taylor Couette flow. Also, the correlation between instabilities and angular speed of the inner cylinder was investigated; it was observed the flow instabilities were influenced by the angular speed of the inner cylinder, resulting in visualizing vortices with a donut shape.

Jeng and Zhu [52] stated a relationship between the fluid volume friction factor and vortices, when the friction factor grows the vortices are compressed toward the inner cylinder. Subsequently, Prima and Swinney [53] have analytically studied the behavior of both Taylor vortices and wavy Taylor vortices flow. Later, Prima et al. [54] establish a correlation between torque and Taylor vortices in laminar flow as a function of radius ratio and Taylor number. Murai et al.[55] performed

a numerical study for a Newtonian solution emphasizing vortex regimes in the TC system over a wide range of Reynolds Number (600 < Re < 4500); they identified five flow regimes, starting at Re < 92 where the flow is laminar, forming Circular Couette flow CCF. As Re increases (92< Re < 138) Taylor Vortex Flow TVF appears, whereas when the critical Re was exceeded, the flow is then known as Wavy Taylor Vortex Flow WTVF with Re values (138 < Re < 1020). In transition flow a Modulated Wavy Vortex Flow MWVF (1020 < Re < 1380) can be observed, finally they observed the Turbulent Taylor vortex Flow TTVF at (Re > 1380).

In addition to the previous numerical and experimental work, many researchers have focused on studying the effect of wavelength, vortices number, and fluid concentration on the flow regimes instability. Peng & Zhu[56], and Landry et al.[57] used Non-Newtonian Bingham fluids to study the linear stability in the Taylor-Couette flow Coles [47] & Snyder[58] investigated both axial and azimuthal wavenumber of the onset of turbulent flow. At high Taylor number (Ta), coexistence evidence of G¨ortler vortices and Taylor vortices has been provided in turbulent flow by Barcilon et al. [59], whereas, Koschmieder [60] used two radius ratios to measure the variations in the wavelength of turbulent Taylor vortices. On the other side, Mullin and Benjamin [61] demonstrated that the flow stability can be influenced by the length of the cylinders.

1.3.5) Non-Newtonian Fluid in Taylor-Couette System:

Several studies are well documented in the literature focusing on flow characterizations of Newtonian fluids in Taylor Couette flow. The Taylor Couette system is considered one of the most appropriate setups to investigate the flow instabilities and regimes for either Newtonian and non- Newtonian fluids [53]. In the last decade, several experiments were carried out to study the vortices' contribution to the flow structure. For example, Mehidi & Amanullah [62] investigated a simulation study of the Bingham fluids' vortices transition between the borehole and rotating string during drilling processes. They depicted that the pressure loss dropped as the vortices elongated at flow transitions. In terms of pressure loss reduction, three different high molecular weight polymers were utilized as Drag Reduction Agents (DRA) by Bhambri et al. [63]–[65] including thermo-responsive polymers, and vera, tamarind powder and pineapple fibers polysaccharides. Whereas Philp et al. [66] & Latrache et al. [67] used diluted shear thinning fluids to conduct experiments on vortex flow characterizations. However, a massive demand to conduct more research on the concentrated shear thinning fluids in the Taylor Couette flow is required.

1.3.6) Applications of Taylor-Couette flow:

Recently, numerous applications are depending on the concept of Taylor Couette flow, including science [52], engineering [52], industrial[62], and fluid processes applications[52]& [62]. The Taylor Couette system employs experts' attention in the oil field to enhance the viscoelasticity properties of the non-Newtonian fluids that are used as drilling muds and to improve the friction reduction ability of drilling muds [52]. Also, these concentrated fluids contribute to the transport of sediments outside the well depending on many factors including their high molecular weight. Thus, the Taylor Couette system is a proper prototype to conduct experiments similar to the borehole wall and rotating string on a laboratory scale level by considering the borehole wall as the outer cylinder and the rotating string as the inner cylinder [62]. Additionally, the Taylor Couette system is also involved in various engineering applications, including journal-bearing lubrication, cooling of rotating machinery among others, and purification of industrial wastewater [52]. Furthermore, it also is used in filtration process applications for different purposes as well as in separation systems such as sperate plasma from blood, and reactors for water purification and animal cell [45].

1.4) Theoretical and Mathematical expressions of Taylor-Couette Flow:

To describe the mass transferring through control volume in a closed Taylor Couette system we identify the first law of fluid mechanics which is the conservation of mass, by introducing the continuity equation:

$$\frac{\partial \rho}{\partial t} + \nabla \cdot (\partial \, \mathrm{p} \, u) = 0 \qquad [3]$$

where ρ is the density of the fluid, t is the time, (∇) is the divergence of a vector field and u is the velocity field. The first term illustrates the amount of mass varied in time, whereas the second term represents the mass flux per unit of volume (mass convection) [68]&[69].

Additionally, the result of the mass and the motion of a body is known as the momentum of the body it can be represented by momentum conservation equations, which depend on Newton's second law of motion containing the sum of external forces acting on a control volume equal to the time rate of change of the linear momentum of the contents of the control volume and the net flux of linear momentum out of the control surface by mass flow. In the case of Newtonian fluids, that

have a proportional correlation between shear stress and shear rate, this equation is called the Navier-Stokes equation and is written as

$$\frac{\partial \rho u}{\partial t} + \nabla\cdot(\partial\, \rho\, uu) = -\nabla p + \nabla.[\mu\,(\nabla u + \nabla u^{T})] + \nabla\left[\left(\mu v - \frac{3}{2}\,\mu\right)\nabla.\, v\right] + F \qquad [4]$$

where ∇ is the gradient, P is the pressure, μ is the dynamic viscosity, T indicates the transpose of a vector, and μv is the volume viscosity. The four terms from lift to right correspond to the following; inertial forces, Pressure forces per unit volume, the sum of viscous forces, and the external forces applied to the fluid [68].

In the case of the flow motion between concentric long cylinders, where the inner cylinder rotates with angular speed ω and the outer one fixed. Thus, the conservation equations will be in cylindrical coordinates as the flow motion around the z-axis. The other dimensions axis are, r and θ present both the radial and the azimuthal coordinates, respectively. The velocity field denote as $U(t; r, \theta, z)$, can be decomposed into three perpendicular components: the azimuthal one, u_θ (t; r, θ, z), the radial one, U_r $(t; r, \theta, z)$ as shown in the Continuity equation in cylindrical coordinates:

$$\frac{1}{r}\frac{\partial}{\partial r}(ru_r) + \frac{1}{r}\frac{\partial u_\theta}{\partial \theta} + \frac{\partial u_z}{\partial z} = 0 \qquad [5]$$

the Navier-Stokes equations for the flow motion in its three cylindrical components are:

At r-axis:

$$\frac{\partial u_r}{\partial t} + u_r\frac{\partial u_r}{\partial r} + \frac{u_\theta}{r}\frac{\partial u_r}{\partial \theta} + u_z\frac{\partial u_r}{\partial z} =$$

$$\frac{1}{\rho}\frac{\partial P}{\partial r} + \upsilon\left[\frac{\partial}{\partial r}\left(\frac{1}{r}\frac{\partial}{\partial r}(ru_r)\right) + \frac{1}{r^2}\frac{\partial^2 u_r}{\partial \theta^2} + u_z\frac{\partial u_r}{\partial z} + \frac{\partial^2 u_r}{\partial z^2} + \frac{2}{r^2}\frac{\partial u_\theta}{\partial \theta}\right] \qquad [6]$$

At θ- axis :

$$\frac{\partial u_\theta}{\partial t} + u_r\frac{\partial u_\theta}{\partial r} + \frac{u_\theta}{r}\frac{\partial u_\theta}{\partial \theta} + \frac{u_r u_\theta}{r} + U_z\frac{\partial u_\theta}{\partial z} = -\frac{1}{\rho\, r}$$

$$\frac{\partial P}{\partial \theta} + \upsilon\left[\frac{\partial}{\partial r}\left(\frac{1}{r}\frac{\partial}{\partial r}(ru_\theta)\right) + \frac{1}{r^2}\frac{\partial^2 u_\theta}{\partial \theta^2} + \frac{\partial^2 u_\theta}{\partial z^2} + \frac{2}{r^2}\frac{\partial u_r}{\partial \theta}\right] \qquad [7]$$

At z-axis:

$$\frac{\partial u_z}{\partial t} + u_r\frac{\partial u_z}{\partial r} + \frac{u_\theta}{r}\frac{\partial u_z}{\partial \theta} + u_z\frac{\partial u_z}{\partial z} = -\frac{1}{\rho}$$

$$\frac{\partial P}{\partial z} + \upsilon\left[\left(\frac{1}{r}\frac{\partial}{\partial r}\left(r\frac{\partial u_z}{\partial r}\right)\right) + \frac{1}{r^2}\frac{\partial^2 u_z}{\partial \theta^2} + \frac{\partial^2 u_z}{\partial z^2}\right] \qquad [8]$$

The velocity components satisfy the no-slip boundary conditions at the cylinder's walls,

$$[\![u'_z = 0 \text{ at } r = r_i,\ r = r_o \quad u' = \omega_i r_i, \text{ at } r=r_i \quad u' = \omega_o r_o, \text{ at } r=r_o \quad u = 0 \text{ at } z = 0,\ z=L]\!]$$

To achieve the similarity conditions to our experimental analysis, we depend on dimensionless parameters, including Reynold number and normalized wavelength. The main reason for using dimensionless analysis is to minimize the number of variables related to the problem's equations by creating a small group of dimensionless parameters. Also, to give us an idea of the correlations between parameters, by identifying which parameters have the most or less impact on the outputs or results. Particularly, in our study, the Taylor-Couette system characterizes by three dimensionless parameters which are as the following:

1)Reynolds Number:

The Reynolds number of the inner cylinder, which represents the ratio between inertial forces to viscous forces, and is defined as

$$Re = \frac{\Omega r_i (r_o - r_i)}{\nu} = \frac{\Omega r_i d \rho}{\mu} \qquad [1]$$

2) The aspect ratio

$$\Gamma = \frac{L}{d} \qquad [9]$$

Also, the viscosity affects and has a clear correlation with shear stress and shear rate as can be seen in the equations below:

Shear Stress

$$\tau = \mu \frac{du}{dy} = \mu \frac{\Omega r_i}{d} \qquad [10]$$

Shear Strain

$$\gamma = \frac{\Omega r_i}{d} \qquad [2]$$

As a result, we can directly infer the value of the viscosity by the relationship between both shear stress and shear rate, confirming the previously mentioned, the viscosity formula can be expressed as::

$$\mu = \frac{\tau}{\frac{\Omega r_i}{d}} = \frac{\tau}{\gamma} \qquad [11]$$

1.5) Study justification:

Based on the above review of the fundamental theory and existing research in the scientific literature, there is an evident need for further analysis of shear thinning fluid behavior in the Taylor-Couette geometry for higher concentrations of additives. Such mixtures have tended to not be studied because of the difficulty in working with such high concentration mixtures. Some of this is because consistent and constant fluid properties are difficult to obtain. This means there is significant justification to characterize more high concentration mixtures and to study flow patterns and behavior at these higher but practical concentrations. The full justification of this research work is laid out below.

I constructed the main hypothesis of this study, are as follows:

- The shear thinning rheology of xanthan gum (XG) and guar gum (GG) gives a unique pseudoplastic flow regime.
- The viscosity and yield stress curves are consistent with the rheology mathematical models that describe the solutions' flow curves.
- The effect of storage time and extra agitation to the (XG) and (GG) solutions affect the rheology and viscoelastic properties.
- The shear thinning affects the flow regimes in the Taylor Couette flow.

The effect of the shear thinning nature of concentrated non- Newtonian biopolymers on the rheology flow curves and the shear thinning nature of all the concentrated solutions is going to be studied by capturing the flow behavior of the viscosity and yield stress points. In addition, the thixotropy response will be investigated for the highly concentrated solutions.

Followed by the rheology flow curve of concentrated biopolymers, the effect of storage time and extra agitation time applied to the concentrated solutions is going to be discussed. The solutions were stored for 1 month, and the measurements performed at the end of each week (4 measurements in total). Whereas extra agitations applied to the solutions, following the sequence of (8 h, 24 h, 48 h) of agitation. After the measurements were carried out at each step, the comparison is taking place at the next step between the sample with storage and agitation effect and the fresh samples that were measured on the first day after preparation.

In addition to the time aging measurements, the viscoelastic frequency sweep is going to be measured in order to study the effect of the shear thinning nature of the viscous and elastic parameters. Also, we are going to characterize and investigate which viscoelastic parameter was dominant at low and high-frequency loads.

After the rheology characterization experiments ended, the main findings obtained after applying the rheology models indicate the characteristics of the shear thinning solutions. These shear thinning characteristics are quantified by the flow index values for each solution. Then, these values are considered the first step of analyzing the flow visualization experiments. Thus, we are going to study the effect of shear thinning fluids on the flow regimes and vortices behavior by using a unique setup called the Taylor Couette system. To link the rheology experiments to the Taylor Couette experiments, the shear thinning flow indices values were used as the main part of our analysis. We are going to depend on the flow indices in analyzing the flow regime variations for all solutions in this study. Also, the characteristics of the vortex flow regimes can be described by the differences in flow indices.

Along with the rheology flow indices values, the viscosity model analysis is also a vital parameter we consider in the flow regime mapping, especially in determining the Reynolds number that is used to characterize the flow regimes, vortices size and wavelength. The Taylor-Couette flow in this study is similar to some extent to the drilling fluids flow behavior observed in the drilling operations. The main goal of using the Taylor-Couette system is to investigate the application of this system on solid sediments transport due to the difference in density between drilling fluid and solid impurities and the gravity effect as well.

Our experimental investigation focuses on observations of the flow regimes mapping in Taylor-Couette flow that have a variety of applications in the oil drilling field [7] . Will be seen in the previous work in the literature review, there is need to conduct experiments in the Taylor Couette system, including characterizing the flow of concentrated shear thinning fluids. The guar and xanthan gum solutions have been characterized by performing rheology investigation to study their yield stress points and viscoelastic behavior. More importantly, the prior studies in the literature addressed several questions on the effect of concentrated (high viscous) shear thinning fluids on flow regimes [108]&[109] critical Reynolds number [49], and vortex axial wavelength [108], which is still unclear, especially beyond the onset of the primary instability over vortex flow range CCF to MWVF. This study aims to bridge the gap and issue by characterizing experimentally the

flow regime mapping by utilizing flow visualization techniques and wide solution concentrations ranging from 1000 ppm to 10000 ppm. A closer look at the literature on the current experiments reveals some gaps and shortcomings in terms of the lack of study of the flow behavior of concentrated non-Newtonian fluids in the TC system. Thus, an important objective of the present thesis is to conduct experimental work with a strong emphasis on flow patterns and vortex analysis behavior in the Taylor Couette system. This goal leads to observing, analyzing the flow mapping for high viscous fluids.

Objectives:

The main objectives of this thesis are as follows:

- Study the behavior of the rheological parameters such as yield stress, viscosity patterns, and viscoelasticity of concentrated non-Newtonian biopolymers including xanthan and guar gums with various ranges of concentrations (1000 ppm to 40000 ppm).
- Investigate the effect of extra storage and agitation time on the viscosity and viscoelasticity stability as well as the yield stress variations of both biopolymers.
- Perform flow visualization experiments in the Taylor Couette system to study the flow behavior characterization of the concentrated solutions and highlight the potential changes in flow structure for all solution concentrations.
- Investigate the effect of shear thinning flow index, which is obtained from the rheology analysis of each solution, on the flow regimes structure, vortices size, vortices number, and vortex flow axial wavelength in the Taylor Couette system.

CHAPTER 2

Rheology Investigation and Yield Stress Characterization of High-Viscosity Xanthan Solutions

Abstract

Rheology characteristics of a viscous non-Newtonian biopolymer xanthan gum (XG) solutions were investigated over a shear rate range of 0.1 s^{-1} to 100 s^{-1}. Four different concentrations of XG solutions (1%wt, 2%wt, 3%wt and 4%wt concentrations) were used to study the yield stress and viscosity rheological behavior of this common non-Newtonian fluid which has a range of practical applications and is a convenient model for understanding the nature of shear thinning fluids that are used in many industrial applications. The rheology experiments were performed using a cylindrical head rheometer manufactured by Anton Paar model number DIN 53019 Rheolab QC.

Before our experiments, all concentrated solutions were carefully prepared to provide uniform concentrations with homogenous mixing. We observed a significant shear thinning dependence between the shear rate and the concentrations, as well as the yield stress points. In addition, the obtained rheology curves were mathematically characterized by using rheological models. We show that as expected when the solution concentration increased, the viscosity and yield stress also evolved with the shear thinning nature being more pronounced at higher solution concentrations. The xanthan gum solutions in this study exhibited flowing conditions when the yield stress points were exceeded at the values of 2.03 Pa, 2.13 Pa, 10.35 Pa, and 12.5 Pa for the concentrations of 10000, 20000, 30000, and 40000 ppm, respectively. Furthermore, the thixotropy "viscosity recovery" was observed for all solutions; all solutions showed a significant thixotropic property, recovering viscosity to the initial state at a low shear load in a short time of fewer than 150 seconds.

To understand the rheological behavior of concentrated XG solutions, different mathematical fitting models were examined, including the power law, Bingham, and Herschel–Bulkley models. The experimentally obtained curves agreed fairly well with the power-law and Herschel–Bulkley models, achieving model fitting accuracy (R^2) of more than 99% matched with the experimental flow curves for both models. The Bingham model did not realistically predict the rheology properties and fluids flow and the model fitting accuracy (R^2) with the experimental flow curves achieved 91% to 92%.

2.1) Introduction

Several studies in the literature in rheological studies focused on structured fluids and yield stress analyses. Yield stress investigations of Xanthan gum solutions and other similar mixtures are essential for several applications, including in a variety of food productions such as paint, foam, grease, and pastes. When it comes to fluid flowability, viscosity and yield stress analysis are also vital to characterize fluid behavior. In some applications, it is important to prevent solutions from aggregation and separation. The overall fluid flow performance and viscous stability of these kinds of fluids can be evaluated by characterizing yield stress and viscosity behavior. Therefore, different flow equations, or "rheological models", were fit to the obtained rheology stress-strain rate curves, aiming to describe the fluid flow behavior throughout yield stress and viscosity characterizations [8]–[11].

2.1.2) Literature Review

In the last decades, several studies in the literature emphasized the rheological properties of *diluted (a relatively small quantity of solute dissolved in a large quantity of solvent) and semi-diluted* XG solutions for numerous industrial purposes. The first attempt by Ochoa et al. who studied the viscosity behavior of diluted solutions implied that the viscosity dropped as the shear rate increased. They confirmed the ordered- disordered molecular transition due to the shearing effect [3]. The viscosity behavior of XG solution at different temperature ranges was studied by Norton et al. [70] who used the *shear rate-viscosity* correlation. They noticed that at low temperatures, the entanglement interactions between XG chains increased, causing a significant increase in viscosity. The recent experimental approach to rheology characterization focused on diluted XG solutions was made by Kang et al. [4] to conduct qualitative and quantitative analysis for both viscosity and yield stress. They investigated the influence of diluted XG concentration on viscosity behavior. They found that the XG concentration fractions in the solution have a significant impact on the solution's rheological properties [4]. They also confirmed the findings reported in the previous studies conducted by Whitcomb & Macosko [8] who investigated the shear flow of diluted XG solution at various ranges of strain rate from 0.1 to 100 s^{-1} as well as different XG diluted concentrations of 0.02 %, 0.03 %, and 0.04 %wt. Whitcomb & Macosko [71] also implied that the diluted XG solution still exhibited Newtonian behavior at a low range of shear rates 0.1-10 s^{-1}. In 1981, Thurston & Pope [72] studied the viscoelastic regimes of XG solution

with a concentration of 0.1 %wt, focusing on the yield stress behavior. They attributed the changes in viscoelastic behavior to the relaxation of the XG solutions. In addition, several studies focused on the effect of the XG concentration on pseudoplastic behavior "shear thinning" by increasing the concentration from diluted to low concentrations up to 0.1 %wt. The concentration effect on shear thinning behavior was investigated over oscillatory shear frequency measurements by Rochefort & Middleman [73]. Similarly, Tiu et al. [74] performed rheology measurements on diluted XG solution, but at different temperatures using steady shear measurements. The diluted solutions exhibited a pseudoelastic response at a low shear frequency up to 10 s^{-1} [74]–[76]. Marcotte et al. [77] later highlighted the influence of concentration on the shear thinning nature. They focused on the viscosity and yield stress analysis of low concentration XG solutions of 0.1 %wt. Later, Ji-Seok et al. [78] conducted a rheology characterization investigation by applying rheology models to the XG solutions' viscosity and yield stress curves. Currently, numerous studies depend on rheometers to conduct the steady flow curves and oscillatory measurements due to rheometers' high accuracy and ease to use [79]

The flow curves, steady shear, and oscillatory measurements were the focus of numerous rheology investigations of XG solutions in the last decade. Murphy et al. [80] & [81] focused on rheology flow curve characteristics of diluted XG solutions. They classified the diluted solutions as structured fluids based on their molecular chain interactions. Launay & Cuvelier [82] followed a similar experimental procedure over different concentrations, paying special attention to quantifying the elastic zone of the XG solutions, while Bejenariu et al. [83] investigated the effect of XG concentrations on the viscoelastic properties and the order-disorder molecular transition by currying out rheology oscillatory measurements. A few years later, Pelletier et al. [84] and Ma & Barbosa [85] performed an experimental work to study the order-disorder confirmations depending on frequency sweep and frequency creep measurements.

Recently, polysaccharide polymers have been extensively involved in the oil field [7], as a thickening agent in drilling muds. Numerous studies were conducted to characterize the main rheological properties that make the gum solutions uniquely suited to additives. Xanthan gum is relatively cheap compared to other mud additives and can maintain the pressure balanced inside wellbores as well as transport drilling cuttings that are generated during the drilling process. Furthermore, the XG solution has attractive heat transfer properties providing favourable

dissipation of heat arising from drilling while acting as an effective lubricant downhole [7], & [15], [86], [87].

2.1.3) Case Study

Rheology measurements of high viscosity XG solution, including steady shear and yield stress, were investigated in this study. Although many studies have been conducted in the rheology characterization of diluted and low concentration biopolymers, the rheological investigation of concentrated XG solutions is still limited. Concentrated XG water-based solutions were selected as a working fluid in this study due to their unique properties, such as viscoelasticity and clean impact on the environment.

2.1.4) Literature Summary

Table 2-1: Literature review studies summary.

Authors	Gum	Rheological Tests	Concentrations	Shear Loads
Whitcomb et al. [71]	XG	Flow Curve Tests	Diluted (0.04 %, 0.03 , 0.02 % wt)	Strain (0.1 - 100 s^{-1})
Thurson and Pope [72]	XG	Oscillatory viscoelasticity	Low (0.1 % wt)	Strain (0.1 - 100 s^{-1})
Ross - Murphy [80], [88]	XG	Flow Curve Tests	Low (0.1 % wt)	Strain (0.1 - 100 s^{-1})
Cuvelier and Launay [82]	XG	Flow Curve and Tests	Medium (0.8 % wt)	Frequency (0.1 - 2 rad/s)
Rochefort and Middleman [73]	XG	Viscoelasticity Measurements	Diluted to low (0.05 to 0.5 % wt)	Frequency (0.1 - 100 rad/s)
Tiu et al. [74]–[76]	XG	Viscoelasticity Measurements	Diluted (0.005 % & 0.01 % wt)	Strain (0.1 - 100 s^{-1}))
Giboreau et al.	XG	Oscillatory viscoelasticity	Low (0.1 % wt)	Frequency (0.1- 100 rad/s)
Hatakeyama et al [79]	XG	Viscoelasticity Measurements	Low (0.1 % wt)	Frequency (0.1 - 10 rad/s)
Marcotte et al. and Ahmed e t al [89] - [90]	XG	Viscoelasticity Measurements	Low (0.1 % wt)	Frequency (0.1 - 300 rad/s)
Bejenariu et al. [83]	XG	Viscoelasticity Measurements	Diluted (0.015 %, 0.02%, and 0.025 %wt)	Frequency (0.1 - 100 rad/s)
Pelletier et al. [84]	XG	Steady Shear Flow and	Moderate ((0.1%, 0.2%and 0.7% wt)	Strain (0.1 - 100 s^{-1})
Ji Seok et al. [78]	XG	Steady flow curve test	Viscous (1 to 4% wt)	Strain (0.1 - 100 s^{-1})

2.2) Experimental Measurements:

2.2.1) Raw Material and Sample Preparation:

The biopolymer selected in this thesis is xanthan gum (XG) powder with high-quality specifications, including viscosity and gelling ability, viscoelastic stability, and shear thinning nature. They can dissolve in aqueous solutions, allowing convenient preparation of shear-thinning solutions that form high viscosity mixtures similar to drilling fluids.

2.2.2) Equipment:

The experimental work in this project was divided into two main steps using modern equipment to complete each step. The first step was the preparation of the non-Newtonian solutions, where we used a weight balance to weigh the exact quantities of XG solute, distilled water and glycerin. Then, we performed the mixing process by utilizing a magnetic stirrer for the lower concentrations and a mechanical homogenizer (model code DX-120D) for the high concentrations. A cylindrical head rheometer manufactured by Anton Paar model number DIN 53019 Rheolab QC was used to perform the second step of the experimental procedure, which was rheology evaluation.

2.2.3) Sample Preparation:

The fundamental materials in the test solution were xanthan gum, deionized water (purity of 99.5%), and glycerin. We weighed the exact amount of all of these materials using a high precision balance (model number 52151646). After that, we dissolved the XG in a small sample of glycerin to avoid lumps and bubble formation until it became a consistent slurry solution. Then, we poured this into the water and mixed it in the magnetic stirrer (model code SH-3) for one hour. Also, we make sure to cover up the container during the mixing process by using parafilm. The final step mixing step is to apply a strong shear load by using a mixing homogenize, starting at 200 rpm for half an hour. Then, increase the load by 200 rpm each half an hour until the solution becomes homogenous. The more concentrated solutions need three to four high mixing round and reaching to more than 1000 rpm load.

In the solution preparation process, we paid much attention to fabricate solutions which were homogenous both in density and gelling appearance without any solid suspension, clumps or bubbles. Our samples consisted of four concentrations: 10000 ppm, 20000 ppm, 30000 ppm, and 40000 ppm.

The final step prior to the rheology measurements was to let the solution sit at rest for at least 24 hours, to decrease the internal stress in the solution due to the mixing process. It was kept cool and at a stable temperature (20 to 22 °C) to make sure there were no changes in the intermolecular interaction force.

Table 2-2: viscous fluids sample composition for the rheology measurements.

Sample Concentration	Sample volume	Water	Xanthan Powder	Glycerin	Mixing Time	Storing Time
1% XG (10000 ppm)	200 ml	86 ml	2 g	12 g	1.5 h	24 h
2% XG (20000 ppm)	200 ml	84 ml	4 g	12 g	1.5 h	24 h
3% XG (30000 ppm)	200 ml	82 ml	6 g	12 g	1.5 h	24 h
4% XG (40000 ppm)	200 ml	80 ml	8 g	12 g	1.5 h	24 h

2.3.4) Rheology Models:

Three different models we used in this study to describe the rheology behavior of non-Newtonian XG solutions and to capture yield stress values as each condition, indicating the ability of solutions to perform under specific conditions similar to what happens in the drilling muds operations inside the annulus. The models are:

Power Law Model "Ostwald Model":

$$\tau = K \gamma^{n} \quad [12]$$

Bingham Model

$$\tau = \tau_O + \mu_p \quad [13]$$

Hershel Buckley Model

$$\tau = \tau_{OH} + K \gamma^{n} \quad [14]$$

Where *n* is the dimensionless solution flow index that indicates the shear thinning degree. *K* is the consistency coefficient associated with the viscosity of solutions. Also, τ_o is the yield point and the unit is Pa. and μ_p is the plastic viscosity and the unit is mPa.s.

2.3) Results and Discussion:

2.3.1) Flow curves analysis:

The yield stress behavior was captured to characterize the fluidity of our XG solutions. Figure 2 - 2 showed the correlation between shear stress and shear rates for different concentrations of XG solutions over a fixed strain rate range of 0.1 to 100 s^{-1}. We observed that the shear stress increased with the shear rate and the yield stress values were obtained for shear rate as low as 10 s^{-1}. Thus, the solution concentrations have a proportional correlation with the applied shear stress and the viscosity curves, resulting in a noticeable increase in yield stress values at higher solution concentrations. As expected, higher yield stress points were obtained in higher concentrations.

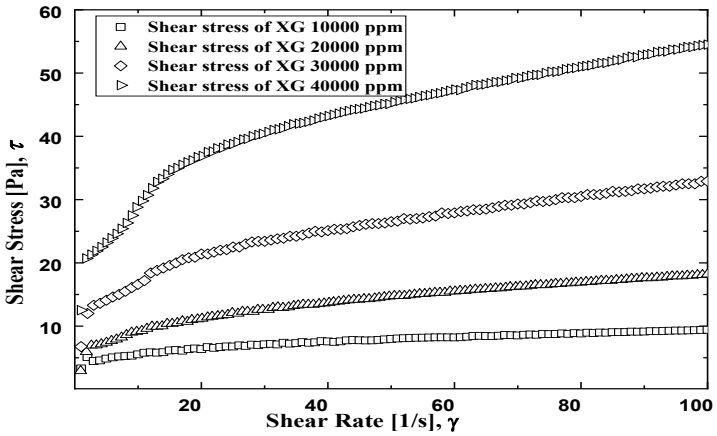

Figure 2-2. The yield stress curves of the Xanthan solutions.

In Figure 2-3, the log-log scale facilitates visually seeing the curve fit the rheological models. We see higher yield stress at higher XG concentrations. But it was noticed that the degree of slopes tended to be quite higher at higher solution concentrations. The yield stress points were quantified and discussed in the next section which contains the rheology models that fit the stress-strain rate curves, as shown in Table3 - 3.

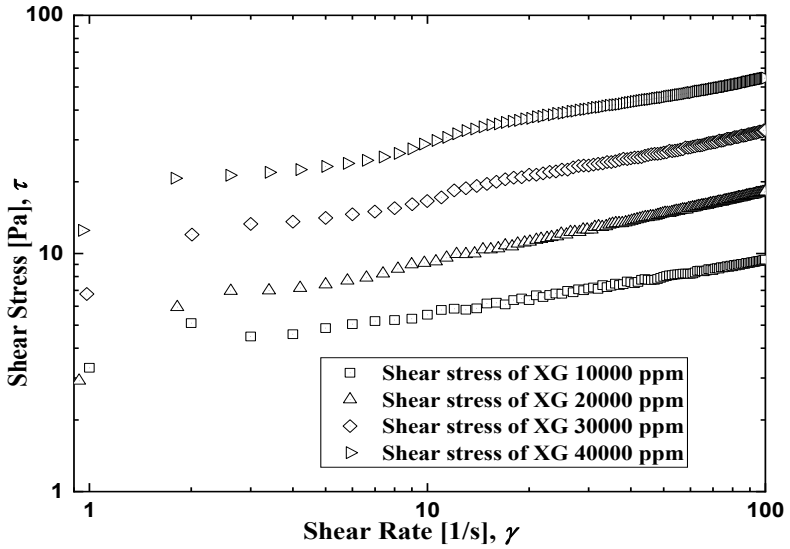

Figure 2-3. Log-log yield stress curves of the Xanthan solutions.

2.3.2) Xanthan gum Replications:

We performed three replications of each test sample concentration performed on different days. Each followed the same sample preparation procedure, including solution quantities, mixing steps and time. The replications were consistent with our first run (replications A) over all concentrations. Our tests were close to some extend with the main findings in literature, when such comparison was possible [5]&[91]. As can be seen in Figure 2 - 4, all curves had the same profile manner with experiencing only one outlier that was noticed in XG 1%wt and the plots for XG 4%wt they were not aligned together. This is might be due to experimental discrepancies in the procedure of sample preparation or the error due to the rheometer performance. In addition, the experimental values of this study were compared to the literature findings, as shown in Figure 2 - 5. The slight discrepancies were due to several factors that could affect the measurements, including the experiments' conditions, the quality of the raw materials of the solutions, and the experimental procedure and equipment used to perform the rheology measurements.

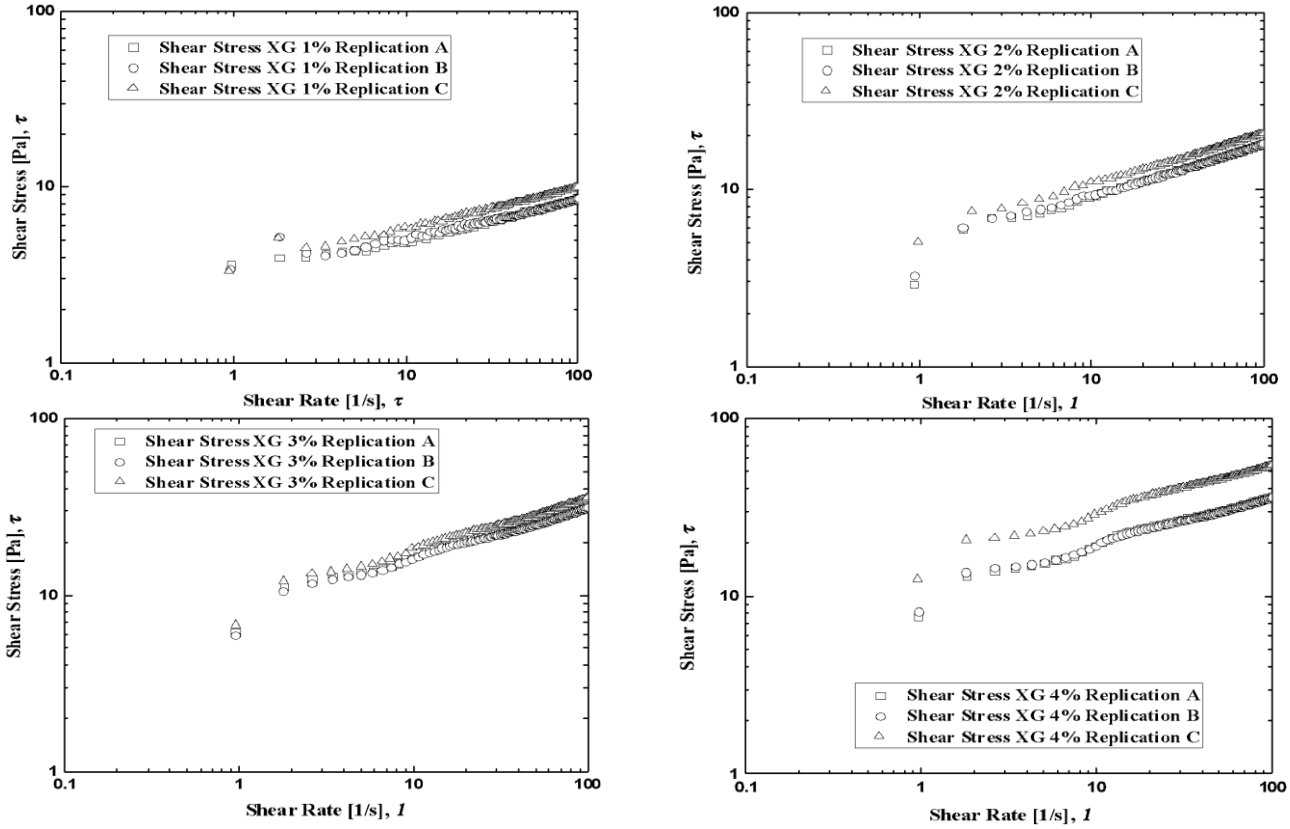

Figure 2-4. The yield stress replications curves of the Xanthan solutions for all concentrations from 1%wt to 4%wt.

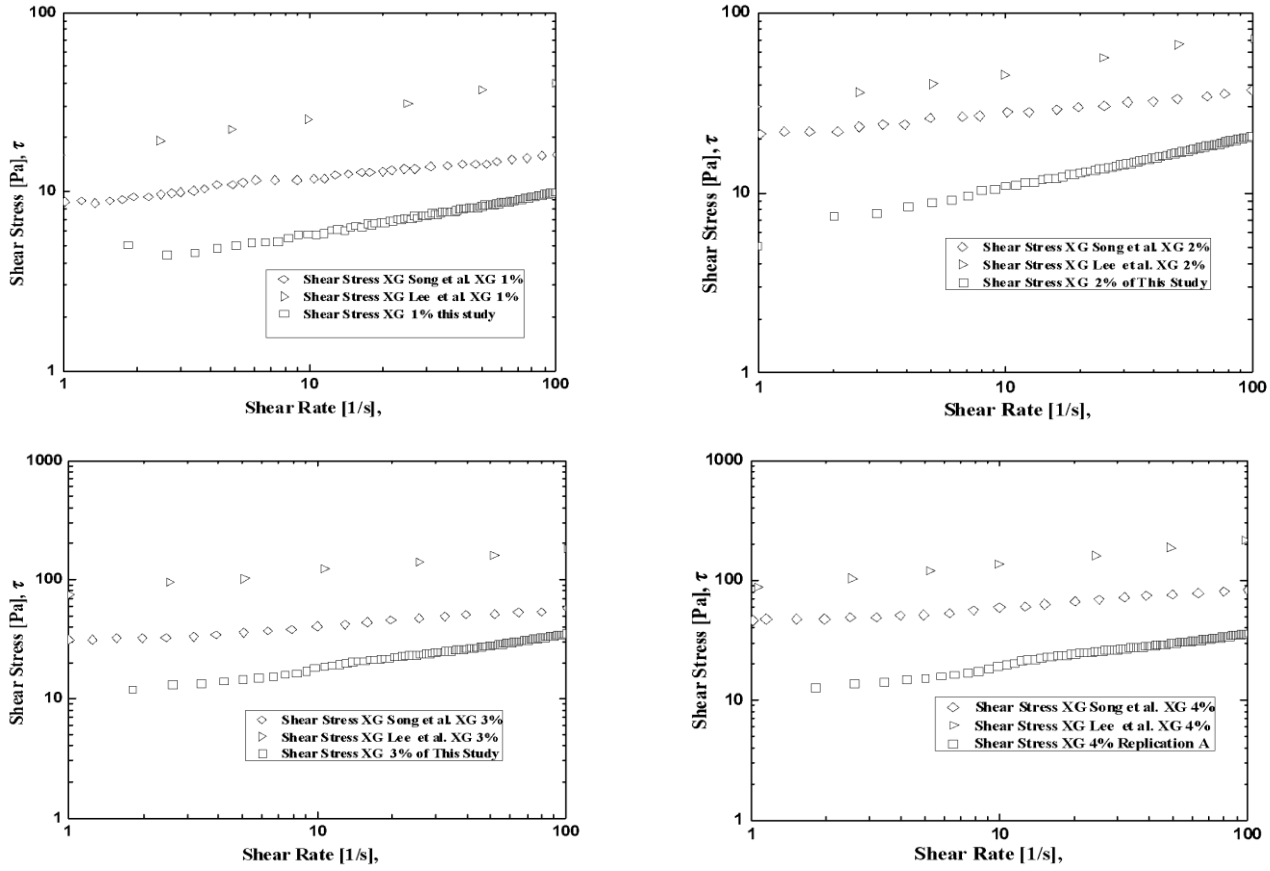

Figure 2-5. the comparison of the yield stress curves of the Xanthan solutions between our study and the literature concentrations from 1%wt to 4%wt.

2.3.3) Viscosity Analysis

Xanthan gum solutions showed pseudoplastic non-Newtonian behavior as the viscosity depended on the shear rate. The rheology curves in Figure 2 -6 exhibited the viscosity characteristics of shear thinning flow behavior at 20 C, where the apparent viscosity dropped as the shear rate increased. Additionally, the curves displayed the expected correlation between the viscosity and solution concentrations, increasing at higher concentrations, resulting in more pronounced shear thinning behavior. This increase is attributed to the interaction forces of the hydrogen bonds connected to the XG chains [5]. Those bonds tend to be weaker at a higher shear rate. Thus, when polymers experience a shear load, their chains stretch, when the high shear is applied they start breaking, resulting in a dramatic drop in the viscosity. The XG molecular structure was entangled at a low shear rate, and the viscosity was observed in higher values for all solutions. As the shear rate increases, the XG solution molecular structure aligns with the flow direction, resulting in a

significant drop in the apparent viscosity due to the drop in the intermolecular interactions and the entanglement [5].

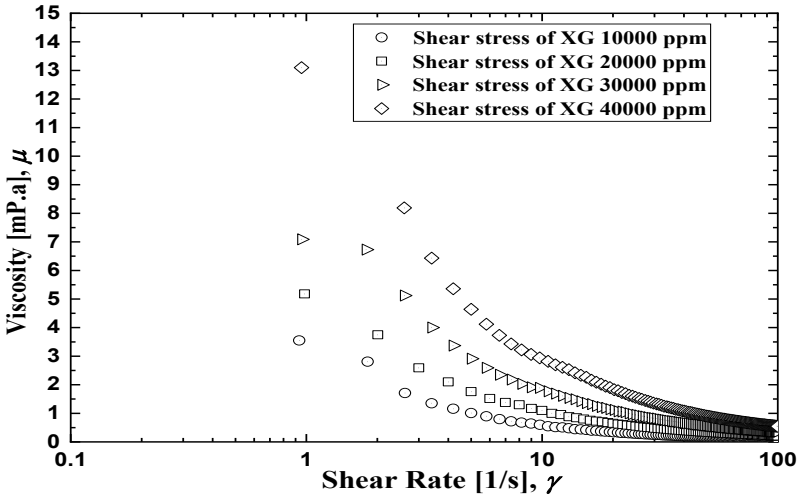

Figure 2-6. The viscosity curves of the Xanthan solutions.

2.3.4) Rheological Fitting Models and Analysis

Different mathematical models associated with rheological analysis were used to describe the rheology flow curves' behavior for the viscosity and yield stress tests. These models were the power law, Bingham, and the Herschel – Bulkley models. The parameters that play a key factor in these rheology models' analysis are the flow index, the yield stress, and the consistency coefficient, as can be seen in Table 2-3. Both yield stress and flow index values incrementally increased as the concentrations increased in all models. The flow index *n* denoted the degree of shear thinning nature. When the flow index approaches zero, it means the solution has a strong shear thinning nature. In contrast, the solution shows more Newtonian nature as the flow index gets closer to 1. Generally, all flow indices indicated that the solution in our study demonstrated a progressive pseudo-plasticity, due to the relatively higher concentrations.

Furthermore, the yield stress curves showed a consistent validation of only the Herschel – Bulkley and the power law models. Both models showed a consistent fitting with the flow behavior of the concentrated XG solutions. The rheology models were applied to fit our experimental obtained data. Also, they used to examine the fitting accuracy (R^2) of each model for each solution. We noticed that a high fitting accuracy of over 99 %was achieved when we used the power law and Hersche l– Bulkley models, as shown in Table 2 -3. However, the Bingham

model did not predict the flow behavior and had fitting accuracy (R^2) of less than 93 % in describing the rheology and flow behavior of the XG solutions. The reason for this poor fit is that the Bingham model is usually used to describe the Newtonian region of the flow curve of drilling muds at an extendedly higher shear rate. Thus, it works precisely beyond the yield stress.

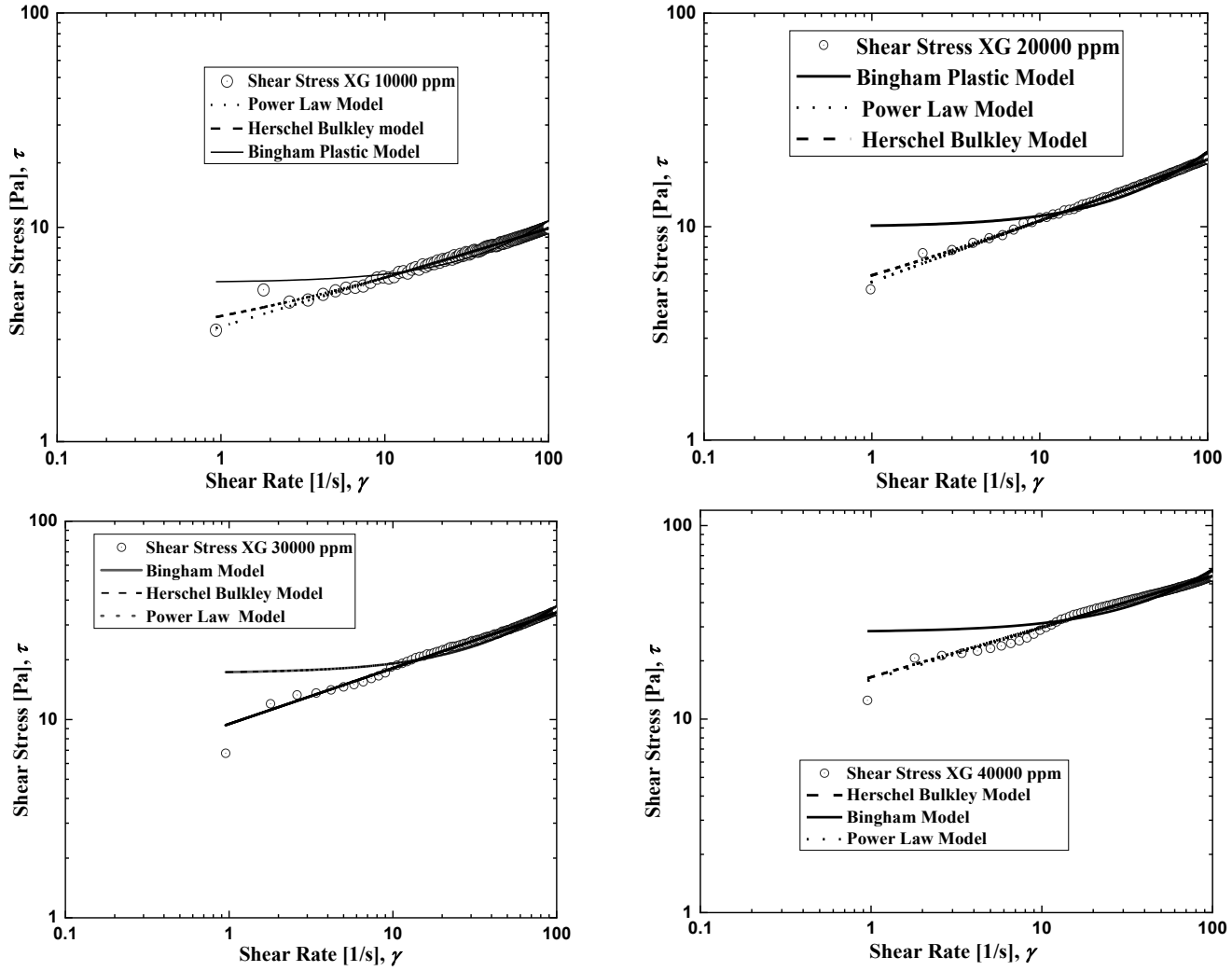

Figure 2-7. The rheology models for yield curves of the Xanthan solutions

Yield Stress Models

Table 2-3: the yield stress rheology models

Rheological Model	Xanthan gum Concentration	Yield Stress τ	Consistency index K	Flow index n	Fitting accuracy R^2
Power Law	10000 ppm	-	3.44	0.23	99.20%
	20000 ppm	-	5.50	0.29	99.80%
	30000 ppm	-	8.11	0.32	96.91%
	40000 ppm	-	16.48	0.26	99.22%
Bingham Plastic					
	10000 ppm	5.62	0.05	-	92.09%
	20000 ppm	10.12	0.12	-	92.60%
	30000 ppm	17.14	0.20	-	91.90%
	40000 ppm	28.18	0.31	-	91.31%
Herschel–Bulkley					
	10000 ppm	2.03	1.81	0.32	99.86%
	20000 ppm	2.13	4.26	0.33	99.50%
	30000 ppm	10.43	8.92	0.29	99.50%
	40000 ppm	12.50	16.47	0.26	99.20%

The following Figure 2 - 8 illustrated the correlation between the flow index n, consistency coefficient K, and yield stress τ trends for all XG concentrations; all parameters were a function of solution concentration. Accordingly, these parameters were obtained from the rheological models that were applied to the flow yield stress curves and the values reported in Table 2-3. The Herschel – Bulkley's yield stress points were consistently showing an incremental trend with the increase of the XG concentrations. The more concentrated solutions started flowing at relatively high yield stress values which were 2.03 , 2.13, 10.35 , and 12.5 Pa. for the concentrations 10000 , 20000, 30000, and 40000 ppm, respectively. This increase in yield stress is attributed to the flow resistance which is more pronounced at higher concentrations at a low shear rate as can be seen in Figure 2 - 8. Additionally, it was observed that concentration played a critical role in yield stress. Hence, the consistency coefficients increased with higher concentrations for both the

power-law and Herschel – Bulkley models compared to the Bingham model. However, the flow index fluctuated as the concentration increased, it increased before it experienced a significant decrease at the highest concentration 40000 ppm. This fluctuation is due to the progressive shear thinning nature of the high-viscosity solutions. Thus, the flow becomes more complex at concentrated solutions, with a strong elastic effect over the entire shear rate range.

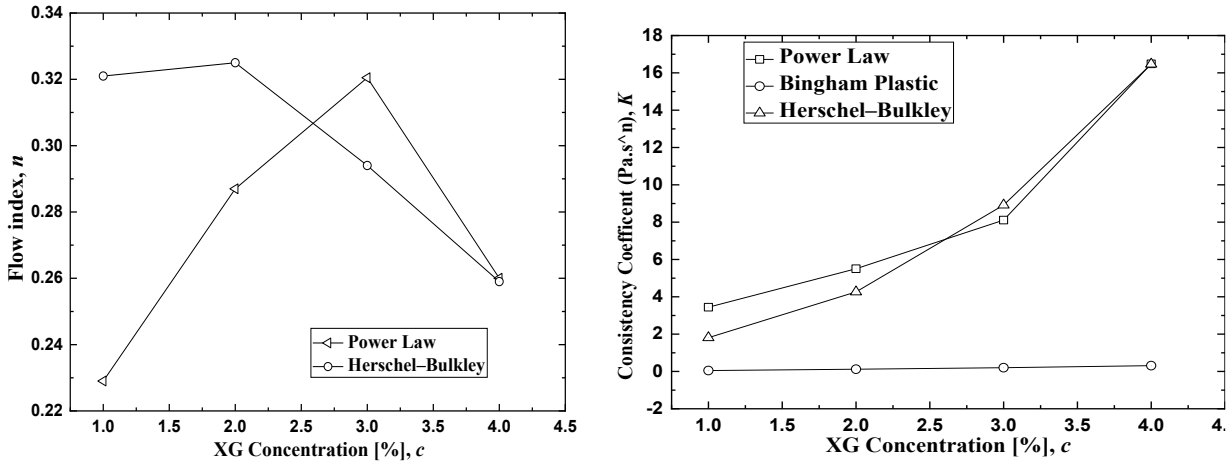

Figure 2-8. The shear thinning flow indices and consistency coefficients analysis for yield stress rheology models.

2.3.5) Thixotropy and Viscosity Recovery

The viscosity recovery or thixotropy behavior of the concentrated XG solutions was investigated over three-step shear rate loads by applying them over three different continuous periods. Firstly, the experiments started by measuring the viscosity at a low shear rate before the highest shear value was applied. After capturing the viscosity behavior in both periods, the load was rapidly reduced to the lowest rate. The recovery in this period was compared to the initial state period to observe the difference. Based on Figure 2 - 9, recovery patterns were shown for all XG concentrations. The viscosities recovered to approximately their initial value after the highest shear stopped. They indicated fast recovery behavior over a relatively short test period, which was 2.5 minutes. The lowest and highest loads were 1 s^{-1} and 100 s^{-1}, respectively.

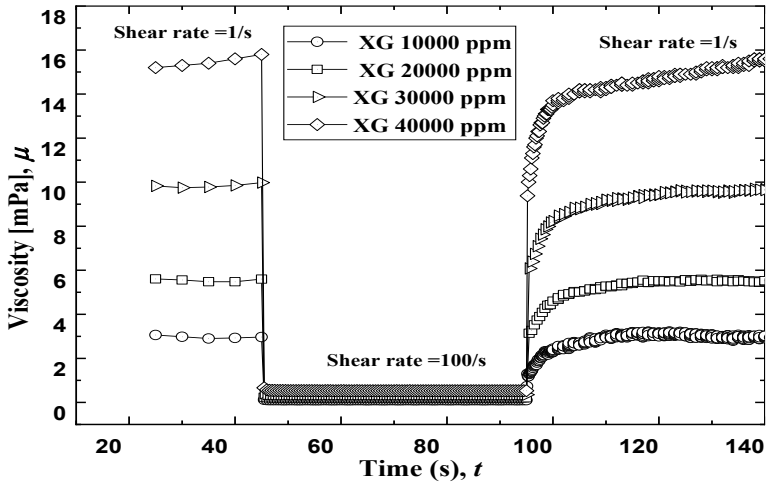

Figure 2-9. The shear thinning thixotropy behavior over a three-step shear rate loads for all xanthan solutions.

Conclusion

The main objective of this study is to analyze rheological properties and to characterize the flow curves of concentrated non - Newtonian XG solutions over a strain range from 0.1 s^{-1} to 100 s^{-1}. The selected concentrations were used to make the solutions similar to drilling muds 'water-based" forming as gel appearance at the rest. The viscosity and yield stress behaviors were well-described and characterized by selecting flow curve rheology tests. Accordingly, the solutions exhibited a relatively lower yield stress value at low shear rate.

All solutions exhibited a pseudoplastic nature, and the shear thinning behavior was strongly pronounced for all concentrated solutions. Additionally, the viscosity showed a significant dependence on the shear rate as well as the solution concentrations. Hence, all viscosities dropped progressively at higher shear load, indicating to the higher concentrations were proportional to the higher apparent viscosities. When the shear rate increased, the intermolecular forces decreased and the XG chains disentangled, causing a significant drop in viscosity under higher shear load.

To validate the obtained flow rheology curves and analysis, three mathematical rheological models were used to quantify the rheology behavior parameters of yield stress, flow index, and consistency index. These models were the power law, Herschel – Bulkley, and Bingham models. The results implied that both power-law and Herschel–Bulkley models were consistent and described the flow curves while achieving high accuracy of more than 99%. The Bingham model

did not accurately describe the flow behavior for all solutions, achieving a fitting accuracy (R^2) of less than 93%.

The thixotropic of the viscosity recovery behavior was studied for all solutions and over three shear-step periods. The thixotropy measurement was carried out to examine the viscosity recovery of the XG gum during and after the shear load was removed. The time taken to approach the initial viscosity was also measured and all solutions demonstrated a fast response of viscosity recovery in a short period of 150 seconds.

CHAPTER 3

Rheology Viscoelastic Characterisations of concentrated Xanthan and Guar Solutions

Abstract

Rheology and viscoelasticity properties of concentrated biopolymers xanthan gum (XG) and guar gum (GG) were studied in aqueous solutions with concentration fractions of 0.1, 0.4, 0.8, and 1%wt for each fluid. The flow curve measurements were performed over the shear rates range of 0.1 s^{-1} to 100 s^{-1}. The rheology experiments were performed using a cylindrical head rheometer manufactured by Anton Paar model number NCR-302. The results show that the yield stress points and viscosity were well characterized and they depended on the solution concentrations. We noticed that a more pronounced shear-thinning nature was observed at higher concentrations and the viscosity of both non-Newtonian fluids. Similarly, the yield stress showed higher values at higher concentrations.

The effect of storage time on the solution viscosity and yield stress of both solutions for the concentration of 1%wt was also investigated with successive viscosity and yield stress stability progress obtained after performing the experiments at the end of each week and lasted for up to 4 weeks of storage period. The apparent viscosity "at zero shear load" increased slightly after 30 days of storage time, this increase was 36.5 % and 22 % for the XG and GG solutions, respectively. Additionally, an extra agitation time was applied for the solutions, and it was evaluated for three different agitation times by 8h, 24 h, and 48h of continuous agitation time. It was observed that a noticeable decrease in viscosity was obtained by 22% for XG and 29% for GG solutions with increasing the agitation time. However, the drop and rise in viscosity and yield stress due to the agitation and storage time "at zero shear load" were considered slight with no huge variation compared to the initial measurements for both viscosity and yield stress values. Therefore, both fluids demonstrated stable behavior of viscosity and yield for long storage and agitation period.

Along with the yield stress and viscosity curves, rheological mathematical models were fit to describe analytically the flow and viscosity behaviors, and these models are the power-law and Herschel–Bulkley and Bingham models. The solutions yield stress points were well described and agreed with the power-law and Herschel–Bulkley models. Whereas the Bingham model was

not as consistent with the observed rheological behaviors. In addition, the viscosity curves of the solutions were consistently fitted with all rheology models associated with viscosity, and these models are the Cross and Careau Yasuda models.

The viscoelastic properties of the XG and GG solutions were characterized by conducting frequency sweep measurements with a frequency range of 0.1 to 300 rad/s and a fixed amplitude (5% of frequency). The results indicated that at low frequency, the elastic effect was only dominant in the XG solutions, but the viscous modulus was dominant in all GG solutions. However, at high frequency, the viscous effect was dominant for both solutions. Based on the solutions' viscoelastic behavior, we conclude that both fluids are still considered good candidates for practical engineering due to their viscoelastic characteristics at high frequency.

3.1) Introduction

3.1.1) Literature Review

There existed in the literature a considerable body of comprehensive descriptions of rheology characteristics of Newtonian and diluted non-Newtonian fluids (small amount of solute dissolved in a large amount of solvent) as well as the influence of temperature and concentration on solutions' viscosity [3]. The viscous behavior of the XG (at 55 ^{O}C) dissolved in distilled water was studied by Norton et al. [70] who indicated an inverse correlation between XG viscosity and the temperature, viscosity increased at low temperatures. This increase is due to the entanglement interactions between polymer chains resulting in an effective increase in the molecule's dimensions and weight. However, in 1993, Kang & Pettit [4] did not report similar observations, hence, they implied that there is no straightforward evidence of the dependency of viscosity with non-Newtonian XG concentrations that exceeded (0.1%wt.). Therefore, Whitcomb & Macosko [71] studied the effect of the steady shear flow of different XG concentrations less than (0.1%wt.) over various shear rate ranges up to 100 s^{-1}. They noticed that the XG solution tended to exhibit a Newtonian behavior at a low shear rate of 0.1 s^{-1}. Later, Thurston & Pope [72] conducted a theoretical and experimental study focused on the viscoelastic behavior of XG solutions and concluded that the change in viscoelasticity behavior due to frequency load (0.1 - 100 rad/s), was attributed to the relaxation processes of the XG solutions.

Recently, extensive efforts have been put into conducting rheology investigations focused on the effect of solution concentration on the viscoelastic non–Newtonian characterizations, as shown in

Table 1. Rochefort & Middlenaon [73] performed an experimental study of rheology behavior using steady and oscillatory frequency measurement of diluted XG solutions. Tiu et al. [74]–[76] focused on steady shear of only diluted XG solutions with concentrations of (0.005% and 0.01%wt) at different temperature conditions. They reported that the shear thinning behavior was observed for the XG concentration of 0.05%wt.

Accordingly, the dependency on rheometers in performing the rheology measurements is widely becoming more common due to several reasons, including their ease of use, their quality and their performance accuracy. Both concentric and parallel plate rheometers were used by Hatakeyama et al. [79] to characterize the viscoelasticity nature of diluted XG solutions. A rheological investigation was conducted by Marcotte et al. [77] to quantify the yield stress behavior of low concentration XG solutions (0.1%wt). The rheology curves of the XG solution were described by using flow equations known as rheology models, including the Power law and Herschel-Bulkley models. Then, Ji-Seok et al. [78] studied the flow rheology properties of the XG solutions and fitted the obtained viscosity and yield stress curves with the rheology models.

Xanthan gum which was dissolved in aqueous solutions was classified as a weak gel based on its viscoelasticity characterizations as reported in two experimental rheology studies that were conducted by Murphy et al [80] & [88]. Similarly, Launay & Cuvelier [82] carried out steady shear and oscillatory tests to investigate the influence of diluted concentrations on the elastic junction zone. Later, the shear thinning influence on viscoelastic properties of biopolymers attracted Bejenariu et al. [83] who studied XG solution behavior in different concentration conditions. The molecules' order-disorder confirmations at different diluted XG concentrations and temperatures were also studied by Pelletier et al. [84] They focused on the viscoelastic parameters' characterization including loss and storage modulus at the molecular level. Whereas Ma & Barbosa [85] performed the frequency sweep and frequency creep measurements to investigate the viscoelasticity of XG solutions that were characterized as weak gel. However, they found that the XG solution's rigidity increased as extra ions were added to the solution.

In the last decade, the rheology characterizations of GG solution were also experimentally studied by numerous scholars, focusing on the effect of concentration on the viscoelasticity behavior [92] & [93]. In 2010 , Bourbon et al. [94] highlighted the variation in the viscoelastic properties of diluted GG solutions including the loss and storage modulus affected by solution concentrations. They used oscillatory frequency sweep and flow shear curve measurements for all

GG solutions concentrations of (0.37% to 0.58%wt). They reported that the shear thinning nature was more pronounced in the viscosity curves, indicating that the elastic behavior was dominant for higher GG concentrations [94]. These findings significantly agreed with Tatham et al. [92] study that was published in 1995.

Currently, Torres et al. [95] examined the Cox-Merz rule of the viscoelastic behavior of diluted GG concentration (0.001%wtto 0.02% wt) by performing oscillatory frequency sweep and steady shear rate measurements. They concluded that the solutions exhibited shear thinning behavior and the flow curves were consistent with the Cox-Merz rule only for low concentrations. On the contrary, it was observed that the solutions did not confirm the Cox-Merz rule at higher concentrations.

Numerous studies have investigated the rheological properties of biopolymers GG solutions. One such study was done by Ross-Murphy [93] who conducted oscillatory and flow curves analysis for GG viscous solutions. They classified the characteristics of diluted GG solutions as a weakly structured gel, concluding that the elastic behavior was dominant at only low oscillatory frequency load. Similarly, Richardson & Ross- Murphy [96] investigated the viscoelastic properties of GG solutions over wide shear and a frequency range from 0.1 to 100 rad/s . In addition, Robinson et al. [97] conducted an experimental rheology study that depicted the effect of different concentrations on the viscoelastic response of GG solutions. They found that all diluted GG solutions depended on the frequency and shear rate [97]. These findings were consistent with the main observations of Wientjes et al. [98] who studied the viscoelastic behavior and properties over various ranges of oscillatory frequency load.

3.1.2) Applications:

Guar and xanthan gums are commonly used in the oil industry as well as in research activities that focus on enhancing the rheological properties of non-Newtonian drilling fluids. Both gums were selected for this study due to their unique rheological properties and their clean impact on the environment. They are considered non-toxic materials to be potentially used in the drilling process, cosmetics and food production. Their viscoelastic rheological properties reinforce their ability to transport drilling cuttings in the drilling process [7] & [15].

Moreover, XG and GG are used to prevent gases and liquids from entering the wellbore by balancing the pressure inside the annulus. Drilling fluids provide an effective lubrication downhole. As the drilling process goes deep, the annulus temperature increases rapidly because of

the friction resulting from the rotation of the string and collar against the wall. The generated heat can be absorbed and both XG and GG provide a favorable heat dissipation inside the annulus due to their heat transfer ability as a heat conductive medium to absorb the heat without changing its properties at a temperature below $70^{O}C$ [15], [86], [87].

3.1.3) Case Study:

Despite decades of research have been done so far, there is an obvious need to investigate the effect of concentrated non-Newtonian biopolymers on the fluid flow properties that show a strong shear thinning nature. The main objective of this study is to investigate the rheological behavior of concentrated biopolymers by studying the viscoelastic behaviors and characteristics over the frequency range (0.1 - 300 rad/s). In addition, this study also aims to study the variation of the shear thinning behavior in yield stress and viscosity for up to one month of storage time, and up to 2 days of the continuous agitation applied to both solutions. The solutions used in this study are considered food-grade biopolymers that could be used as drilling fluids “water-based mud”. Both XG and GG were selected for this study due to their unique properties such as the gelling capacity, high shear thinning nature, and their environmental impact.

Table 3-1. Literature Summary

Authors	Gum	Rheological Tests	Concentrations	Shear Load
Whitcomb et al. [71]	XG	Flow Curve and Yield stress Tests	Diluted (0.04%, 0.03, 0.02%wt)	Strain (0.1-1000 s^{-1})
Thurson and Pope [72]	XG	Oscillatory viscoelasticity	Low (0.1%wt)	Frequency (0.1- 100 rad/s)
Ross-Murphy [80], [88]	XG	Flow Curve and Yield stress Tests	Low (0.1%wt)	Frequency (0.1- 100 rad/s)
Cuvelier and Launay [82]	XG	Flow Curve and Yield stress Tests	Medium (0.8%wt)	Frequency (0.1- 2 rad/s)
Rochefort and Middleman [73]	XG	Viscoelasticity Measurements	Diluted to low (0.05 to 0.5%wt)	Frequency (0.1- 100 rad/s)
Tiu et al. [74]–[76]	XG	Viscoelasticity Measurements	Diluted (0.005%and 0.01%wt)	Frequency (0.1- 100 rad/s)
Giboreau et al.[99]	XG	Flow Curve and Oscillatory viscoelasticity	Low (0.1%wt)	Frequency (0.1- 100 rad/s)
Hatakeyama et al. [79]	XG	Viscoelasticity Measurements	Low (0.1%wt)	Frequency (0.01- 60 rad/s)
Marcotte et al. and Ahmed et al. [89] [90]	XG	Flow Curve Measurements	Low (0.1%wt)	Strain (0.1- 400 1/s)
Bejenariu et al. [83]	XG	Viscoelasticity Measurements	Diluted (0.015%, 0.02%,and 0.025%wt)	Frequency (0.1- 100 rad/s)
Pelletier et al. [84]	XG	Steady Shear Flow and Viscoelasticity Measurements	Moderate ((0.1, 0.2 and 0.7%wt)	Frequency (0.1- 100 rad/s)
Ji-Seok et al. [78]	XG	Steady flow curve test	Viscous (0.1 to 0.4%wt)	Strain (0.1-100 s^{-1})
Ross-Murphy [93]	GG	Steady Shear Flow and Viscoelasticity Measurements	Viscous (0.1 to 0.4%wt)	Frequency (0.1- 1000 rad/s)
Richardson and RossMurphy [96]	GG	Steady Shear Flow and Viscoelasticity Measurements	Moderate (0.1 and 0.5%wt)	Strain (0.1-100 s^{-1}) Frequency (0.1- 100 rad/s)
Bourbon et al.[94] and Tatham et al[92]	GG	Steady Shear Flow and Viscoelasticity Measurements	Moderate ((0.37-0.58%wt)	Frequency (0.1- 100 rad/s)
Torres et al [95]	GG	Steady Shear and Oscillatory Measurements	Diluted (0.001%wt to 0.02%wt)	Frequency (0.01- 10 rad/s)
Robinson [97]	GG	Steady Shear and Oscillatory Measurements	Low (0.2%wt)	Frequency (0.1- 100 rad/s)
Roland et al [98]	GG	Oscillatory Measurements	Low (0.2%wt and 0.4%wt)	Frequency (1-100 rad/s)

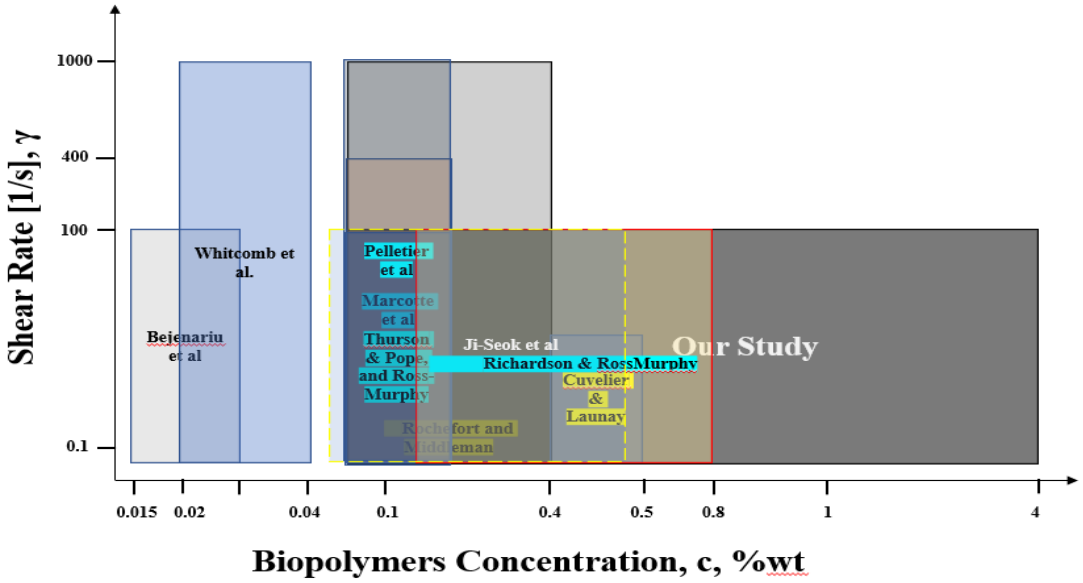

Figure 3-1. Literature Comparison with solutions concentrations in our study.

3.2) Experimental Measurements:

3.2.1) Raw Material and Sample Preparation:

Both XG and GG powder used in this project was produced by miniScience Inc. in the United States. They have unique specifications and hydrocolloid rheological properties. They are in white powder appearance form and can dissolve easily in both cold and hot water. They have a viscosity range of 1.0 to 1.5 Pa.s at rest for 1 %wt solution concentration. They are considered excellent candidates to prepare viscous non-Newtonian solutions, forming viscous solutions similar to drilling fluids with good gelling ability as well as their high pseudoplastic nature that makes them compatible with the applications that require thickening agents.

3.2.1) Equipment:

Four different types of equipment are used in this study. These devices are utilized for sample preparation and mixing, as well as rheology measurements. The first device is a high precision balance (model number 52151646) which was used to weigh the XG solute, deionized water, and glycerin before the mixing step. Also, a magnetic stirrer (model code SH-3) was utilized to provide a gentle mixing of the solution. To make sure the solutions were homogenously mixed, a high shear homogenizer with steel blades (model code DX-120D) was used to add a strong shear rate to the samples. The rheology measurements followed the mixing process. The rheology process is

performed by using a cylindrical head rheometer manufactured by Anton Paar model number NCR-302.

3.2.3) Sample Preparation:

The sample preparation process aims to achieve consistent dissolving of each powder in aqueous solutions. As mentioned before, the unique properties of both gums enable them to dissolve in both hot and cold water. We should be aware of avoiding the formation of bubbles and lumps during preparing the XG and GG solutions.

The solutions are prepared by weighing the proper amount of the XG by using a high-accuracy electronic weight balance. Then, instead of dissolving the XG powder directly in the water, it was dissolved in a small amount of glycerin (6 g/100 ml) to make a slurry solution in order to avoid lumps and bubbles formation. Then, the slurry solution was mixed slowly in distilled water using the magnetic stirrer for 1 hour. To avoid dust and contaminants dissolving in the solution during the mixing, the solution is sealed from the top by using parafilm. After this step, the mixing homogenizer is used to apply a high shear rate to the solution by applying agitation at 200 rpm for 30 minutes. Then 500 rpm for another 30 minutes, before it reaches 700 rpm for another 30 minutes. The total mixing time is 1.5 hours to make sure the solution is well mixed.

The final step prior to the rheology measurements is to let the solution be kept at a cool and stable temperature (20 to 22 ^{o}C) for at least 24 hours to decrease the internal stress in the solution due to the mixing process and to make sure there are no changes in the intermolecular interaction force, thus not affecting the rheology measurements.

Table 3-2. Fluids sample composition for the rheology measurements.

Sample Concentration	Sample Volume	Water (ml)	Gums	Glycerin	Mixing Time	Storing Time Before Rheology
0.1% XG and GG (10000 ppm)	100 ml	93.9 ml	0.1 g	6 ml	1.5 h	24 h
0.4% XG and GG (4000 ppm)	100 ml	93.6 ml	0.4 g	6 ml	1.5 h	24 h
0.8% XG and GG (8000 ppm)	100 ml	93.2 ml	0.8 g	ml	1.5 h	24 h
1% XG and GG (10000 ppm)	100 ml	93 ml	1 g	6 ml	1.5 h	24 h

3.2.4) Rheological Tests:

Rheology flow curve tests are performed for XG and GG over a selected range of shear rates from 0.1 to 100 s^{-1} in order to study the viscosity behavior, flow characteristics, and yield stress points for all concentrations. Then, other flow curves are performed to study the effect of the storage and agitation time on the yield stress, and viscosity. Each storage time measurement was selected to perform at the end of each week for up to 1 month long. On the other side, the extra agitations experiments were performed by increasing the agitation time for a period of 8 h, 24 h, and 48 h of continuous agitation. Both tests aimed to study the behavior of yield stress, viscosity, and flowability over the shear rate.

Furthermore, the frequency sweep measurements are also performed to investigate the viscoelastic properties and parameters of the solutions, to report which of these parameters are dominant at various ranges of frequency ranging from 0.1 to 300 rad/s. In addition, we paid special attention to the behavior of the fluids at low frequency.

3.3) Result and Discussion:

3.3.1) Viscoelastic Flow Curves

The biopolymers XG and GG solutions were prepared at different solute concentrations of (0.1% wt, 0.4% wt, 0.8% wt, and 1% wt) before currying out the rheology measurements including the flow curve and frequency sweep oscillatory over the shear rate ranging from 0.1 to 100 s^{-1}. Both solutions exhibited shear thinning behavior as can be seen in Figures 4- 2 and 4-3. It was obvious in Figure 3-2 that the yield stress values for XG evolved when the solution concentrations increased; these yield values were quantified from the rheological models such as the Bingham plastic, and Herschel-Bulkley models. The shear thinning effect is more obvious at higher concentrations. In addition, the yield stress point and apparent viscosity were affected by the concentration and their values are shown in Table 3- 3. As the shear rate increased, the shear stress showed a monotonic increase for the entire shear load. Whereas the apparent viscosity curves in Figures 3-2 and 3-3 consisted of 3 regions or segments: 2 of them are the linear regions at low shear rates so-called zero viscosity and at high shear rates “so-called infinite viscosity”. The last region is the non-linear region which is located in between the linear regions. The apparent viscosity started with the first linear region plateau at a very low shear rate before the yield point followed by a significant drop in viscosity with exhibiting shear thinning

behavior. Then, it reached the second linear region at the maximum shear rate. The solution concentrations showed a significant pseudoplastic influence on the yield stress, apparent viscosity, and shear stress increased. This pseudoplastic nature occurred due to the biopolymer hydrogen bonds and molecular structure that caused entanglements. The hydrogen bonds break at a high shear rate, indicating a significant drop in the intermolecular forces when polymer chains align at a shear rate direction [5].

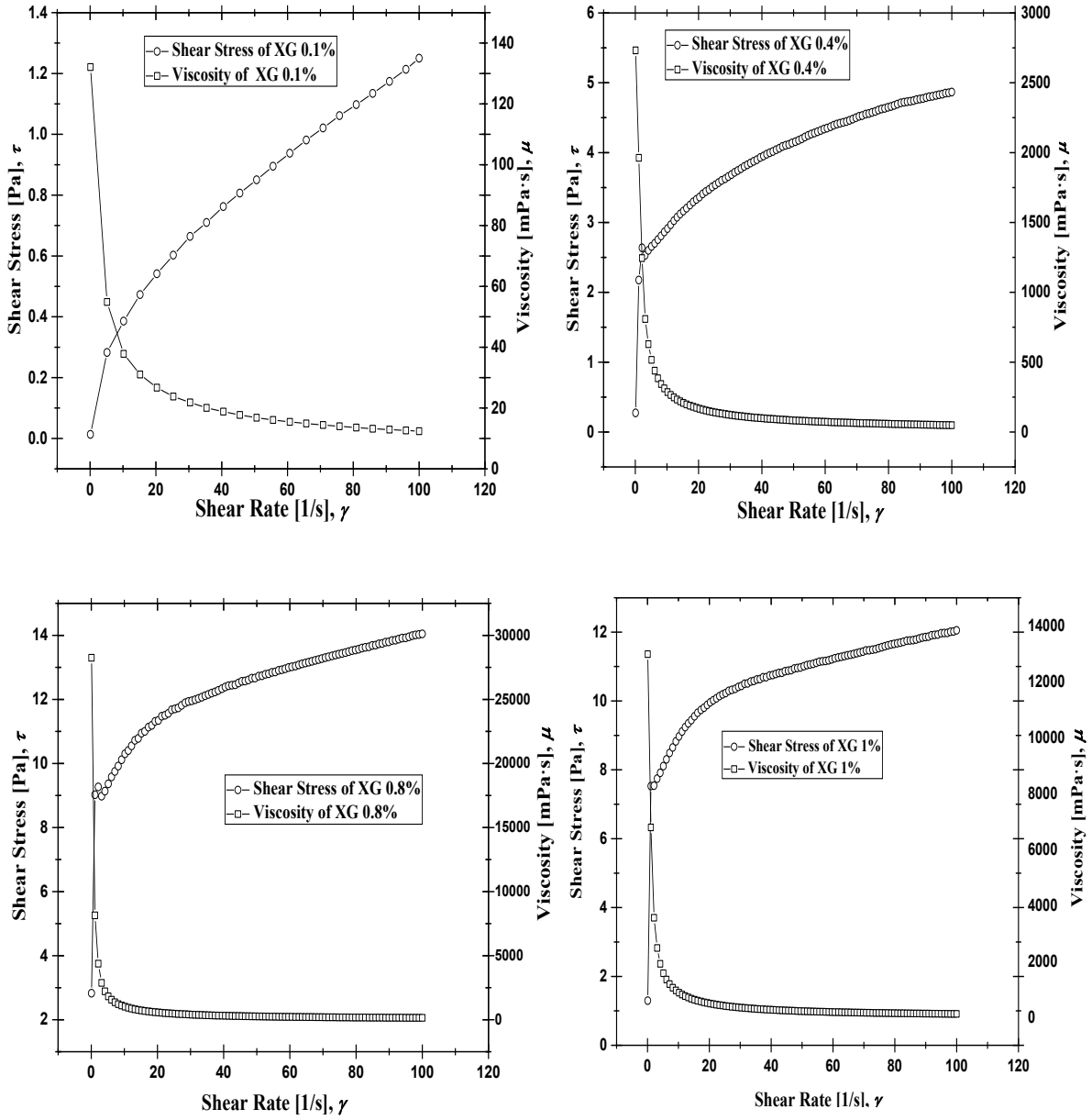

Figure 3-2. The viscoelastic flow curves for Xanthan Gum at all concentrations A) XG 0.1%wt, b) XG 0.4%wt, c) XG 0.8%wt, d) XG 1%wt

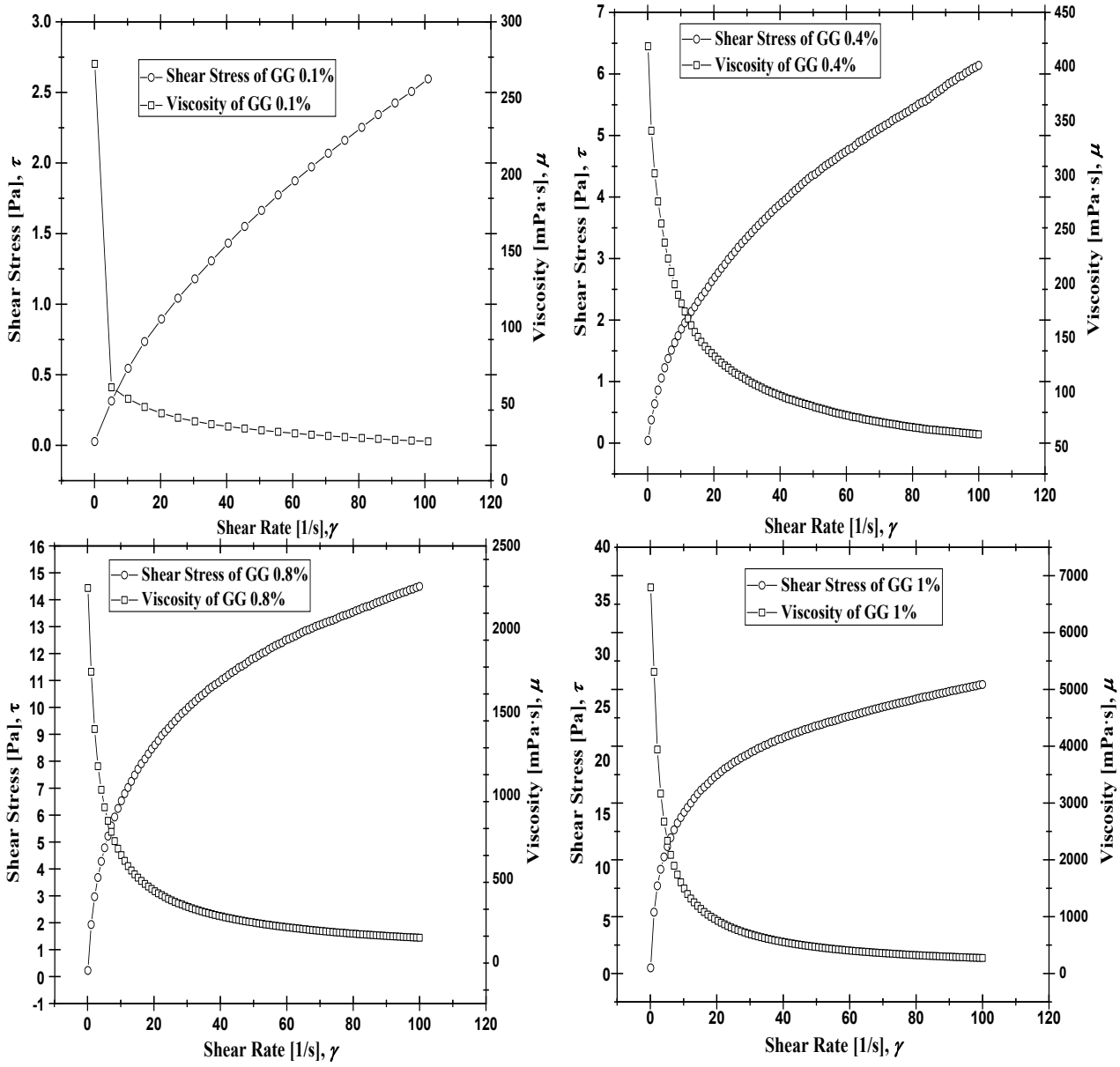

Figure 3-3. The viscoelastic flow curves for Guar Gum at all concentrations A) GG 0.1%wt, b) GG 0.4%wt, c) GG 0.8%wt, d) GG 1%wt

3.3.2) Rheological Models:

The logarithmic scale in Figure 3-4 facilitates the curves visualization to fit with the rheology models. To understand the rheology behavior of XG and GG solutions, conventional flow

equations are known as rheology models used to describe the concentrated fluid flow manners by fitting them with the obtained rheology curves. These models are the power law, Bingham, and Herschel– Bulkley models were also used to quantify the shear stress curves and capture the yield points for each solution. Whereas the Carreau Yasuda and Cross models were used to quantify the viscosity curves, as can be seen in Table 3-4. The results describing the yield stress agreed with the main findings that were highlighted in previous studies as shown in Table 3-3 [77]&[78]. Also, an inverse correlation between flow indices and solution concentrations was reported when the strong non-Newtonian nature was noticed in the solutions as the degree of shear thinning flow indices decreased. The yield stress curves were consistent with the Power law and Herschel–Bulkley models achieved fitting accuracy (R^2) of more than 99 % matching the obtained flow curves for both models for all solutions. Whereas the Bingham plastic had a less fitting accuracy as low as 92 %, as can be seen in Table 3-3.

Table 3-3. The rheology models' outputs for yield stress

Rheology Models	Gums Concentration	Yield Stress τ	Consistency index K	Flow Index n	Fitting accuracy R^2
Power Law Model	0.1%wt XG	-	0.70	0.05	99.96%
	0.4%wt XG	-	1.70	0.22	99.87%
	0.8%wt XG	-	5.40	0.15	98.80%
	1%wt XG	-	6.45	0.14	95.80%
	0.1%wt GG	-	0.12	0.66	99.70%
	0.4%wt GG	-	0.69	0.47	99.24%
	0.8%wt GG	-	2.90	0.35	99.20%
	1%wt GG	-	8.25	0.26	98.40%
Bingham Plastic					
	0.1%wt XG	0.53	0.01	-	99.30%
	0.4%wt XG	2.70	0.02	-	84.40%
	0.8%wt XG	8.60	0.04	-	67.00%
	1%wt XG	9.90	0.05	-	73.00%
	0.1%wt GG	1.10	0.01	-	98.4%
	0.4%wt GG	1.71	0.05	-	92.00%
	0.8%wt GG	5.00	0.10	-	86.00%
	1%wt GG	5.90	0.15	-	79.00%
Herschel–Bulkley					
	0.1%wt XG	0.25	0.02	0.79	99.85%
	0.4%wt XG	0.30	1.76	0.22	97.70%
	0.8%wt XG	1.02	5.41	1.35	96.10%
	1%wt XG	1.30	6.50	0.14	94.00%
	0.1%wt GG	0.10	0.11	0.60	99.97%
	0.4%wt GG	0.38	0.69	0.47	99.90%
	0.8%wt GG	2.10	3.08	0.33	99.23%
	1%wt GG	5.80	8.25	0.26	98.34%

Table 3-4. The rheology models for viscosity behavior

Rheology Models	**Gums Concentration**	***Zero shear viscosity*** η_0 **(mPa.s)**	**Infinite viscosity** $\eta^*_{infinity}$ **(mPa.s)**	**Fitting accuracy** R^2
Careau Yasuda Model	0.1%wt XG	135.00	4.80	99.96%
	0.4%wt XG	2731.00	26.02	99.95%
	0.8%wt XG	28245.00	56.00	99.90%
	1%wt XG	12978.00	40.35	99.98
	0.1%wt GG	444.00	1.90	99.87%
	0.4%wt GG	512.80	60.10	99.97%
	0.8%wt GG	2115.00	60.30	99.92%
	1%wt GG	6857.70	130.00	99.70%
Cross Model				
	0.1%wt XG	142.00	5.54	99.70%
	0.4%wt XG	2806.00	58.30	99.70%
	0.8%wt XG	34920.00	103.10	99.99%
	1%wt XG	13714.00	128.50	99.78%
	0.1%wt GG	2385.00	1.60	99.80%
	0.4%wt GG	492.20	60.00	99.94%
	0.8%wt GG	492.20	60.20	99.70%
	1%wt GG	7274.70	116.71	99.89%

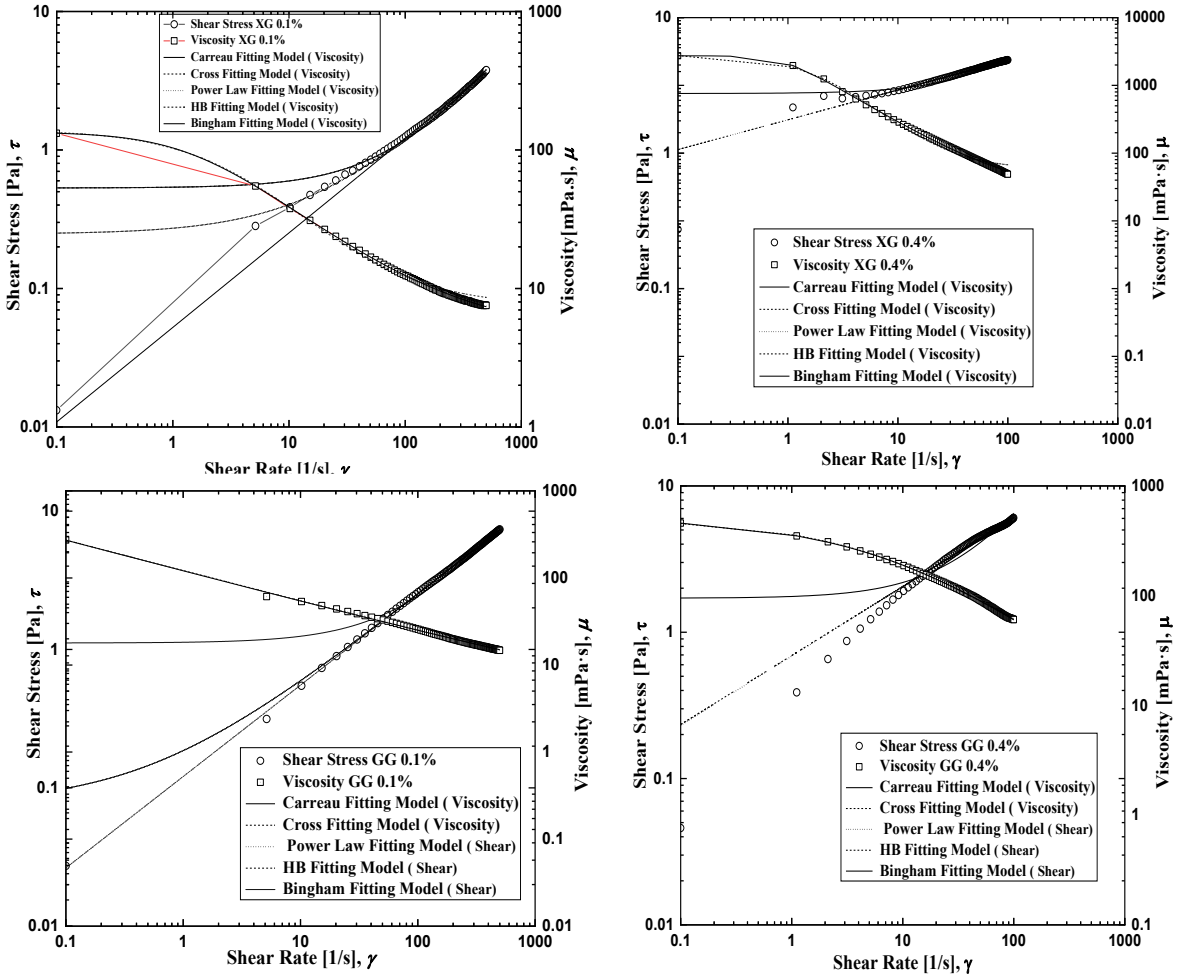

Figure 3-4. The viscoelastic flow Models for xanthan and guar gum A) XG 0.1%wt, b) XG 0.4%wt, c) GG 0.1%wt, d) GG 0.4%wt

3.3.3) The Effect of Storage and Extra Agitation Time on the Viscosity and Yield stress

Figures 3-5 to 3-7 depicted the effect of storage and agitation time of XG and GG solutions on the yield stress flow points and apparent viscosity behavior for 1 %wt solution concentration. The measurements for the effect of storage time on viscosity were measured at the end of each week, and it lasted for 1 month long for all solutions. Whereas the time of applying extra agitation to the solutions was: (8h, 24h, and 48h). It was observed that the viscosity in all plots exhibited a monotonic increase with longer storage time measurements, resulting in a strong shear thinning nature for higher concentrations. This increase in zero shear viscosity of the XG solution on day 30th was quantified as about 36.5 % more than the fresh solution viscosity, which was measured on day 2nd after the preparation of the solutions, as illustrated in Figure 3-7. Similarly, the increment variation in viscosity of the GG sample in the fourth week was 22%. Accordingly, Figure 3-7

showed that yield stress analysis at the same storage period exhibited an increase of 29% and 22% for XG and GG solutions, respectively. Hence, it was noticed that the viscosity and yield stress were higher in the XG solutions than in the GG solutions. The effect of flow index "degree of shear thinning" is more obvious in the XG solution compared to the GG solution.

Unlike the storage time analysis, the extra agitation time measurements illustrated an obvious drop in the shear stress, viscosity, and yield stress compared to the initial measurements that were performed with 8 h of agitation time, as can be seen in Figure 3-5. The drop variation in zero viscosity was quantified by 30% for GG solution and 40% for XG at the longest agitation period "48 h". Whereas the drop variation in yield stress for both solutions was about 30% at 48h of agitation. Overall, both solutions showed a stable viscosity and yield stress manner beyond the zero shear viscosity and critical yield stress points "at 1 s^{-1}" throughout the one-month storage period. Similarly, the drop in both parameters due to extra agitation time was also slight beyond zero shear viscosity. This gives us a clear indication of the characteristics of the XG and GG solutions that achieved convergent viscosity stability behavior beyond the shear rate of 1 s^{-1}.

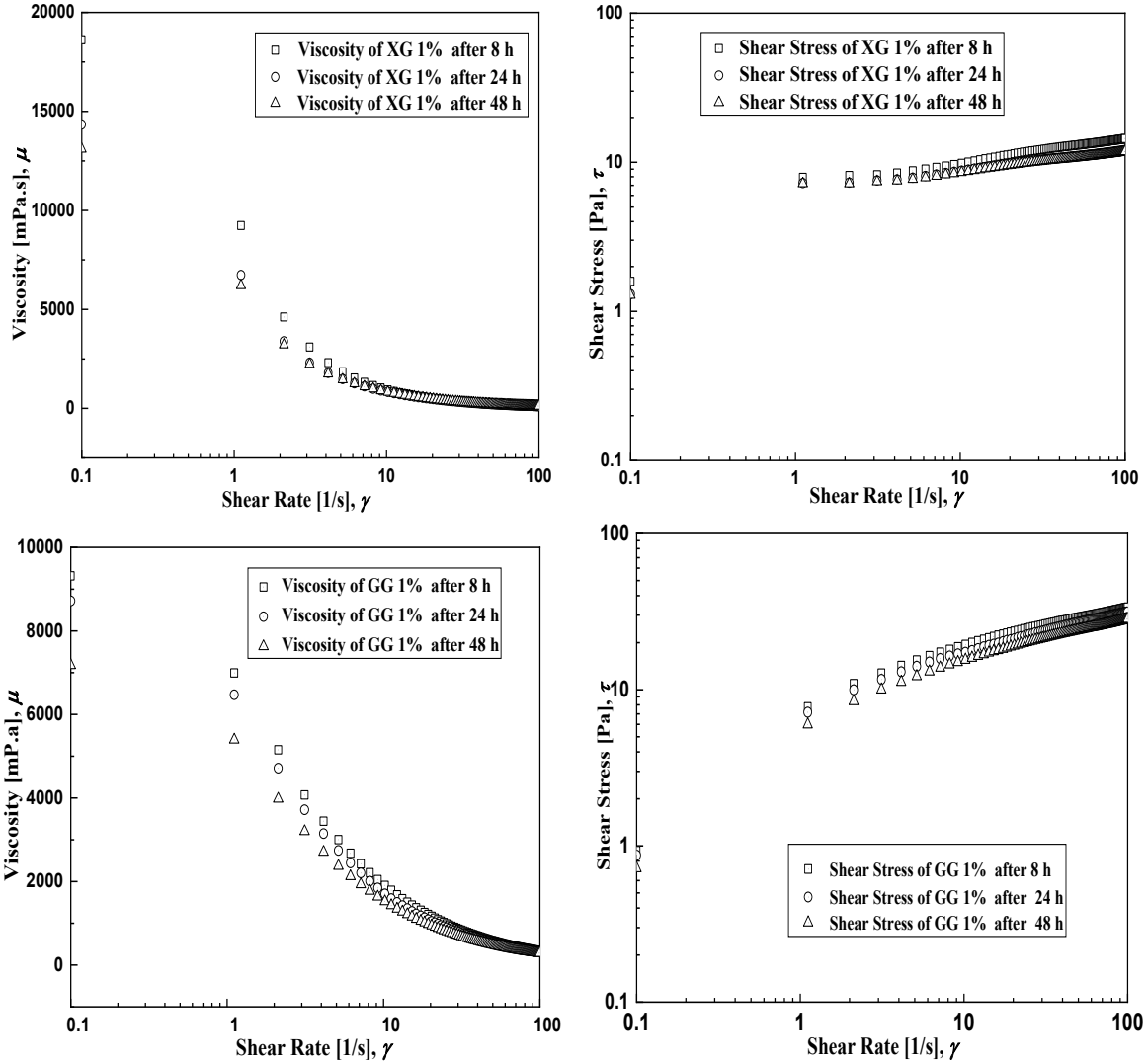

Figure 3-5. The effect of extra agitation on viscosity and yield stress the Xanthan and Guar solution.

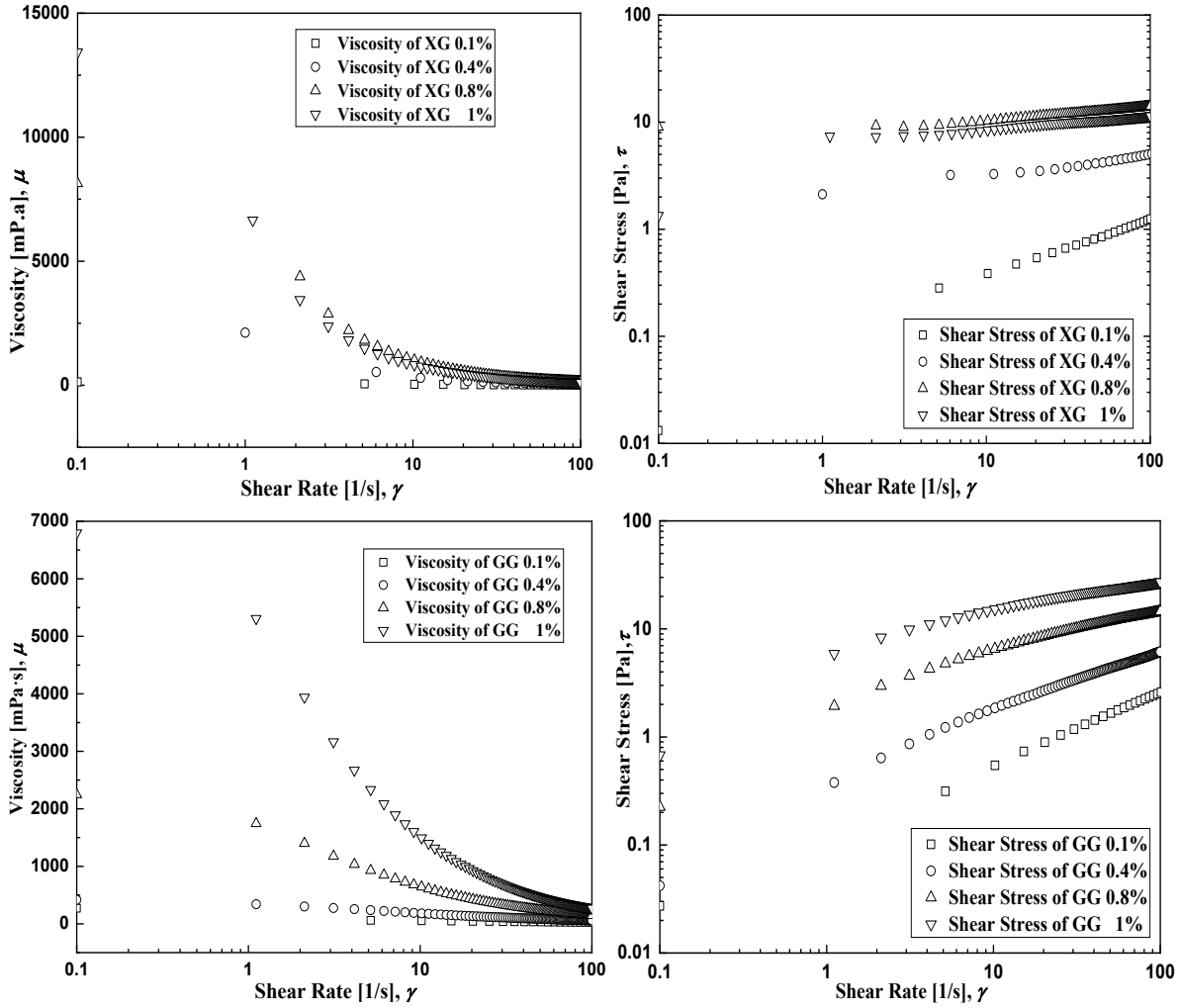

Figure 3-6. The viscosity and yield stress curves of the Xanthan and Guar solution.

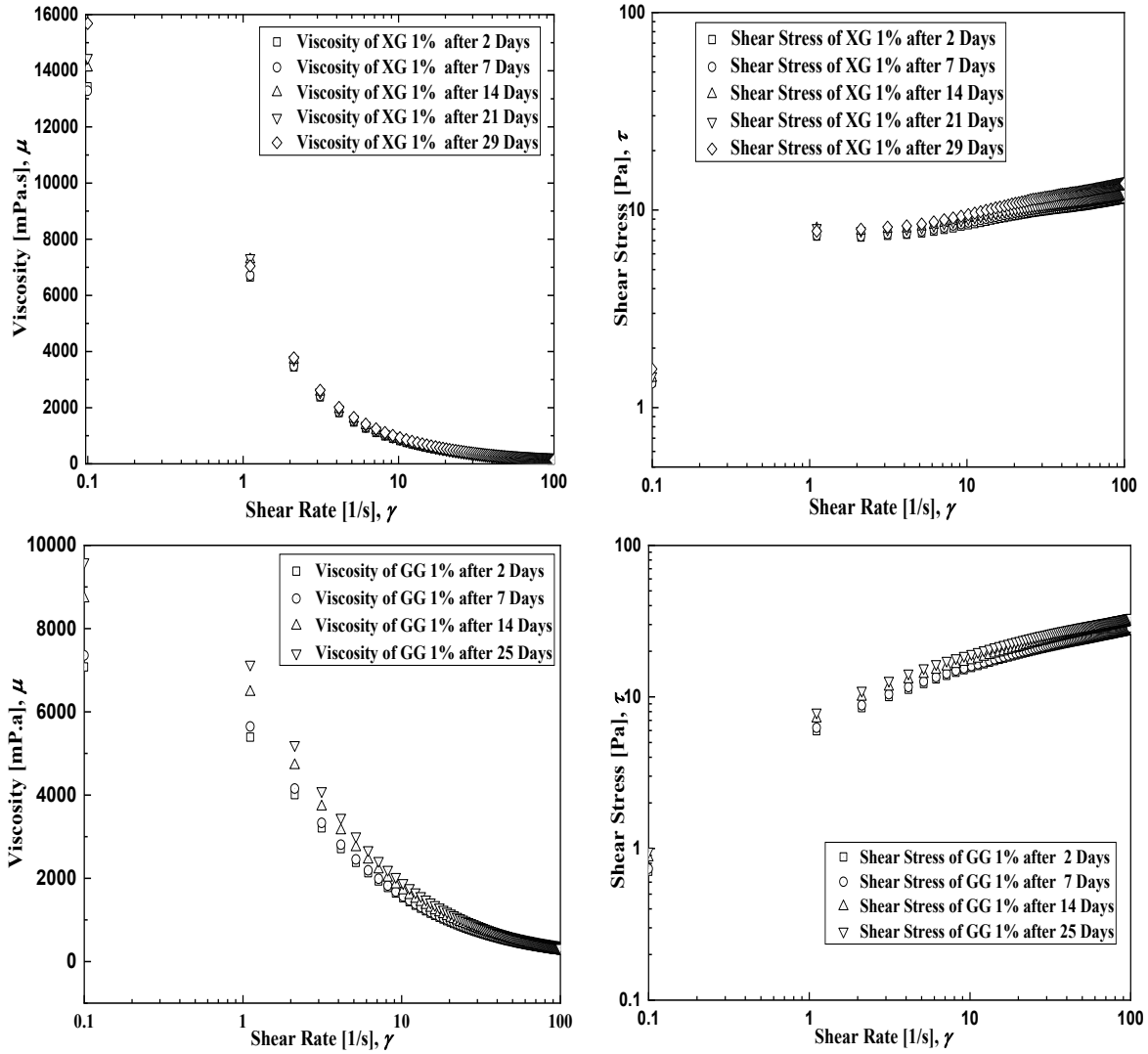

Figure 3-7. The effect of time storage on viscosity and yield stress for the Xanthan and Guar solutions.

3.3.4) Viscoelastic Frequency Sweep

Frequency sweep measurements were performed for all solutions, aiming to investigate the behavior of viscoelastic parameters, including storage "***G'***" and loss " ***G"*** " modulus. The storage modulus denotes the elastic effect of solutions "the rigidity degree" and the high capacity of the reversible energy stored in solutions. On the other hand, the loss modulus is associated with solutions viscous effect, and the irreversible energy dissipated by the fluid. The solution's viscoelasticity can be characterized by other parameters such as phase angle, which is the angle between the viscous and elastic deformation amplitude. The viscous effect on the fluid was considered dominant if the tangent phase angle is less than 1.

The results were consistent as expected, the solutions were categorized as structured fluids "weak gels" based on their viscoelastic parameters' behavior. At low-frequency load, the elastic effect "storage modulus" was dominant for XG solutions, whereas the viscous effect "loss modulus" was dominant at a higher frequency beyond 100 rad/s, as can be seen in Figure 4-8. These analyses indicated that the XG solutions at low strain load behave as gels. They also behaved like a liquid at high frequency. The cross-over regions were captured in all XG solutions, which occurred at a higher frequency load for higher concentrations. Figure 3-8 shows that both G' and G" are dependent on oscillatory frequency. Thus, at low frequency, the XG solutions show more rigidity than liquids. Whereas the viscous effect was dominant for all GG solutions over the entire frequency range, as illustrated in Figure 3-9. The plots depict that the GG solutions experienced higher flowability even at a low-frequency load, indicating that both loss and storage were dependent on frequency.

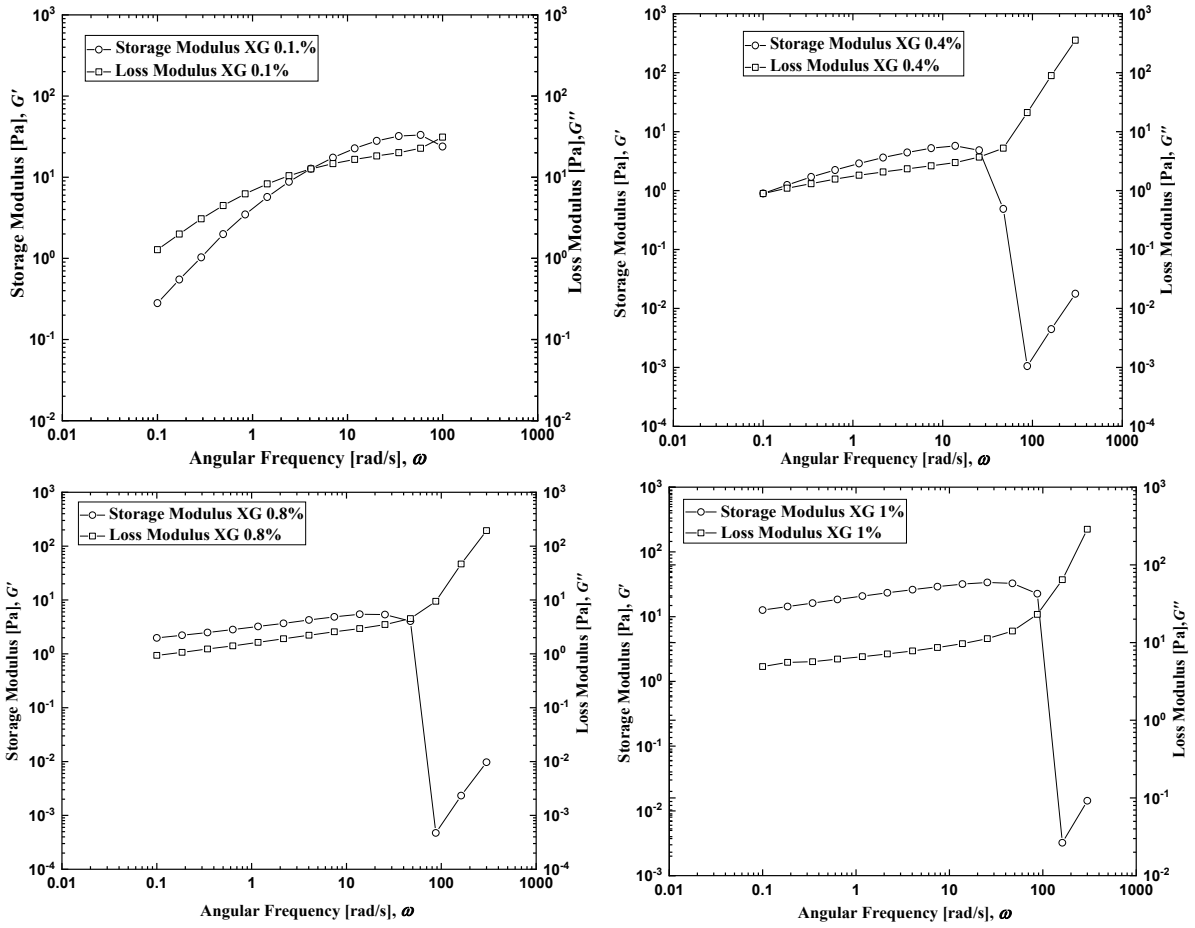

Figures 3-8. the Frequency dependence of G' and G" at different xanthan solution concentrations.

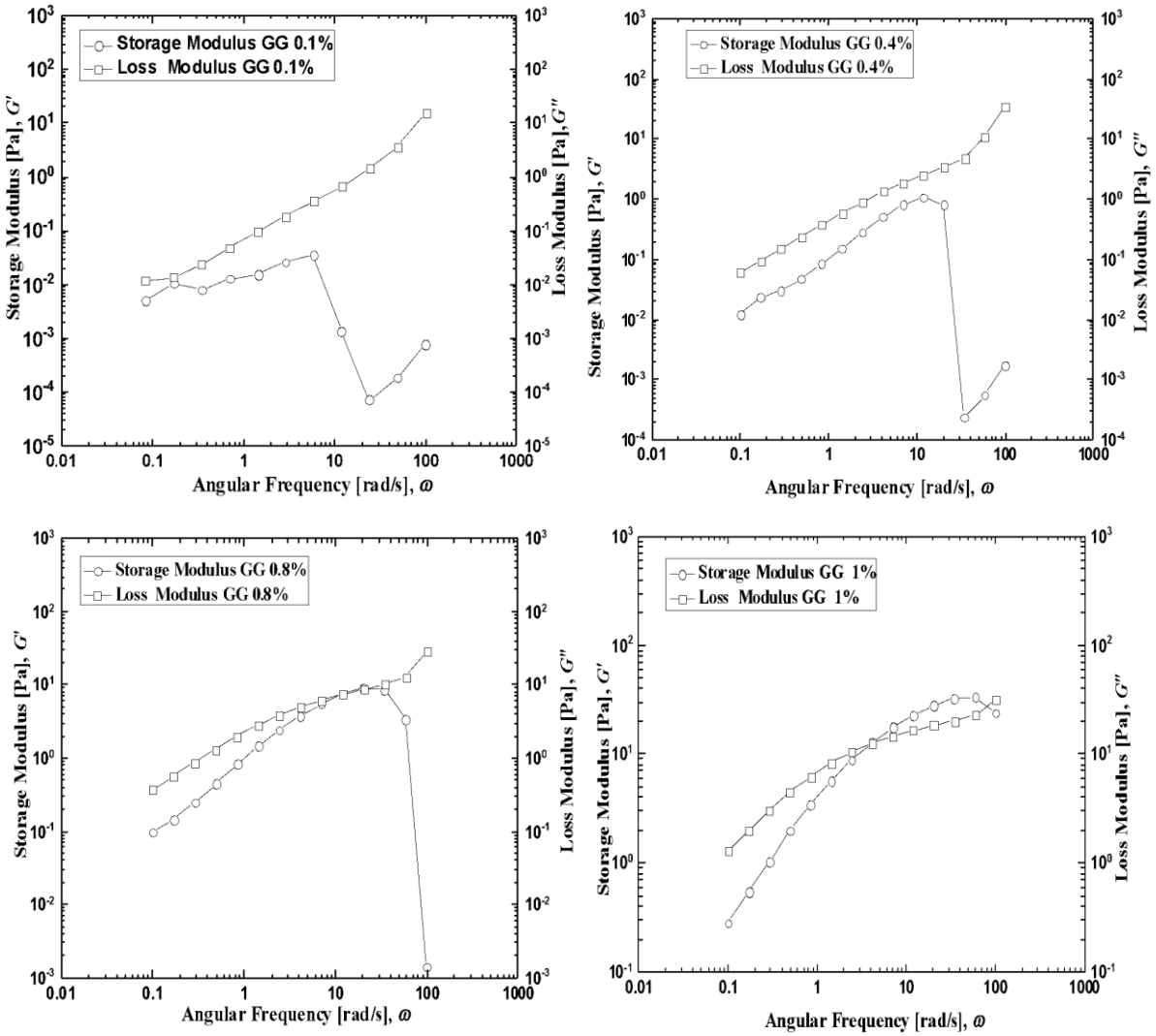

Figures 3-9. Dynamic response of G' and G" at different Guar solution concentrations.

3.3.5) Viscoelastic Complex Viscosity Tan delta and Phase Angle

The complex viscosity, phase angle, and tangent phase angle were measured to characterize the solutions' viscoelastic behavior. Higher energy efficiency and flowability were achieved by obtaining low storage modulus, high loss modulus, and high tangent phase angle for both solutions. The complex viscosity showed similar shear thinning behavior and matched the apparent viscosity for all concentrations which confirmed the Cox-Merz rule as can be seen in Figure 3-10. Additionally, the phase angle decreased at higher concentrations; hence the viscoelastic main trends were reported by characterizing tangent phase angles of both fluids, as shown in Figures 3- 11 and 3-12. At low frequency, the higher XG concentrations (0.8%wt and 1% wt) have

a tangent phase angle of less than 1 value, whereas the lower concentrations have more than unity of tangent phase angle, indicating that the elastic behavior of XG solutions was more pronounced as the concentration increased. Whereas all GG concentrations show tangent phase angle higher than 1 at low frequency, resulting in the viscous behavior being dominant over the entire frequency range, and we observe that there is no direct correlation between the concentrations and the elastic behavior in this study.

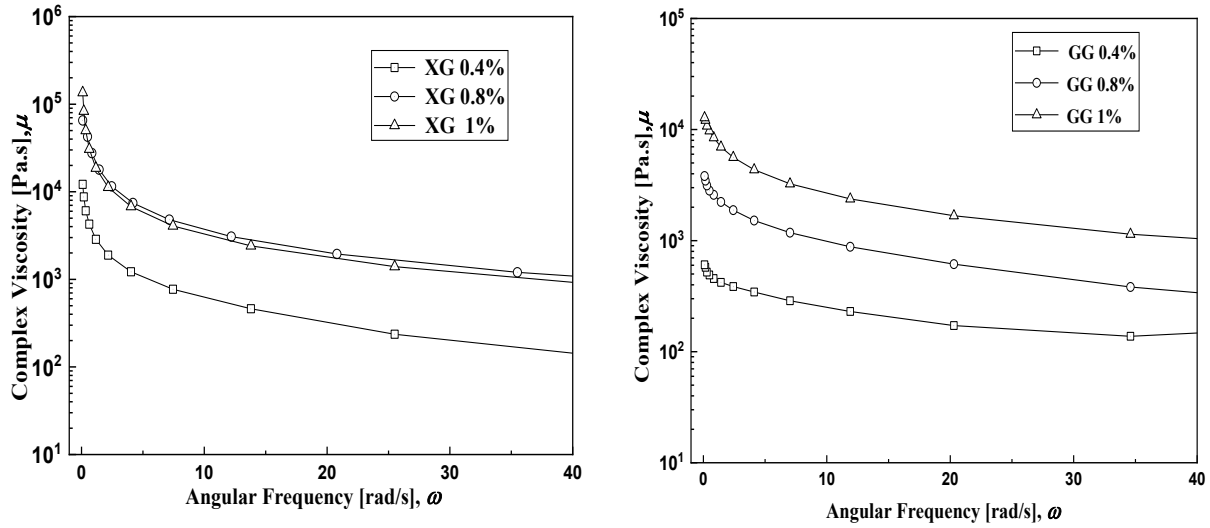

Figure 3-10. Frequency Sweep depicting the complex viscosity for Xanthan and Guar solutions at different concentrations

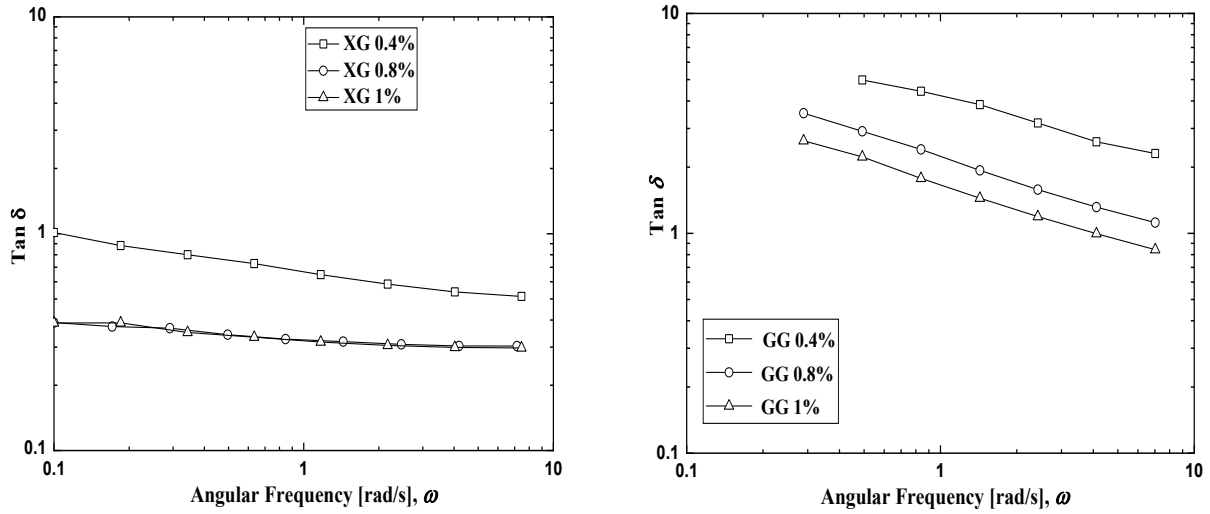

Figure 3-11. Frequency Sweep depicting the Tangent phase angle for Xanthan and Guar solutions at different concentrations

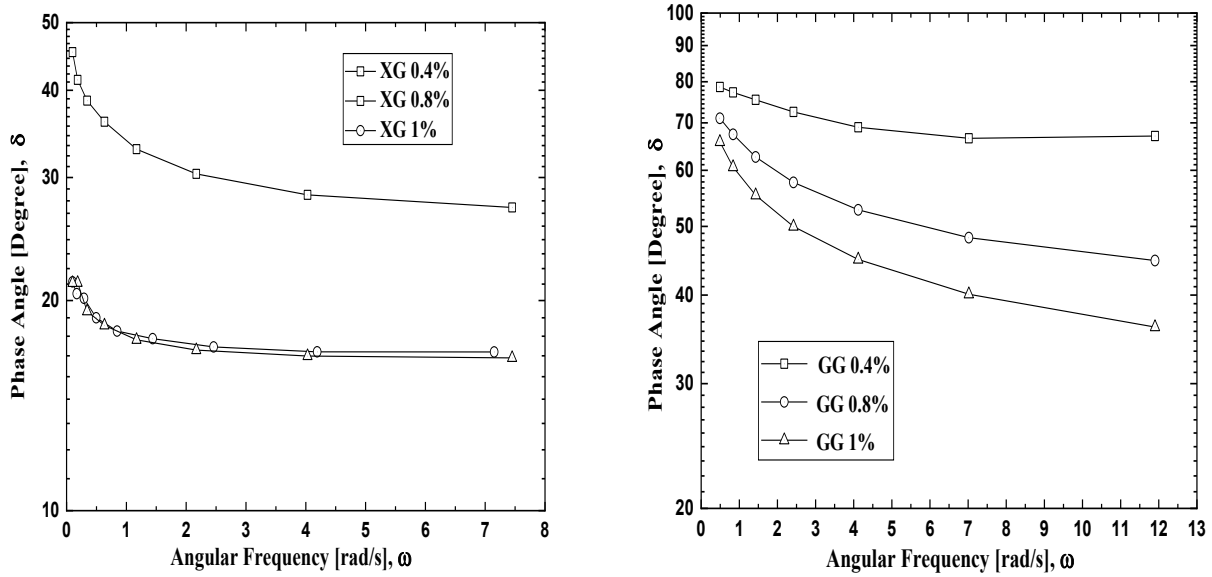

Figure 3-12. Frequency Sweep depicting the phase angle for Xanthan and Guar solutions at different concentrations

Conclusion:

Oscillatory rheology investigations were successfully performed for concentrated biopolymers XG and GG solutions with the following concentrations (0.1%wt, 0.4%wt, 0.8%wt and 1%wt). These solutions were prepared carefully to ensure they are homogenous and have uniform mixing prior to the rheology measurements. The flow curve measurements were carried out over a wide range of strain rates from 0.1 s^{-1} to 100 s^{-1} to characterize the viscosity behavior and to capture yield stress values. Furthermore, the effect of storage and the agitation time on the viscosity and yield stress was studied, and the measurements were conducted at the end of the day 7th of each week for up to 1 month of storage time. Whereas, the extra agitation time tests were performed by increasing the agitation time applied to the solutions as follows: (8 h, 24 h, and 48 h). An obvious correlation between the shear rate and the solutions concentration, viscosity, and yield stress was reported with noticing a strong shear thinning behavior for all solutions. The reason behind the pronounced shear thinning behavior at higher concentrations is attributed to the intermolecular hydrogen bonds that where are connected to the biopolymer's chains.

The viscosity reached higher values for higher concentrations, resulting in increased yield stress. It was noticed that the viscosity data point of both solutions collapsed into approximate same line over the one-month storage time by 22%, and a 36.5% difference in the low shear viscosity along this period for XG and GG solutions, respectively. In contrast, both viscosity curves and yield

stress points of the solutions decreased at high extra agitation loads by 29% for GG and 22% for XG solutions. The stress-strain rate plots agreed with the rheological models that describe the non-Newtonian fluids, indicating that the flow characteristics of both XG and GG solutions were well fitted by the Power Law "Ostwald" and Herschel–Bulkley models. Whereas the Bingham model failed in describing the flow curves of both XG and GG solutions.

Frequency sweep measurements were performed for all the XG and GG solutions at fixed strain amplitude (5%). The frequency load was applied decreasingly from high to a low level from "300 to 0.1 rad/s". The elastic effect was dominant for XG solutions at low frequency, whereas the viscous effect was dominant at a higher frequency. Compared GG to XG solutions, GG solutions exhibited a viscous behavior for all concentrations at low and high frequencies, resulting in higher flowability properties even at low frequencies.

At higher frequency, all solutions showed lower storage modulus and higher tangent phase angle, resulting in increasing the solutions' flowability and fluids energy efficiency. In addition, the apparent viscosity was consistent with the complex viscosity, which both exhibited a similar shear thinning manner and confirmed the Cox- Merz rule. In addition, all XG phase angles in this study showed an inverse correlation with the concentrations, hence the tangent phase angle dropped to less than one for higher XG concentrations (0.8%wt and 1%wt), confirming the elastic behavior was dominant for these concentrations at low frequency. However, the viscous behavior was dominant for all GG concentrations which achieved tangent phase angle values of more than one.

CHAPTER 4

The influence of concentrated shear-thinning guar and xanthan solutions on flow patterns in Taylor Couette flow

Abstract:

This experimental investigation aims to study the flow transition characteristics in the Taylor Couette system with fixed out cylinder and rotating inner cylinder, focusing on the flow regimes structure at the onset of the flow instabilities for non-Newtonian biopolymer fluids including guar gum (GG) and xanthan gum (XG) solutions. We characterize the flow structure due to the solutions' viscoelastic and yield stress behavior over a wide range of concentrations (1000 ppm, 4000 ppm, 8000 ppm, and 10000 ppm) for each fluid. The main goal of this study is also to observe the influence of the high viscosity shear thinning nature on the flow patterns for all solutions as well as to measure the vortices' key parameters associated with the flow patterns such as vortices' axial wavelength, and the number of vortices for concentrated XG and GG solutions in the Taylor Couette system at various Reynolds number range from 0 to 800.

The effect of shear thinning behavior on the flow structure, flow instabilities and critical Reynolds number (Re) was investigated by quantifying the flow indices for each solution concentration obtained from the rheology experiments as follows: (0.520, 0.220, 0.361 and 0.136 for XG solutions) and (0.661, 0.494, 0.350, and 0.263 for GG solutions). It was noticed that the critical Re_c values have an inverse correlation with the shear thinning flow indices, it altered the vortex flow back as the solution concentration increases over the captured flow regimes between the Taylor vortex flow (TVF) to the Modulated Wavy vortex flow (MWVF). In addition, two new non-axisymmetric flow regimes were observed, which were Spiral vortex flow (SVF) for high concentrations of (8000 ppm and 4000 ppm) and Coil vortex flow (CVF) for low concentrations of (1000 ppm and 8000 ppm). The effect of the flow indices on the axial wavelength and vortices number were identified for all non-Newtonian fluids. At the onset of the first and second instabilities, the axial wavelength experienced a significant increase with the critical Re_c The increase turned monotonically sharper as the solution concentration increased.

The number of vortices showed a significant drop between the secondary and tertiary flow instabilities, indicating the decrease was slight at the first transition and it was more pronounced as the vortex flow evolved. The maximum vortices numbers were highlighted as 30 and 22 vortices that were achieved for the concentrations of 4000 ppm at TVF of

the GG and XG, respectively. The effect of shear thinning on vortices aspect ratio was noticed and measured for all solutions. The vortices aspect ratios are influenced by the flow indices and the onset of the flow regime instability at TVF. It was also observed the vortices' aspect ratios varied at each concentration, however, the vortices at both ends of the setup chamber elongated with a larger size than the vortices in the middle of the chamber.

4.1) Introduction

4.1.1) Historical Background

The circular motion of fluid between two or one rotating coaxial cylinders was discovered and investigated by Geoffrey I. Taylor in 1923 [30]. In the past decades, Maurice Couette [30] was the first scientist who performed his experiments by using a similar experimental setup, called a viscometer, depending on the rotation of the outer cylinder. The early days of this flow type referred back to the most influential pioneers and scientists in this field such as Newton, Stoke, Margules, Mallock, Couette, Taylor, and Chandrasekhar [30], [32], [33]. They discovered the basic concepts and manifestations of the flow regimes' behavior in the system known as the Taylor Couette system [30]. One of the reasons that make the Taylor Couette system suitable for conducting research in the fluid mechanics field, is the obtained flow patterns and transitions that occurred due to the variation of the angular velocity. One primary problem of the flow complex behavior associated with the flow instabilities is the difficulty to characterize and explain them in the early days of investigations. To simplify the matter, it is difficult to find the exact solution of the Navier-Stock equation for Taylor-Couette flow instances. To bridge the gap, researchers were conducting experiments and then confirm the results with the theoretical and numerical solutions. This method was much easier to construct [30], [32], [33].

Numerous existing studies in the broader literature have focused on the flow regimes behavior in the Taylor Couette system, starting with the study investigated by Newton [30]. Along with Newton's experiments, George Stokes [31] investigated the fluid velocity profile in the TC system. The main findings were the motion of the inner cylinder produced less stability of the flow; thus, eddies appeared as a result of the motion of fluid outward the inner cylinder by the centrifugal force. In 1881, the famous instrumentalist Margules [32] proposed the initial design scheme of the viscometer. Then, a few years after that it was constructed by Mallock & Couette [33], and they both carried out the first viscometer experiment. Hence, Mallock [34] reported a nonlinear correlation between the angular velocity and the torque. Subsequently, the flow, in this case, was

unstable when the velocity exceeds the critical speed. As a result of this instability, new vortices were formed, which are called Taylor Vortices [34]. Mallock's [34] experimental work was investigated by Kelvin [35] who was obsessed with the concept of flow stability. The flow stability has been studied by Rayleigh who was the first scientist concentrated his effort to explain the flow stability. He demonstrated that a stable flow is achieved when the outer cylinder rotates, and unstable flow is more pronounced as the inner cylinder rotates [36]. Eight years after Margules' proposal of constructing a viscometer, Couette finished his first experiment in viscometer and he highlighted that two types of fluids can be tested in this system including, Newtonian and non-Newtonian fluids [37]. The previous experimental findings make research on the TC system almost inactive until the linear stability of diluted viscous flow has been studied by Taylor [39]. A few years later, Chandrasekhar [30] published his book about hydrodynamic stability, focusing on different experimental and theoretical aspects of Taylor-Couette flow.

4.1.2) Flow visualization and mapping:

Most early studies and the current investigations in the modern era have been full of attempts to achieve a valuable contribution and well understanding of the Taylor-Couette flow, especially in the onset of instability where the turbulence, chaos, and bifurcations appear. Studying the flow behavior beyond the stability stage is unpredictable and not easy to observe. To fill this gap, by using visualization techniques through modern ways and devices, enabling researchers to observe the flow patterns and regimes. For an instant, Taylor [30] & [36]. utilized ink in his experiments to visualize the flow patterns by injecting ink into the system. According to Liao et al. [41], Taylor-Couette flow has significant flow pattern types, including both spatial and temporal flows that were captured by using the same flow visualization technique used by Taylor. What makes the Taylor-Couette flow practical system is the noticeable transition of flow regimes between laminar and turbulence. This behavior is due to the non-linear flow patterns which appear at the onset of flow instabilities [42]. The instabilities occur when the massive inertia force overcomes the viscous force by maximizing the Reynolds number. Accordingly, the flow instabilities in Taylor-Couette flow appear as toroidal vortices form, which is called Taylor vortices. These vortices are influenced by main dimensionless parameters such as Taylor number (Ta) "denoted to the characterization of the balance between the centrifugal force due to fluid rotation to the viscous force in Taylor-Couette system" and higher Reynolds number (Re). The formula of Re for Taylor Couette flow is shown in the equation below:

$$Re = \frac{\Omega\, r_i\, (r_o - r_i)}{\nu} \qquad [1]$$

where ρ is the fluid density, μ is the viscosity, is the rotational speed of the inner cylinder, R_i is the inner cylinder radius, and $d = r_o - r_i$ is the gap between the cylinders. The Taylor-Couette system can be geometrically characterized by the radius ratio, $\eta = \frac{r_i}{r_o}$ where r_o is the outer cylinder radius, and the aspect ratio, $\Gamma = \frac{d}{L}$, where L is the length of the cylinder axis.

Earlier at the beginning of the twentieth century, the standard of instabilities has created for the first time as well, which relied on cylinder angular speed, causing a donut shape of vortices around the inner cylinder [39]. Starting with, Jeng and Zhu [52] stated the correlation between the volume friction factor and vortices, when the friction factor grows the vortices are compressed toward the inner cylinder. Then, Prima and Swinney [53] studied analytically the behavior of both Taylor vortices and wavy Taylor vortices. Later, Prima et al. [54] established a correlation between torque and Taylor vortices in laminar flow as a function of radius ratio and Taylor number. Murai et al. [55] performed a numerical study of flow characterization of Newtonian solutions, emphasizing vortex regimes in the TC system over a wide range of Reynolds Number (600 < Re < 4500); they identified five flow regimes, starting at Re < 92 where the flow was laminar, forming Circular Couette flow CCF. As Re increases (92< Re < 138) Taylor Vortex Flow TVF appears, whereas when the critical Re was exceeded, the flow is then known as Wavy Taylor Vortex Flow WTVF at Re values of (138 < Re < 1020). In transition flow a Modulated Wavy Vortex Flow MWVF (1020 < Re < 1380) was observed.

In addition to the previous numerical and experimental findings, many researchers have focused on the explanation of the flow instability behavior such as Peng & Zhu [56], and Landry et al. [57] who utilized Bingham fluids to study the linear stability of Taylor-Couette flow. Stuart [100] analytically studied the energy transfer in TC flow. Coles [47] investigated both axial and azimuthal wavenumber of the onset of turbulent flow, while Snyder [58] implied that the wavenumber was influenced by the flow initial condition. Furthermore, a spectral analysis to study the onset of chaotic regimes in the Taylor-Couette flow was done by Gollub & Swinney [101]. At a high Taylor number, obvious evidence of G¨ortler vortices and Taylor vortices was reported at the onset of TC turbulent flow by Barcilon et al. [59]. Koschmieder [60] utilized two different radius ratios to study the variation of the wavelength of Taylor vortex flow (TVF),. On the other side, Mullin [61] and Benjamin [102] demonstrated that the flow stability can be influenced by the

length of the cylinders. Also, a large number of vortices were observed as increasing a TC aspect ratio, with a monotonic increase in vortices number.

As far as we know, the previous studies utilized Newtonian solutions as working fluids in the TC system. However, limited experimental work in the literature focused on the effect of concentrated shear thinning fluids on the transition regimes in the TC system [103]&[104]. Also, the effect of the flow stability and instabilities due to shear thinning fluids was investigated in the TC system by many researchers, including Lockett et al. [105] . They used the finite element method to study the effect of diluted non-Newtonian solutions such as XG on the critical Reynolds number and axial wavelength which both were influenced by the onset of the flow instability. Then, the drift of vortices in the axial position was noticed as a result of the non-Newtonian effect of XG solution by Escudier et al. [106]. Different diluted polymers were used as shear thinning additives to investigate the flow instabilities and regimes by Yi & Kim [107]. They implied the flow regimes and transitions were similar to the regimes observed in the case of using Newtonian solutions in the TC system.

In the last decade, many authors have driven experimental studies with extreme dependence on the rheology findings by linking the rheology characteristics such as the flow index obtained from the rheology power-law models' analysis with the flow regimes characterizations [108]&[109]. In 2006, Caton et al. [108] study depended on the correlation between the flow index to flow regime characteristics, wavelength, and the transitions. They observed that there was a slight drift in the onset of the instabilities, also the vortices transition was non-symmetric. In 2012 the variation in wavelength due to the non-Newtonian effect was demonstrated by Alibenyahia et al. [51] by studying different flow indices of XG solutions. Three years later, Bahrani et al. [110]conducted a similar experimental study, and they concluded that there was a significant increase in vortices wavelength due to increasing the shear thinning effect (at a low flow index). Therefore, they observed the onset of the instability regimes and the critical Reynolds number were altered due to the pseudoplastic nature. The previous results have been confirmed by Cogney & Balabani [111] who noticed the same trends in increasing the wavelength, resulting in compressing the vortices size. Majji et al . [112] investigated the influence of particles size on the TC flow regimes. They observed at a laminar flow, there was the formation of new vortex flow formed at the top and the bottom of the TC system between the onset of CCF to TVF transition such as Spiral Vortex flow (SVF) and Ribbons (RIB).

Numerous research attempts are continuing to investigate the influence of the flow index on flow regimes, critical Reynolds number, and vortices wavelength in the TC system. In 2020, Huseyin & Bulent [49] conducted an experimental study focused on the influence of the low XG concentration shear thinning solutions on critical Reynolds number and wavelength. Their results confirmed the previous studies that concluded the wavelength depended on the flow index and the critical Re; additionally, the vortices drifted towards the axial direction as the flow index decreased.

Recently, wide range of engineering applications depend on the concept of Taylor-Couette flow, including science, engineering, industrial, and fluid processes applications. The TC system employs massive the experts' attention in the oil field to enhance the viscoelasticity properties of the Non-Newtonian fluids that are used as drilling muds and to improve the friction reduction ability of drilling muds by selecting viscous Drag Reduction Agents (DRA) to reduce the pumping power required to pump fluids [63]. Also, they contribute to the transport of sediments outside drilling holes, by using relatively viscous muds. Thus, the Taylor Couette system is a proper prototype to conduct experiments similar to the borehole wall and rotating string on a laboratory scale by considering the borehole wall as the outer cylinder and the rotating string as the inner cylinder [62]. Additionally, the TC system is also observed in various types of engineering applications, including journal bearing lubrication, cooling of rotating machinery among others, and purification of industrial wastewater [52]. Furthermore, the TC system is used in filtration processes in many fields for different purposes. Also, it is used in separation systems such as sperate plasma from blood, and reactors for the purpose of water purification and animal cell [45].

Case Study

The current experimental investigation focuses on observations of the flow regimes mapping in the Taylor- Couette system that have a variety of applications in the oil drilling field. As discussed in the previous studies in the literature, massive need to conduct experiments in the TC system including characterizing the flow regimes behavior of concentrated shear thinning fluids. The GG and XG solutions have been characterized by performing rheology investigation to study their yield stress points and viscoelastic behavior. More importantly, the prior study addressed several questions on the effect of concentrated (high viscous) shear thinning fluids on flow regimes, critical Reynolds number, and vortices axial wavelength, which are still unclear, especially beyond the onset of the primary instability within the vortex flow range from CCF to MWVF. This study

aims to bridge this gap by characterizing experimentally the flow regimes mapping and utilizing flow visualization techniques to examine wide solution concentrations ranging from 1000 ppm to 10000 ppm. A closer look at the literature on the current experiments, however, reveals some gaps and shortcomings in terms of the lack of studying the flow behavior of concentrated non-Newtonian fluids in the TC system. Thus, the main objective of the present thesis is to carry out experimental work with a strong emphasis on flow patterns and vortices analysis behavior in the Taylor Couette system. Furthermore, observing and analyzing the flow mapping for high viscous fluid as well.

4.2) Experimental Setup and Procedure

4.2.1) Taylor-Couette Chamber

The Taylor Couette system consists of the main chamber which is the most vital part of the system. It contains two concentric cylinders, outer and inner cylinders, which are covered by base plates on the top and bottom sides. The cylinders are hollow and made from transparent cast acrylic plastic to provide better flow visualization inside the chamber. The inner diameter of the inner cylinder is 10.16 cm, and the outer diameter is 14.06 cm. Also, the height of the inner cylinder is 28.03 cm. The cast acrylic was selected due to its transparency properties and its high tensile strength, which can bear up to 7.75 x 107 N/m^2. A hollow inner cylinder was designed to reduce the required torque that rotates the inner cylinder. The reason behind this is to make sure the system is still operating even at low torque. There were two acrylic base plates were covered on both ends of the inner cylinder with 1-inches thickness.

The inner diameter of the outer cylinder is 15.875 cm, and the outer diameter is 17.78 cm with a height of 28.08 cm. The outer cylinder was covered by two cast acrylic bases with 1-inches thickness. Also, an adhesive seal was used to fix the cover plate on the inner cylinder, also a Buna N O-ring (Dash no. 215) and stainless-steel shaft collar were used to seal the plates and hold the shaft. The shaft diameter was reduced to 1.27 cm at the end to connect with the motor shaft by using a shaft coupling. The detailed assembly of the inner cylinder is shown in Figure 1.

A grooving was provided on both the plates to hold the bearing and seal. A double-sealed stainless-steel bearing (BocoBearing) with a ceramic ball material was used. Also, a graphite-reinforced PTFE seal (provided by McMaster Carr), was selected due to a lower coefficient of friction and good wear resistance. An o-ring was placed in the grooving of both the top and base plates to seal the TC chamber. Six threaded tie rods were placed to provide force support to the

chamber, and the base plate was connected to a machine table using bolts and nuts. The complete assembly of the TC chamber is shown in Figure 4-1.

4.2.2) Bio-Polymers fluids and Flow visualization Procedure:

Both GG and XG powders used in this study were produced by miniScience Inc**.** in the United States with unique specifications and hydrocolloid rheological properties. They have a white powder appearance, with a shear-thinning non-Newtonian nature due to their ability to dissolve easily in both cold and hot water. Their viscosity ranges from 1.0 to 1.5 Pa.s at rest conditions for 10000 ppm solution concentration, allowing them to prepare viscous non-Newtonian solutions similar to drilling fluids. Also, they have a consistent gelling ability as well as a high pseudoplastic behavior that makes them compatible with the applications that require stabled viscosity agents.

To visualize our non-Newtonian concentrated solutions flow regimes, a special type of rheoscopic flow visualization flakes was utilized. It contains tiny stearic acid particles with dimensions ranging from 5 to 50 μm and their thickness is 0.3 μm. These tiny reflective particles align with the flow direction and reflect the light due to their anisotropy, resulting in clear flow qualitative characterization by the direction of the reflective light from the aligned flakes. The rheoscopic fluid exhibited a Newtonian behavior similar to water. Thus, the viscosity of our non- Newtonian fluids is not going to be affected as reported by. Borrero-Echeverry et al.[113]

4.2.3) Image processing techniques

In addition, a high-speed camera is used to record the experiments with frames per second of 20 fps. All frames have equal pixels size of 2048 x 1024. Also, the flow visualization experiment depends on a sufficient illumination source. The experiment was performed in quite dark rooms to eliminate light stray. The illumination comes from two directions in front of the setup to get better vision and remove the shade. We recorded each flow for about 40 seconds after we make sure it reached to vortex stable condition.

We used the image processing method to capture the variations of flow regimes for all concentrations that can be observed in the space-time plots in Figures 5- 3 to 5-9. We depended in our procedure on line scan camera image processing, by selecting the mid column of pixels that is located right the mid image of each frame. The program extracts the column of pixels from each frame and moves to the followed frame. It attached all columns beside each other as a stitched image for each run, each image contains 800 columns.

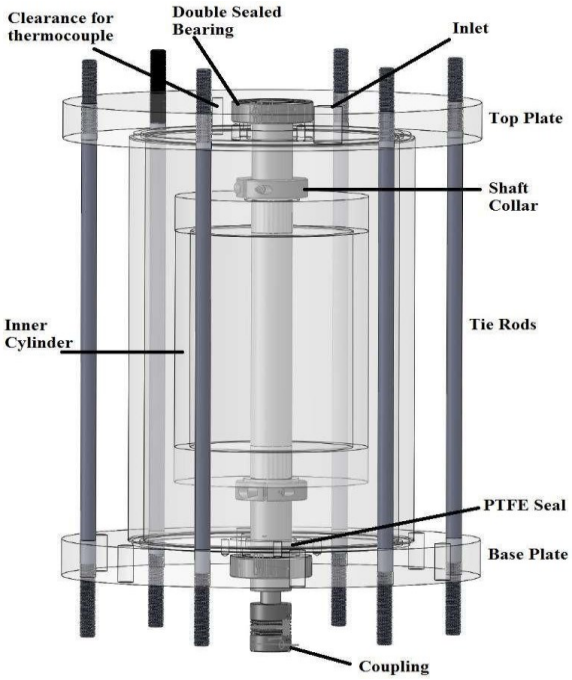

Figure 4-1. Complete assembly of TC Chamber adapted from [65].

The Taylor-Couette flow instability between coaxial cylinders occurs in the transition from laminar to turbulent regimes as the only inner cylinder rotates, creating massive inertia force required to overcome the viscous force that is reflected in higher Reynolds number. Accordingly, the flow instabilities in Taylor-Couette flow appear as toroidal vortices form, Taylor vortices (TVF). These vortices are influenced by main parameters such as fluids viscosity and Reynolds number (Re). The Reynolds number can be represented by the followed equation below:

$$Re = \frac{\Omega\, r_i\, (r_o - r_i)}{v} \qquad [1]$$

where ρ is the fluid density, μ is the viscosity, is the rotational speed of the inner cylinder, R_i is the inner cylinder radius, and $d = r_o - r_i$ is the gap between the cylinders. The Taylor-Couette system can be geometrically characterized by the radius ratio, $\eta = \frac{r_i}{r_o}$ where r_o is outer cylinder radius, and the aspect ratio, $\Gamma = \frac{d}{L}$, where L is the length of the cylinder.

Since we used non-Newtonian viscous fluids that exhibit shear thinning nature, when the viscosity of these fluids depends on the shear rate load; it changes its behavior as the shear rate evolves. Thus, to quantify the Re values for the shear thinning fluids, different definitions of Re have been used in the literature[49]–[51]. We define the Re values in our study based on viscosity values observed at the average nominal shear rate value as

$$\gamma = \frac{\Omega\, r_i}{d} \qquad [2]$$

Table 4-1. Summary of the flow instabilities regimes for all solutions.

Solutions	Concentration	First Re_{C1}	Second Re_{C2}	Third Re_{C3}
Xanthan Gum	1000 ppm	194.80	-	246.80
	4000 ppm	38.45	57.70	134.60
	8000 ppm	36.70	48.40	54.70
	1000 ppm	33.4	42.80	82.80
Guar Gum	1000 ppm	200.7	-	264.80
	4000 ppm	49.30	54.70	69.90
	8000 ppm	64.80	94.90	116.20
	1000 ppm	43.30	48.70	56.30

4.3) Result and Discussion

4.3.1) Flow Regimes Snapshots:

The flow regime patterns occur when the inner cylinder rotation exceeds the critical Reynolds number, as a result of flow instabilities formations. Three different instabilities (Primary, secondary and tertiary) were reported in this study at the flow regimes of the TVF, WVF, and MWVF as can be seen in the snapshots and the space-time plots in Figures 4-2 to 4-8. The cylindrical Couette flow (CCF) was observed at a minimum rotation speed (90 to 95 rpm) in the laminar flow for the XG solutions. Then the first critical speed and Reynolds number were achieved at the onset of the first instability where the Taylor vortices appeared and known as the Taylor Vortex Flow (TVF) at Re_{c1} = 195 for the XG 1000 ppm. As shown in Table 4-1, the critical Reynolds numbers for the XG concentrations were observed earlier at higher concentrations. Therefore, the onset of the first and second instabilities was observed and occurred earlier for the high solution concentrations at Re_{c1} = 38, 36, 33 for the XG concentrations 4000 ppm, 8000 ppm, and 10000 ppm, respectively. This drift in the critical Reynolds number is attributed due to the obvious increase in the solutions' viscosity, and the changes in the balance between the centrifugal force and viscous variation at each solution.

The flow started progressively evolving from CCF to TVF at the bottom of the chamber where the Ekman vortices occurred. This development also happened due to the change in balancing of the viscous and centrifugal forces. It was noticed that the TVF contains pairs of counter-rotating vortices along the axial direction. The secondary instability occurred when the TVF developed into wavy flow patterns as illustrated in Figures 4-2 to 4-8. This waviness affected the stability and magnitude of the TVF, resulting in noticeable variation in the axial wavelength through axisymmetric wavy patterns. This flow regime is known as Wavy Vortex Flow (WVF), and it was captured in concentrations of 4000 ppm, 8000 ppm and 10000 ppm XG solutions, at the corresponding secondary critical Re_{c2} = 58, 48.5, and 43. Whereas the WVF was skipped and not observed over the entire Reynolds number range Re = 100 – 650 for the 1000 ppm concentration of both XG and GG.

The tertiary instability "bifurcation" occurred at Re_{c3} = 246 for 1000 ppm XG solution where the amplitude of the vortices evolved to a non-axisymmetric periodic waviness which is known as Modulated Wavy Vortex Flow (MWVF). The vortices' wavelength, frequency and amplitude were time-dependent, it periodically changed for all XG and GG concentrations. Then, when the speed increased the periodic regime became more complex, showing a progressively strong MWVF regime. The vortices at this regime have a higher wavelength than the secondary instabilities at Re_{c3} = 64, 54, and 66 for the followed XG concentrations.

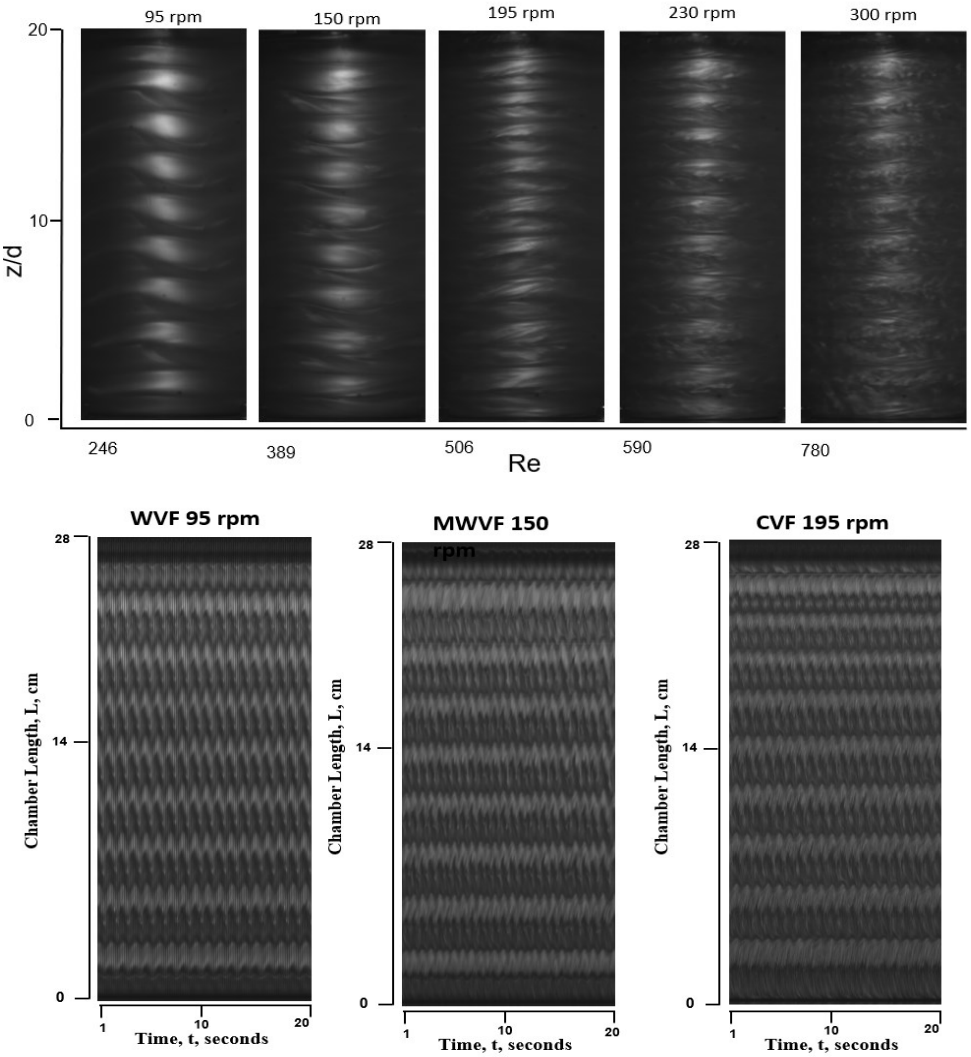

Figure 4-2. a) Recorded picture of the flow regimes for xanthan gum 1000 ppm solution vs Re. b) Spatio-temporal plots at the narrow gap for the 1000 ppm xanthan gum solution.

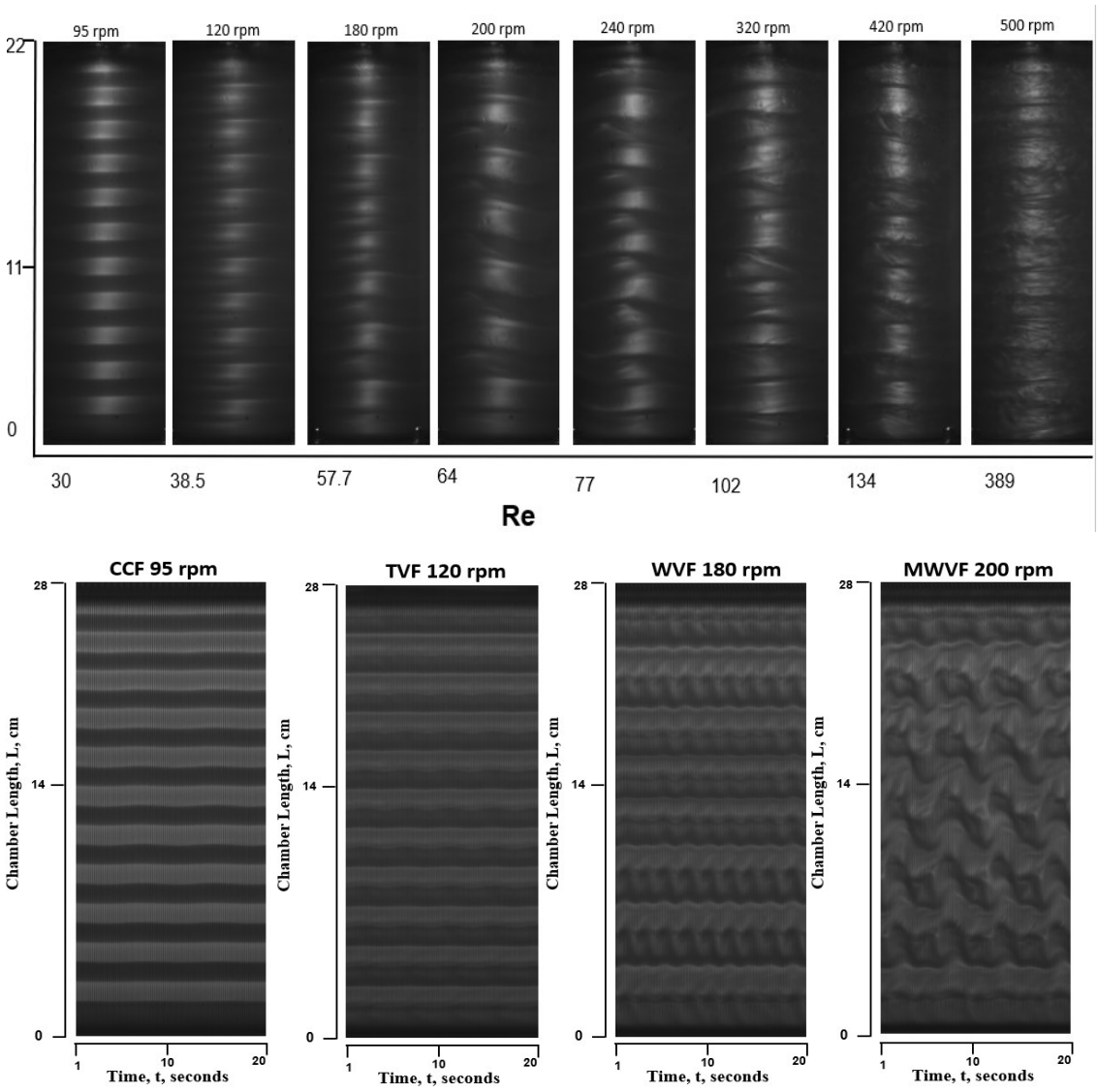

Figure 4-3. a) Recorded picture of the flow regimes for xanthan 4000 ppm solution vs Re. b) Spatio-temporal plots at the narrow gap for the 4000 ppm xanthan solution.

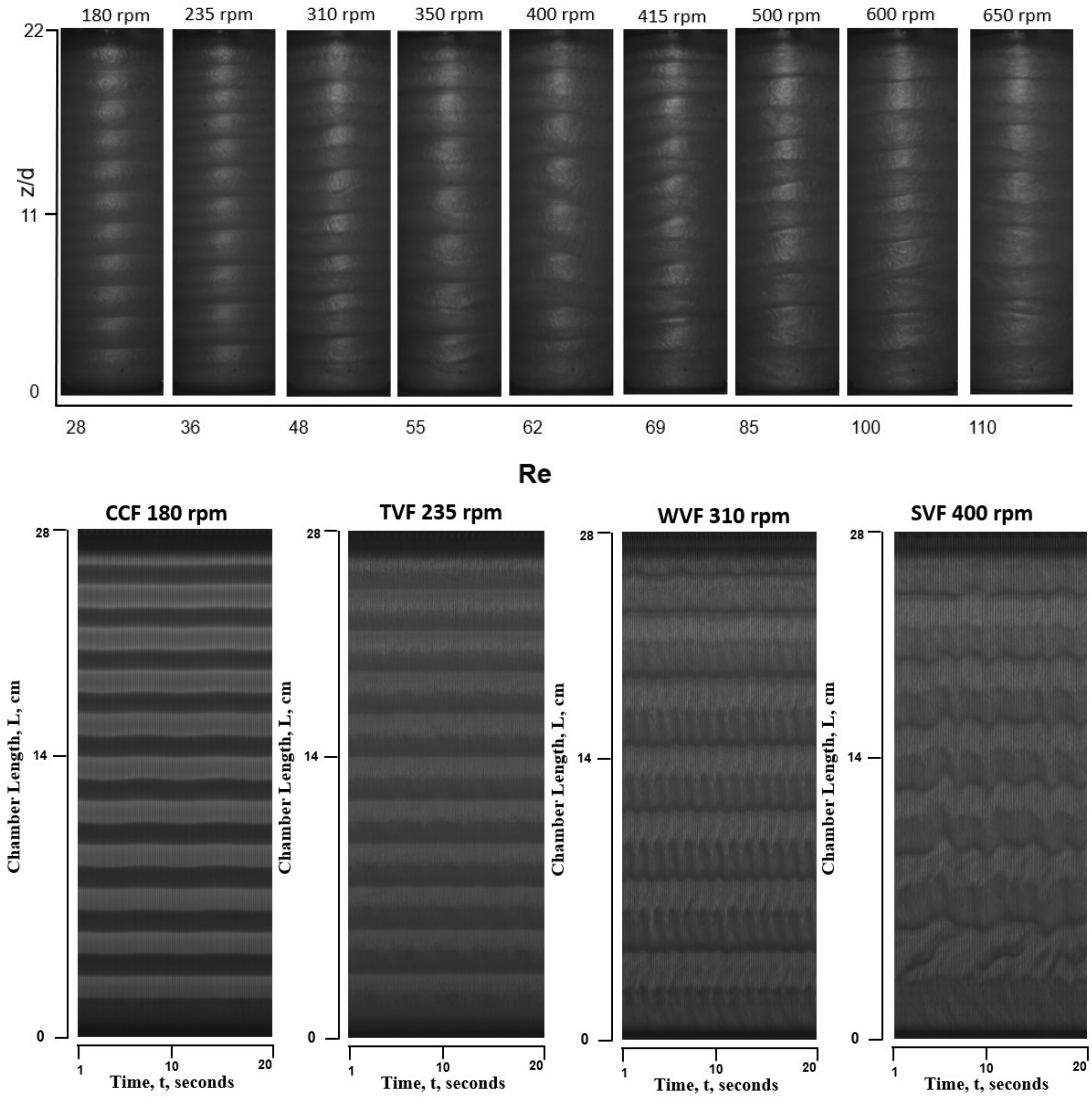

Figure 4-4. a) Recorded picture of the flow regimes for xanthan gum 8000 ppm solution vs Re. b) Spatio-temporal plots at the narrow gap for the 8000 ppm xanthan gum solution.

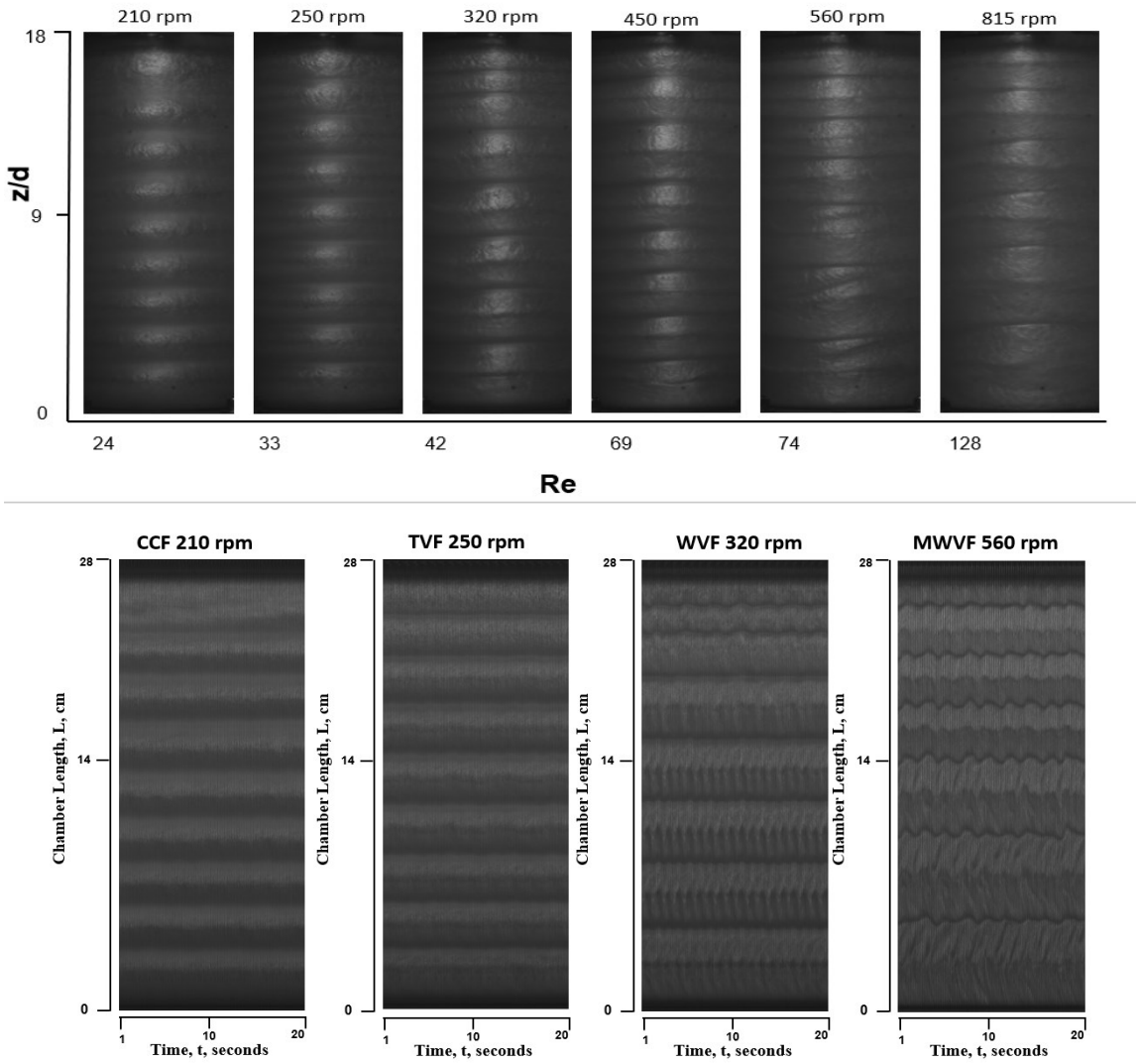

Figure 4-5. a) Recorded picture of the flow regimes for xanthan gum 10000 ppm solution vs Re. b) Spatio-temporal plots at the narrow gap for the 10000 ppm xanthan gum solution.

For the GG solutions, the flow regimes behavior was observed quite similar to the XG solutions. Thus, the first instabilities of the TVF occurred at $Re_{c1} = 200, 49, 64,$ and 43 for the concentrations 1000 ppm, 4000 ppm, 8000 ppm, and 10000 ppm. Whereas the secondary instabilities at the onset of WVF were captured at $Re_{c2} = 54, 94, 49$ for the concentrations between 4000 ppm to 10000 ppm with no observation of the WVF for the GG 1000 ppm. Unlike the critical Reynolds numbers behavior at all XG flow regimes the which depicted an obvious decreasing Re_c pattern, the Re_c for GG solutions experienced the same drop in Re_c, but it is not monotonic with experiencing a slight increase at GG 8000 ppm concentration flow regimes which we are going to discuss that in Figures 4- 13 and 4-14.

The variations of flow regimes for all concentrations can be observed in the space-time plots in Figures 4- 3 to 4-9. These plots were prepared by using line scan camera image processing, by focusing on extracting the mid columns of pixels with the size from each frame, and this process will be applied to all frames at each flow regime. The program extracts one column from each frame and then attached them beside each other as a stitched image for each run, each image contains 800 columns. The space-time plots showed all detailed flow regimes to illustrate a clear vision of the flow structure starting from Cylindrical Couette Flow (CCF) to Modulated Wavy Vortex Flow (MWVF). According to Figures 4- 2 to 4-9, the number of vortices experienced a significant drop as the flow evolved along with each instability. There are 20 vortices counted for the XG 1000 ppm at the onset of the primary instability before it dropped to 18 vortices at the onset of the followed flow regimes from WVF to MWVF. As a result of this reduction in vortices count, the vortices at the top and bottom merged with neighboring vortices, creating a noticeable increase in vortices' axial wavelength which will be discussed in the following sections.

For XG and GG solutions, the common merging vortex flow characteristics occurred at the cylinder's both ends, where the vortices at the top and bottom were larger than the vortices in the middle of the chamber. This merging can be noticed obviously at the onset of the WVF and beyond. The switch from the vortices' high frequency and low amplitude to the low frequency and high amplitude occurred at 4000 ppm of XG and GG solutions. Furthermore, we observed a non-axisymmetric vortex disordered flow characteristic at the upper part of the setup rather than the lower part for 4000 ppm XG solution at the onset of WVF. This is attributed to the end effect and viscoelastic properties of solutions as reported by Huseyin & Bulent [49]. On the other hand, the vortices size of GG solutions at the upper and lower part of the setup was larger than the

XG solutions' vortices. It was observed that all vortices elongated at the onset of MWVF for all GG concentrations, where disordered flow structure occurred specifically at MWVF for the 8000 ppm and 10000 ppm GG concentrations.

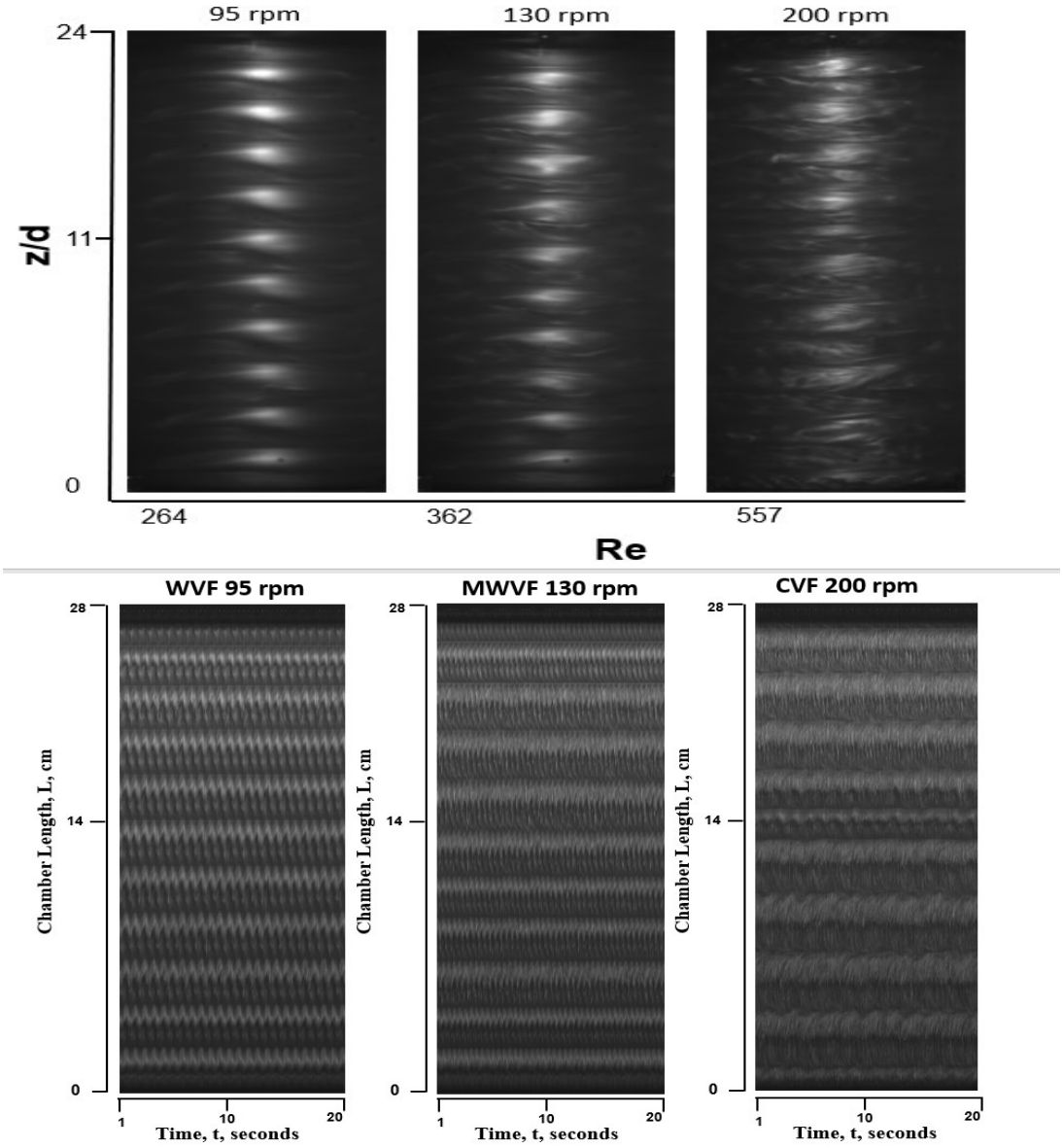

Figure 4-6. a) Recorded picture of the flow regimes for guar gum 1000 ppm solution vs Re. b) Spatio- temporal plots at the narrow gap for the 1000 ppm guar gum solution.

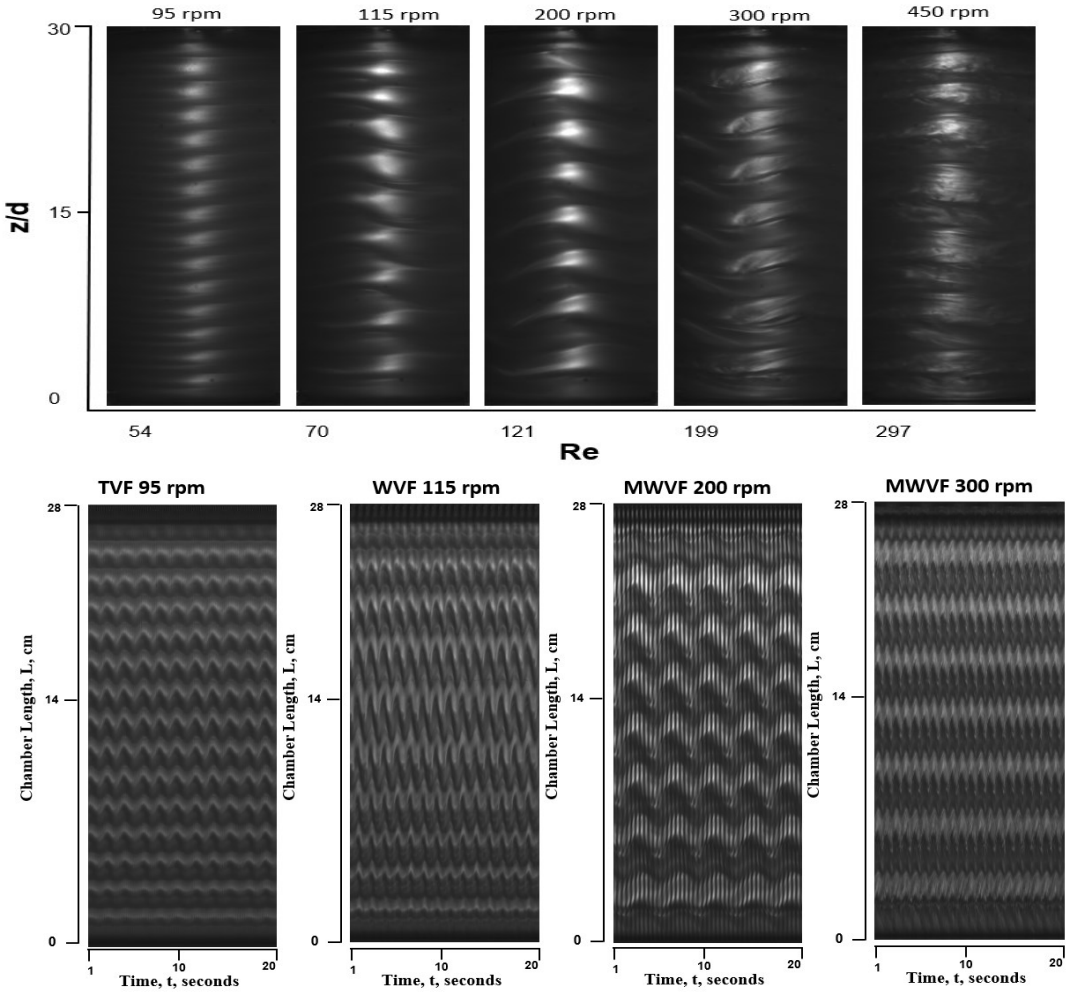

Figure 4-7. a) Recorded picture of the flow regimes for guar gum 4000 ppm solution vs Re. b) Spatio- temporal plots at the narrow gap for the 4000 ppm guar gum solution.

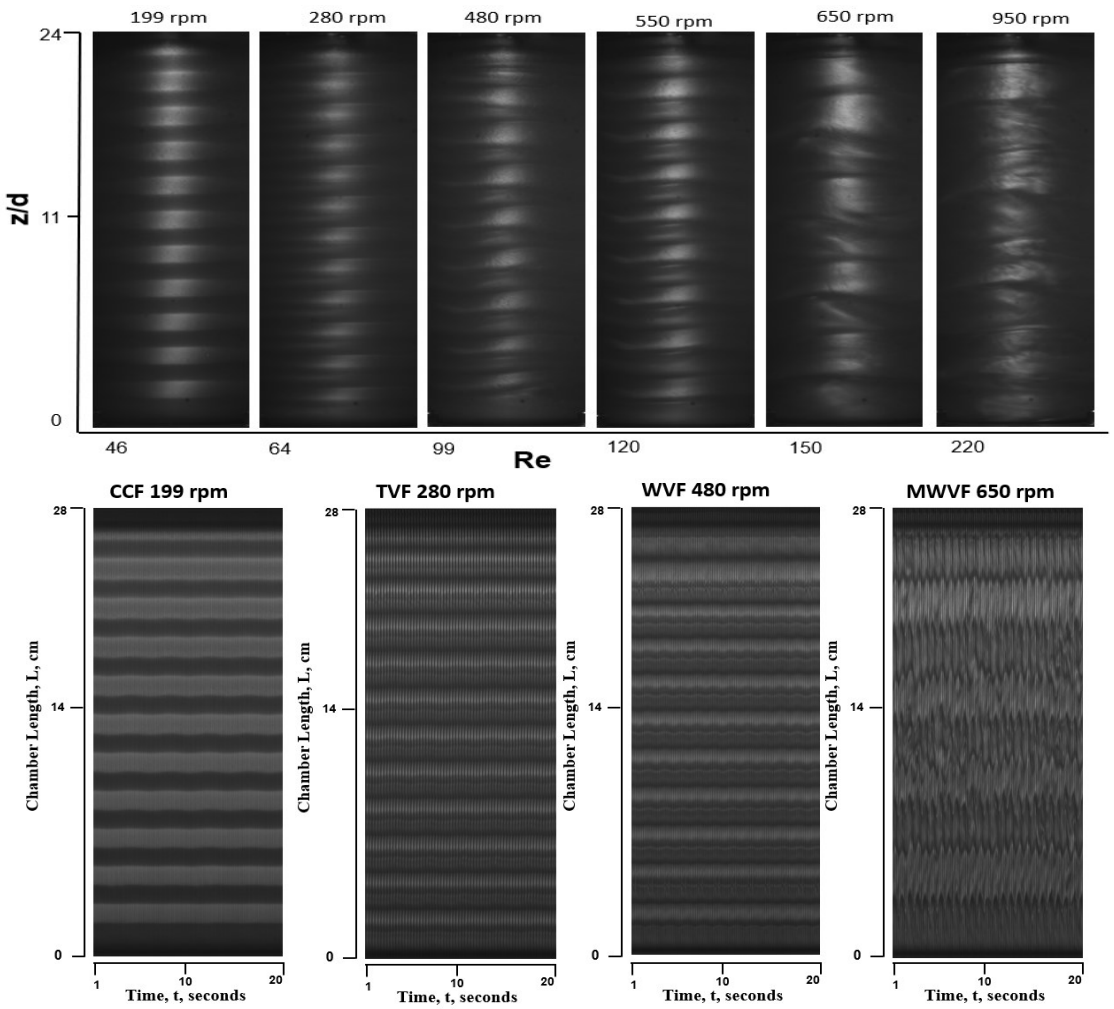

Figure 4-8. a) Recorded picture of the flow regimes for guar gum 8000 ppm solution vs Re. b) Spatio- temporal plots at the narrow gap for the 8000 ppm guar gum solution.

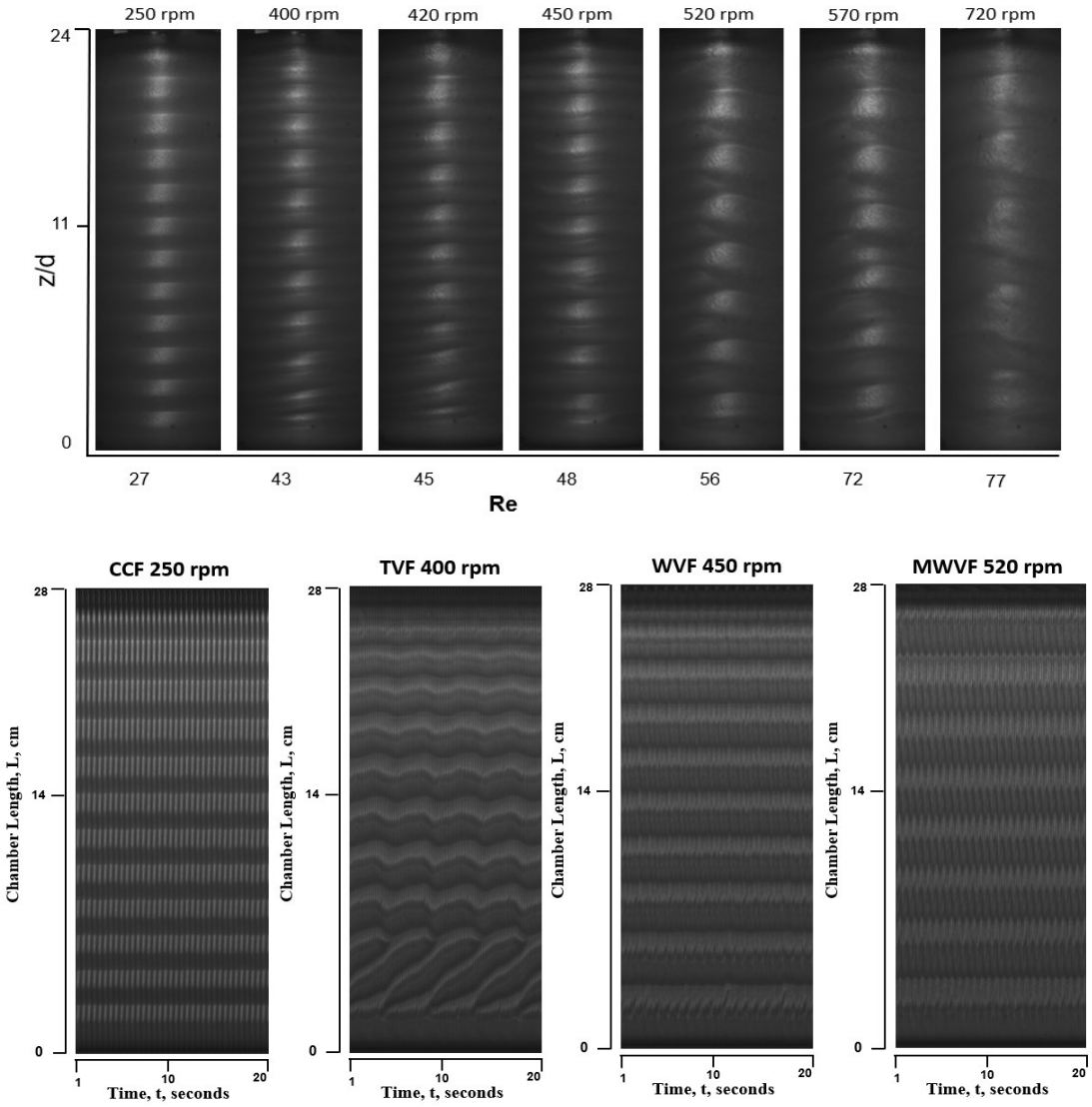

Figure 4-9. a) Recorded picture of the flow regimes for guar gum 8000 ppm solution vs Re. b) Spatio- temporal plots at the narrow gap for the 10000 ppm guar gum solution.

Figures 4-3 to 4-9 showed different new non-axisymmetric regimes captured in this study such as the Spiral Vortex Flow (SVF) and Coil Vortex Flow (CVF) for GG and XG solutions. The SVF regimes occurred at the highest concentrations for the XG 8000 ppm and 10000 ppm at the onset of the secondary transition from WFV to MWVF at the bottom and the top ends of the outer cylinder, as can be seen in Figure 4-10. The first two spiral vortices from the bottom end for the XG 8000 ppm were captured at 450 rpm with a total axial size $z/d = 6.13\ cm$ as illustrated in Figure 5- 10. Moreover, the SFV occurred twice for the XG 10000 ppm at speeds of 450 rpm and 550 ppm with noticing that only the third vortex from the top changed its structure to an oblique pattern with occupying axial size $z/d = 2.45\ cm$. Whereas, the SVF occurred at the bottom side of the chamber occupying about half of the cylinder with a total axial cell size $z/d = 10.8\ cm$ for XG 10000 ppm. The SVF bifurcations were more pronounced at high solution concentrations due to their strong elastic characteristics obtained from the rheology analysis.

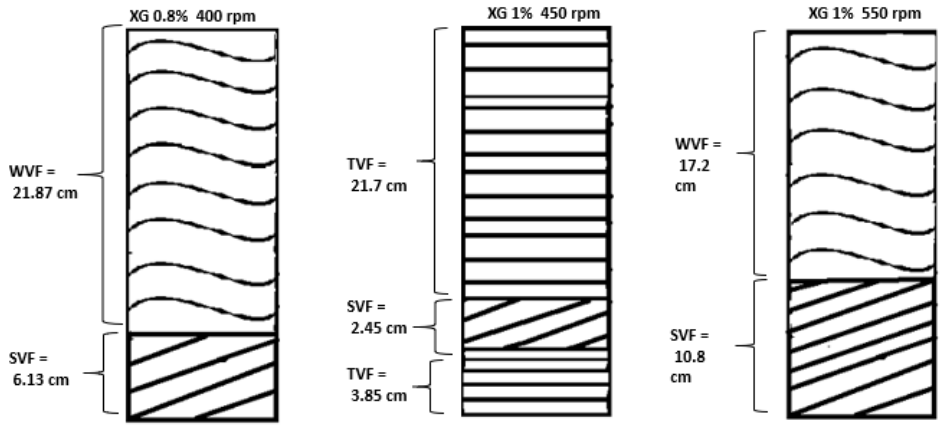

Figure 4-10. shows the flow structure scheme of the flow regimes between TVF and WVF for xanthan gum 8000 ppm and 10000 ppm solutions.

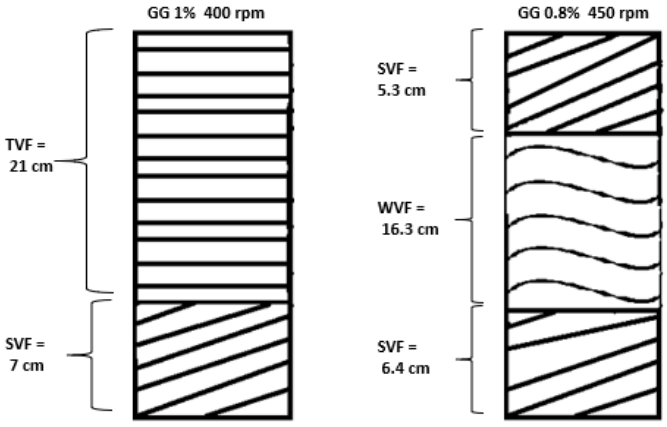

Figure 4-11. shows the flow structure scheme of the flow regimes between TVF and WVF for guar gum 8000 ppm and 10000 ppm solutions.

Similarly, for same SVF regimes were also observed at the highest GG concentrations of 8000 ppm and 10000 ppm. As can be seen in Figure 4-11, the, the SVF occurred for GG solution 8000 ppm at the transition between WVF and MWVF forming the first three vortices from both the top and bottom side of the TC chamber with total cell size *z/d = 5.3 cm and 6.4 cm* for the top and bottom axial position, respectively. Whereas it was noticed for GG solution 10000 ppm in the onset of the WVF at the first three vortices from the bottom with total size *z/d = 7 cm* as seen in Figure 4-11.

On the other hand, the CVF was illustrated only for the lowest GG concentrations (1000 ppm and 4000 ppm). It was captured beyond the speeds of 300 rpm for the

XG 1000 ppm and 500 rpm for XG 4000 ppm. The CVF was at 200 rpm and 420 rpm for GG 1000 ppm and 4000 ppm, respectively. As shown in Figures 4- 12 and 4-13, the CVF instabilities observed and reported beyond the MWVF for all fluid samples in this study confirmed the main findings of Huseyin & Bulent [49] where the coil structure was reported beyond MWVF.

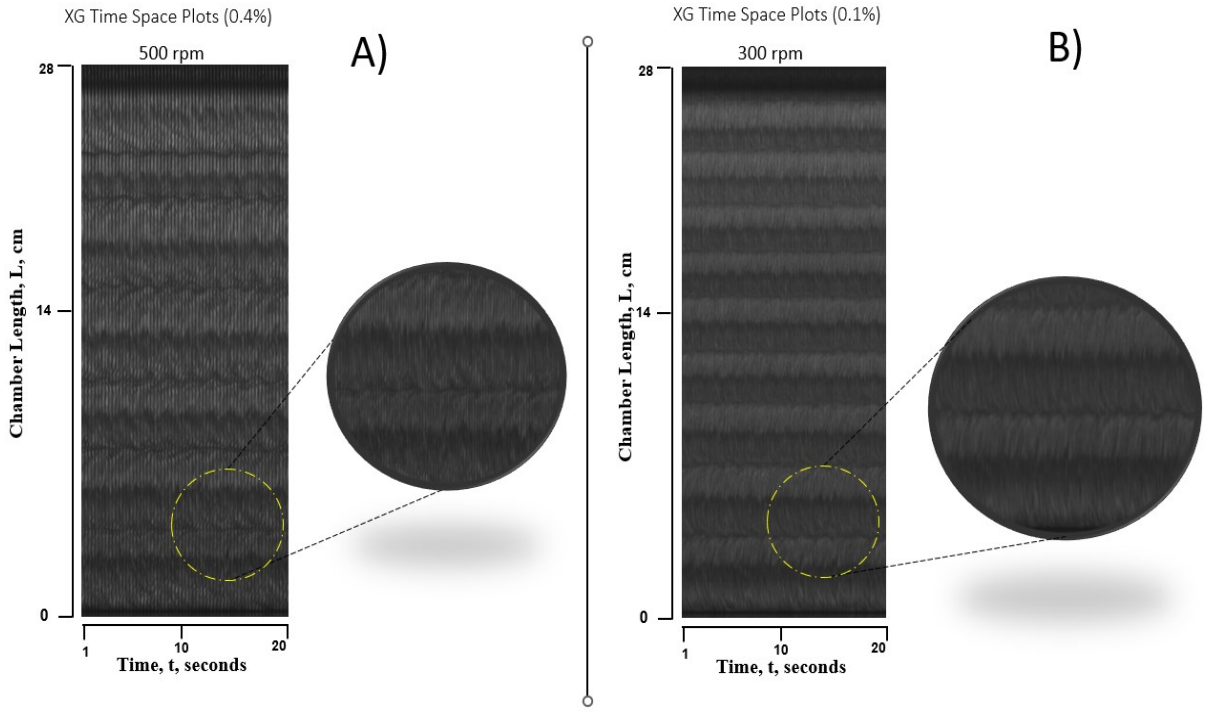

Figure 4-12. shows a magnified view of the CVF flow for xanthan gum a) 4000 ppm and b) 1000 ppm solutions.

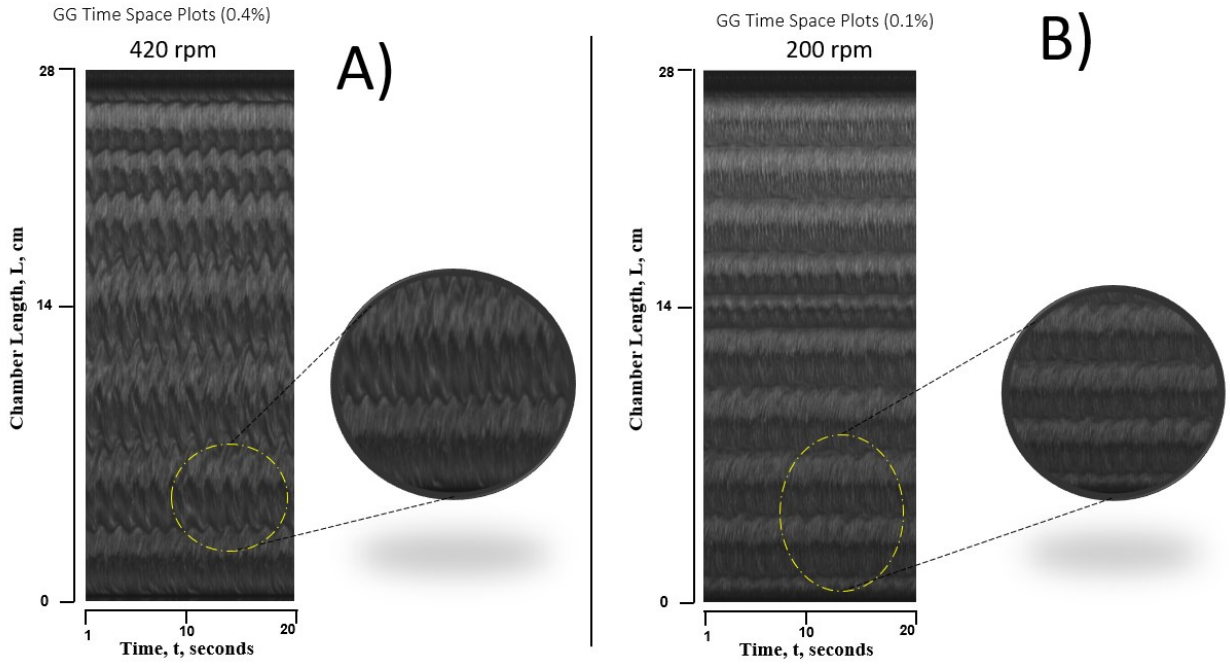

Figure 4-13. shows a magnified view of the CVF flow for guar gum a) 4000 ppm and b) 1000 ppm solutions.

4.3.2) Critical Reynolds Number vs Flow Index:

Figures 4-14 show the critical Reynolds number at the onset of the flow instabilities, namely the TVF, WVF, and MWVF, as a function of the shear thinning flow indices obtained from the rheology power-law model analysis. The flow indices showed similar rheology behavior in both fluids. It was noticed that there was a clear inverse correlation between the shear thinning concentration and the critical Reynolds numbers Re_c. For the XG solutions, the critical Reynolds numbers in each transition flow (TVF, WVF, and MWVF) experienced monotonic decreasing patterns as the vortex flow evolved. Figure 4-14 illustrated the critical Re_c was observed earlier as the shear thinning concentration increased for all flow instabilities between TVF and MWVF regimes. Also, a steep decline in the Re_c was noticed at a flow index of $n = 0.35$ for the concentration of 4000 ppm.

The GG flow indices showed a decreasing manner as the concentration increases with a significant reduction in the Re_c occurring at flow index $n = 0.5$ "4000 ppm", however, the manner of the Re_c beyond $n = 0.5$ experienced a non-monotonic behavior; it experienced a slight increase before it decreased again to the lowest value at flow index of $n = 0.26$. Based on many studies, this fluctuation is attributed to the strong viscoelastic shear-thinning nature of the GG where the

viscous effect was dominant for the entire frequency load as well as the variation in the applied power-law model to the rheological analysis of the solutions [50].

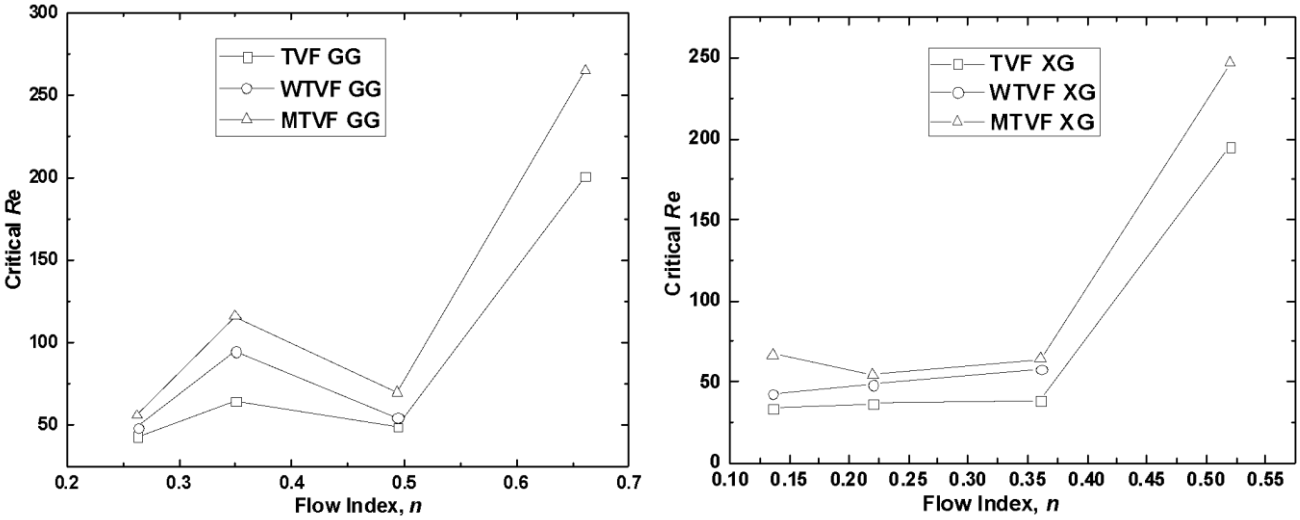

Figure 4-14. the variation of the critical Reynolds numbers on the onset of the flow instabilities between TVF and MWVF, over shear thinning flow indices for a,) xanthan gum and b) guar gum solutions

4.3.3) Vortices Aspect Ratio along the cylinder length

The axial size and the aspect ratio of the Taylor Vortex flow regime along the outer cylinder wall were investigated in this study. The size of each cell was measured and calibrated by converting the pixel size to SI unit such as mm or cm, was associated with the flow regimes, resulting in different aspect ratios at each regime in the Taylor Couette system. The aspect ratio of Taylor vortex flow versus the axial wall was plotted for both solutions as can be seen in Figures 5- 15 A and B. The vortices count at the TVF were 22 , 22 and 18 vortices for the XG concentrations of 8000 ppm, 4000 ppm and 10000 ppm that corresponded to the following averaged vortices aspect ratios of 1.4 , 1.5 and 1.6, respectively. For the XG 8000 ppm concentration, the aspect ratio varied from 1 to 1.5. However, the 4000 ppm and 10000 ppm concentrations showed slight differences in the vortices' aspect ratios along the chamber wall. These variations in vortices aspect ratios were quantified and they formed a zig-zag pattern, as can be seen in Figures 4-15A. These zig-zag-shape variations are attributed to the trapezoid shape of the vortices cells that affected the dimensions of each vortex due to the strong elastic behavior. The variations in the aspect ratios for the XG and GG solutions were higher as the concentration

increased; whereas they were negligible at lower concentrations where the viscoelastic nature is less pronounced. Additionally, the vortices at both chamber ends elongated with higher aspect ratios; they reached up to 2.5 aspect ratios for the XG 10000 ppm as shown in Figure 4-15B.

As can be seen in Figure 4-15B, the vortices aspect ratios for the GG 8000 ppm and 10000 ppm were 1.2 and 1.4, respectively. The GG 8000 ppm obtained about 24 vortices, but there are only 22 vortices are captured for the GG 10000 ppm. Similar to the XG solutions, the vortices at both ends of the chamber elongated, achieving the aspect ratios of 1.8 for the GG 8000 ppm. Also, the aspect ratio of both ends vortices varied from 1.4 to 2.3 for the GG 10000 ppm concentration. Overall, the vortices elongation at both ends for all fluids is attributed to the chamber's end effect as well as the viscoelastic nature.

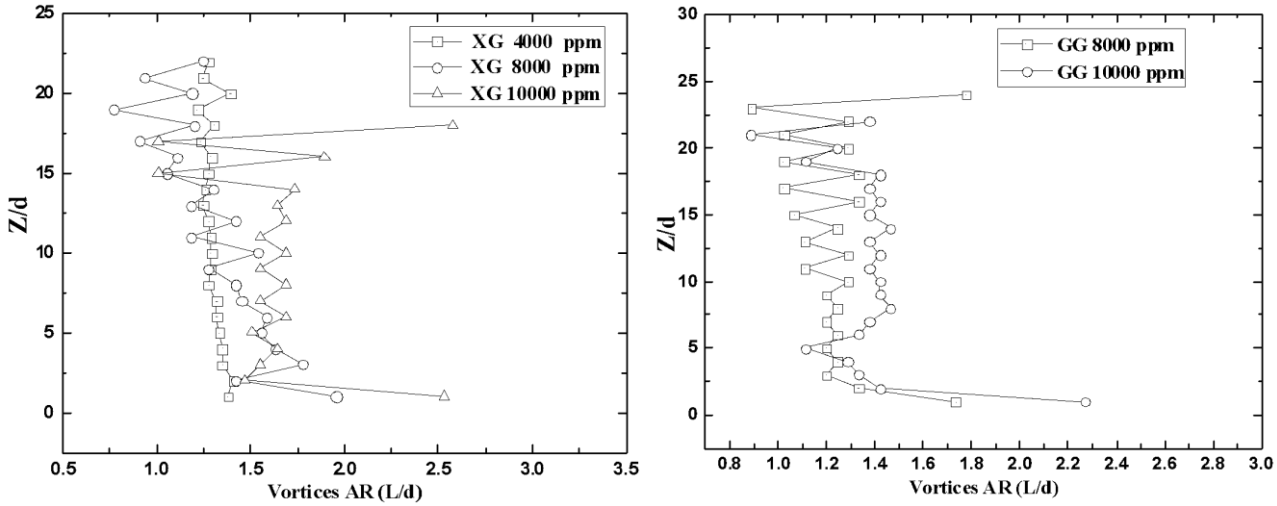

Figure 4-15. The aspect ratio of the Taylor vortices along the axial axis for a) The xanthan gum on the right-hand side, b) guar gum solutions in the left-hand side.

4.3.4) Number of Vortices

We observed an inverse correlation between the magnitude of the axial wavelength and the vortices count. As the wavelength increased the number of vortices experienced a noticeable drop. It was also obvious that the variation in the number of vortices was slightly small at low solution concentrations, whereas it was higher as the solution concentration increased, as can be seen in Figure 4-16. The highest vortices number was at the primary instability between CCF and TVF regimes for all solutions. It decreased monotonically at the onset of the WVF. Then it continued dropping at the onset of the MWVF regimes. The lowest vortices number was 12 vortices that were obtained for the XG 8000 ppm at the onset of the MWVF. Whereas the highest vortices

number is 22 vortices obtained for the XG 4000 ppm and 8000 ppm concentrations as illustrated in Figure 4-16A. For GG solutions, the highest vortices number were 30, 24, and 24 vortices observed at the primary transition for the 4000 ppm, 1000ppm, and 8000 ppm concentrations, respectively. Also, 10 vortices were captured at 650 rpm for 8000 ppm GG solution, indicating the correlation that as the concentration of the solution increased at a high Reynolds number, a significant drop in vortices count was reported and vice versa.

Both GG and XG plots showed a consistent behavior for all concentrations, confirming similar decreasing patterns in all solutions. This agreement is because of the consistent shear thinning viscoelastic behavior of both solutions at high shear load.

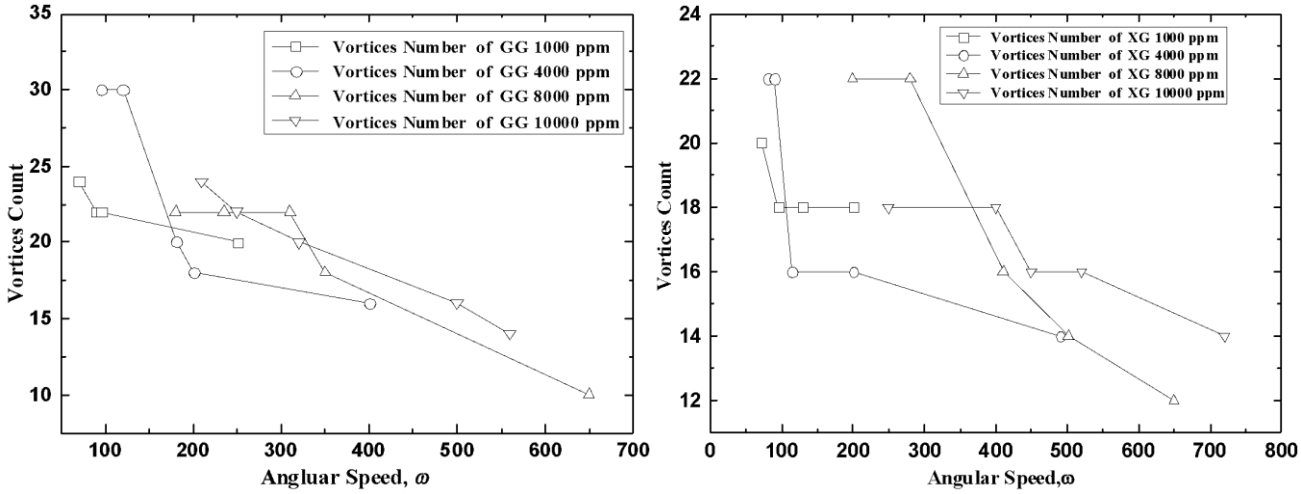

Figure 4-16. The vortices number corresponding to each flow regime along the axial axis for a) the xanthan gum on the right-hand side and b) guar gum solutions on the left-hand side.

4.3.5) Vortices Characterized by Axial Wavelength (Axial Wavelength vs Reynolds Number)

The variation in the axial wavelength versus Reynolds number for the XG and GG solutions was reported in Figures 4-17 and 4- 18. The data points were collected from flow transition regimes including TVF, WVF, and MWVF. The axial wavelength (per the gap between the cylinders) formula is $\lambda/d = AR/2N$ (where N is the number of pair vortices), was applied to determine the wavelength of the vortices. The axial wavelength for all concentrations increased with the critical

Reynolds number. Thus, the transition regimes have an obvious impact on the wavelength. At high solution concentrations, a monotonic increase in axial wavelength was noticed. The wavelength plot for the XG solution 1000 ppm turned slightly flat beyond Re = 200. All GG and XG plots in Figures 4-17 and 4-18 experienced a slight plateau manner in the axial wavelength beyond the MWVF regimes. Overall, the general manners for all plots were similar among all fluids.

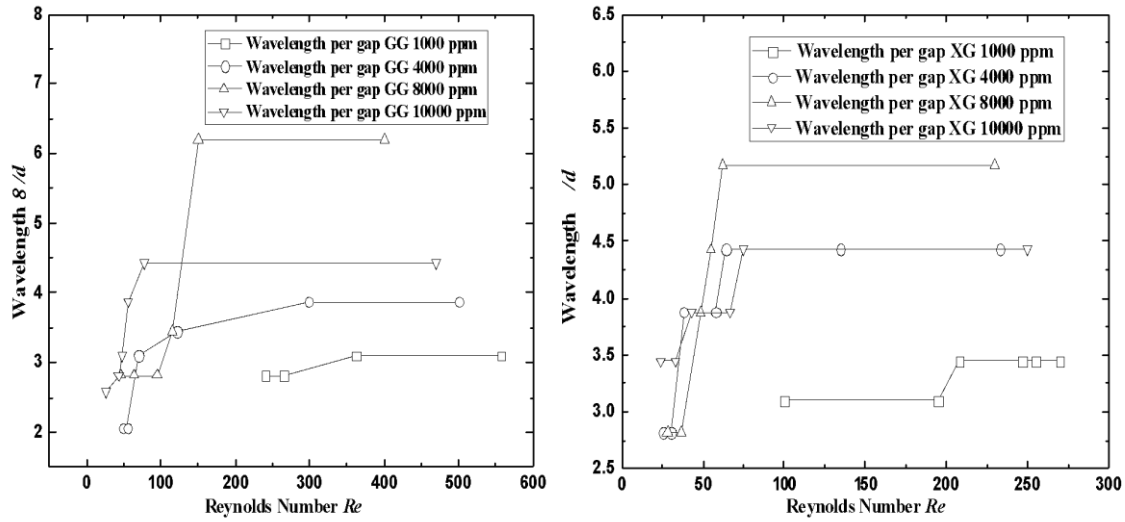

Figure 4-17. The variation in the flow structure axial wavelength for the flow regimes from the CCV to MWVF for a) the xanthan and b) guar solutions.

Conclusion:

The effect of shear thinning of concentrated biopolymers on the flow regimes in the Taylor Couette system with only inner cylinder rotates was investigated. Four concentrations of the GG and XG solutions were experimentally tested including 1000 ppm, 4000 ppm, 8000 ppm, and 10000 ppm each. The flow visualization experiments were performed to characterize the flow patterns between the laminar to the per turbulent regimes, and four symmetric flow regimes are observed such as CCF , TVF , WVF, and MWVF for the GG and XG solutions within the Reynolds number ranges from 0 to 800. On the other hand, two different non-axisymmetric are noticed in the transition between TVF to WVF including SVF and CVF for the 8000 ppm and 1000 ppm XG and GG solutions. The flow modes between CCF to MWVF experienced a non- axisymmetric merging of the periodic vortices, including the vortices at both ends elongated and with large axial size for all concentrations compared to the other vortices. This propagation occurred progressively at the

second instability and beyond. Both biopolymer solutions exhibited a switch in vortices' amplitude and frequency from high frequency and low amplitude to the opposite at 4000 ppm concentrations in each solution.

The influence of the shear thinning flow indices on the critical Reynolds number was also investigated for all concentrated solutions. The shear thinning flow indices obtained from rheology experiments were (0.520, 0.220,0.361 and 0.136 for XG solutions) and (0.661, 0.494, 0.350, and 0.263 for GG solutions). The critical Re at the onset of the flow instabilities is observed earlier as the flow indices decreased, indicating an inverse correlation between the solution concentrations and Re; as the critical Re drifted back as the concentrations increased. Furthermore, the vortices number, axial wavelength, and aspect ratio were measured corresponding to the onset of each flow instability and transition that occurred at critical Re for all solutions. The vortices' aspect ratios have an almost fixed value for the vortices in the middle of the outer cylinder wall, however, the vortices at both ends elongated with a significantly larger aspect ratio for both GG and XG solutions. This increase is speculated to be the end effect at the bottom and the top of the cylinder. Additionally, the axial wavelength has been inversely affected by the vortices number; the wavelength experienced a significant increase as the number of vortices decreased. The vortices number dropped when the flow evolved at a higher inner cylinder's speed, resulting in a quite small variation in the reduction in vortices number at low solution concentrations.

CHAPTER 5

Conclusion, Recommendations

This thesis aims to study the rheology behavior of concentrated shear thinning biopolymers focusing on the main parameters such as yield stress, viscosity patterns, and viscoelasticity. Additionally, we investigated the viscosity stability of these parameters for all non-Newtonian fluids focusing on the influence of storage time and agitation amount on the viscosity and yield stress variations. More importantly, after the rheology characterizations, we investigated the effect of rheological shear thinning parameters such as flow indices on the flow regimes and patterns by using flow visualization experiments in the Taylor Couette system.

The effect of high-viscosity shear thinning biopolymers on Taylor Couette flow characterization has rarely been studied in the last decades. It was recommended in the literature that there is a need to study the flow mapping behavior of viscous fluids in the Taylor Couette system. Also, we focused on the influence of the shear thinning nature on the vortex flow regimes, and critical Reynolds numbers at the onset of the flow instabilities between CCF to MWVF.

5.1) Yield stress rheology investigation

The first goal of this work is to study the rheological behavior of high-viscosity xanthan solutions to quantify the yield stress values, viscosity, and viscosity recovery behaviors over shear rate range from $0.1s^{-1}$ to 100 s^{-1}. The selected XG concentrations were 10000 ppm and 20000 ppm, 30000 ppm, and 40000 ppm making the solutions take a gel formation similar to drilling fluids “water-based”. The results obtained were compared with the previous studies in the literature and they were consistent. The solutions exhibited strong shear thinning nature and it confirm the effect of solution concentrations on the yield stress, resulting in lower yield stress values even at high concentrations and low shear rate in this study.

Furthermore, the viscosity depended on the shear rate load, showing an inverse relationship that highlighted as the shear rate increased the viscosity showed an obvious shear thinning behavior for the entire shear load. This shear thinning nature was more pronounced at higher xanthan concentrations. The viscosity recovery thixotropy” of XG was investigated by applying three-step shear loads as follows: starting with a low shear load at 0.1 s^{-1}, then a sudden high shear load applied by 100 s^{-1}, and ending up with the low shear load of 0.1 s^{-1} in sequence. The recovery was

achieved quickly at the low shear load, where the viscosity recovered back to the initial state after approximately 150 seconds.

Therefore, three rheological models including the *power-law, Herschel–Bulkley, and Bingham* models were applied to the rheological flow curves in this study to quantify the yield stress behavior as well as describe the shear thinning properties. The rheology properties of the xanthan solutions were found in good agreement with only the *power-law*, and *Herschel–Bulkley* models. Whereas, the *Bingham* models did not predict accurately our rheology flow curves, showing less fitting accuracy compared to the other models.

5.2) Viscoelastic Characterizations of concentrated Xanthan and Guar Solutions

In this chapter, two different biopolymer non-Newtonian solutions were used to study the viscoelastic properties of the solutions over various ranges of concentrations. The GG and XG solutions were well prepared to form concentrated solutions with concentrations of 1000 ppm, 4000 ppm, 8000 ppm, and 10000 ppm each. Also, the experiments were conducted by performing flow curves and oscillatory frequency sweep measurements. The flow curves aim to characterize the viscosity and yield stress properties in sort and long period conditions of storage time for about 1 month, and in a condition of extra agitation time for approximately 2 days of a continuous agitation for all solutions. The storage time tests were conducted at the end of each week for a 1-month period of storage time. Whereas, the extra agitation time tests were performed over increasing the agitation time applied to the solutions as follows: (8h, 24h, and 48h). It was reported that the viscosity and yield stress experienced a slight increase in the zero-shear viscosity at a shear rate less than 0.1 s^{-1} after one month of storage time, indicating consistent behavior at infinite viscosity values for all solutions. The viscosity of GG increased by 22% after one month, and by 36.5% for XG solutions. On the other hand, the viscosity and yield stress exhibited a slight drop in their values at the zero shear viscosity region as the agitation period increased, indicating both GG and XG showed about 29% and 22% drop in viscosity for XG and GG, respectively.

Moreover, the viscoelasticity analysis was performed over frequency ranging from 300 to 0.1 rad/s. the GG solutions exhibited a viscous effect that was dominant for all solutions over the entire frequency range, indicating the loss modulus "*G"* " was dominant. Whereas, the viscous effect was dominant for the XG solutions only at high frequency, and the elastic effect "*G'"* was dominant at the low-frequency load.

Both GG and XG solutions exhibited higher tangent phase angle and lower storage modulus at a higher frequency. Therefore, these characteristics contributed directly to increasing the solutions' flowability and fluids' energy efficiency. Also, both the apparent viscosity and complex viscosity of all solutions confirmed the Cox-Merz rule., Additionally, the phase angle has an inverse correlation with the concentrations, resulting in a significant drop in the tangent phase to less than one for higher XG concentrations beyond 4000 ppm. They confirmed that at low frequency the elastic behavior was more pronounced for XG solutions.

5.3) The influence of concentrated shear-thinning guar and xanthan solutions on flow patterns in Taylor Couette flow

The influence of the non-Newtonian XG and GG solutions on the vortex flow structure in the Taylor Couette flow was investigated for four different concentrations of each solution. In addition, four flow regimes were captured for all solutions by using flow visualization experiments over the entire Reynolds number range ($0 < Re < 800$), and they are CCF, TVF, WVF, and MWVF. However, two non-axisymmetric regimes were observed, they were Spiral Vortex Flow (SVF) and Coil Vortex Flow (CVF) at the secondary transition before the onset of the WVF. The SVF was reported at only higher concentrations of 8000 ppm and 10000 ppm, whereas the CVF was at the low concentrations of 1000 ppm and 4000 ppm of both solutions. Furthermore, we observed a non-axisymmetric vortex merging at both ends of the Taylor chamber, resulting in obvious elongation of the vortices size at both Taylor chamber's ends. At the concentration of 4000 ppm of both fluids, the vortices frequency and amplitude experienced a significant switch from the higher frequency and low amplitude to low frequency and high amplitude.

Accordingly, the vortex regimes were affected by the solutions' shear thinning viscoelastic nature. Thus, the flow regimes mapping altered back and observed earlier at lower critical Reynolds numbers Re when the solution concentrations increased. We concluded that the solution concentration has a direct influence on the onset of flow instabilities. Moreover, the shear thinning viscoelastic nature had a significant impact on the vortices count, vortices axial wavelength and aspect ratios. The vortices count dropped as the critical Re and shear thinning flow indices increased, resulting in an obvious increase in the vortices' axial wavelength in this case. On the other side, the aspect ratios of the vortices on both ends elongated significantly. This attributes to the existence of the ends effect. Whereas the vortices in the middle of the chamber experienced fluctuations in the aspect ratio forming as zig-zag patterns; these fluctuations were more

pronounced at higher solution concentrations and the vortices' aspect ratios have very slight variations for lower solution concentrations.

5.4) Future Recommendations:

The following recommendations could be made for future work on this study.

- Conducting more investigation into the variation of the vortex flow due to the non-Newtonian effect by using Fast Fourier Transformation (FFT) analysis. These variations also occur in the merging regimes where vortices' frequency and amplitude switched behavior due to the non-linear effect of the solutions.
- Studying the effect of non-Newtonian fluids on Reynolds shear stress near the wall over a narrow and wide gap between our setup cylinders in the Taylor Couette system by using the Particle Image Velocimetry (PIV) experiments.

Focusing on the phenomenon behind the fluctuations of vortices size along the axial direction by performing flow visualization experiments using (PIV) techniques.

Appendices

Uncertainty Analysis and

A.1) Concentrated XG solutions (10000 ppm to 40000 ppm):

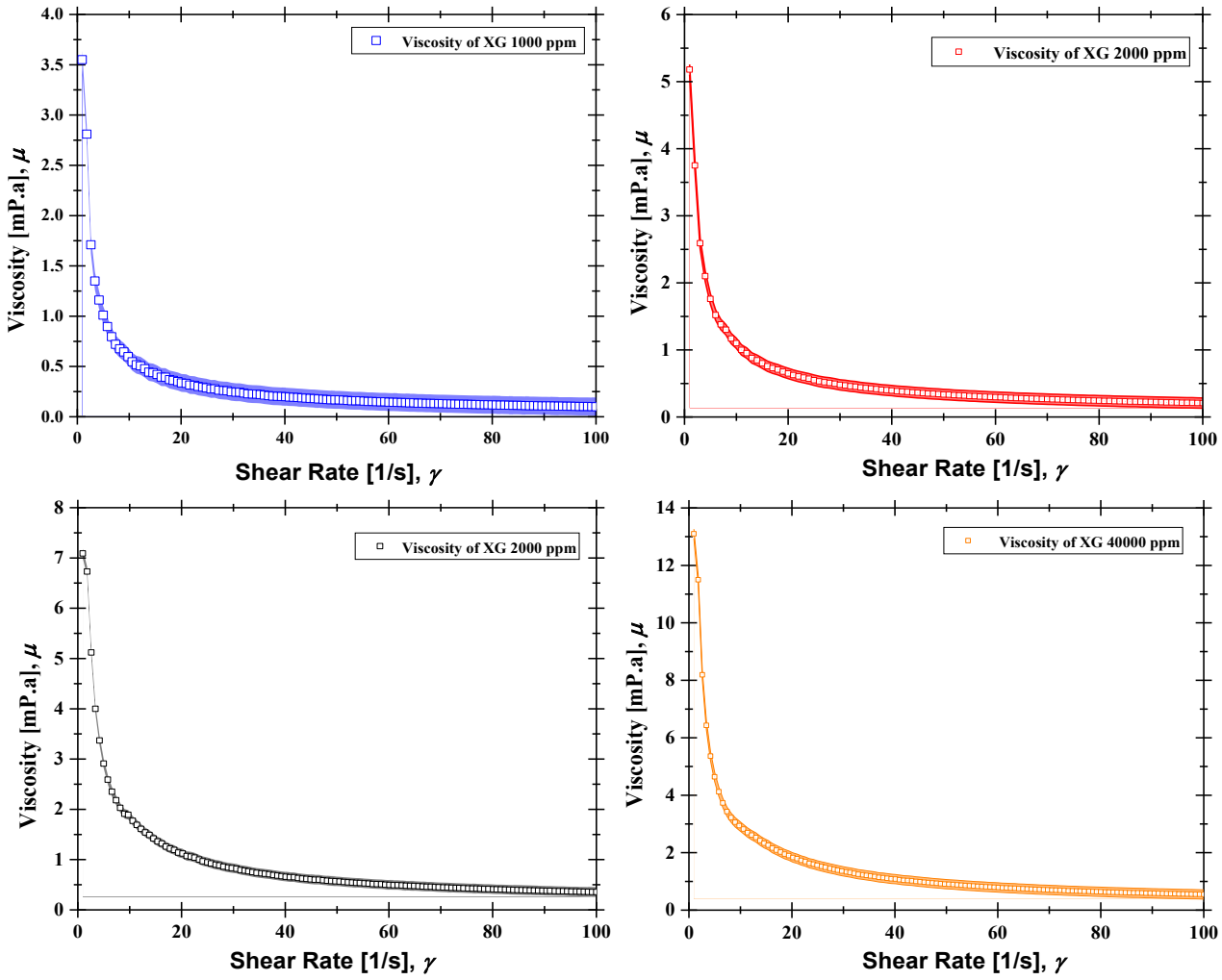

Figure A1. The viscosity curves of high concentrated XG solutions with standard error shown as shadow zones.

	10000 ppm	20000 ppm	30000 ppm	40000 ppm
Standard Deviation	**0.45**	**0.69**	**1.05**	**1.81**
Square Errors	**11.18**	**11.18**	**11.18**	**11.18**
Standard Errors	**0.04**	**0.07**	**0.09**	**0.16**

Table A1. The uncertainty analysis of the viscosity curves of XG solutions.

A.2) Concentrated XG and GG solutions (1000 ppm to 10000 ppm):

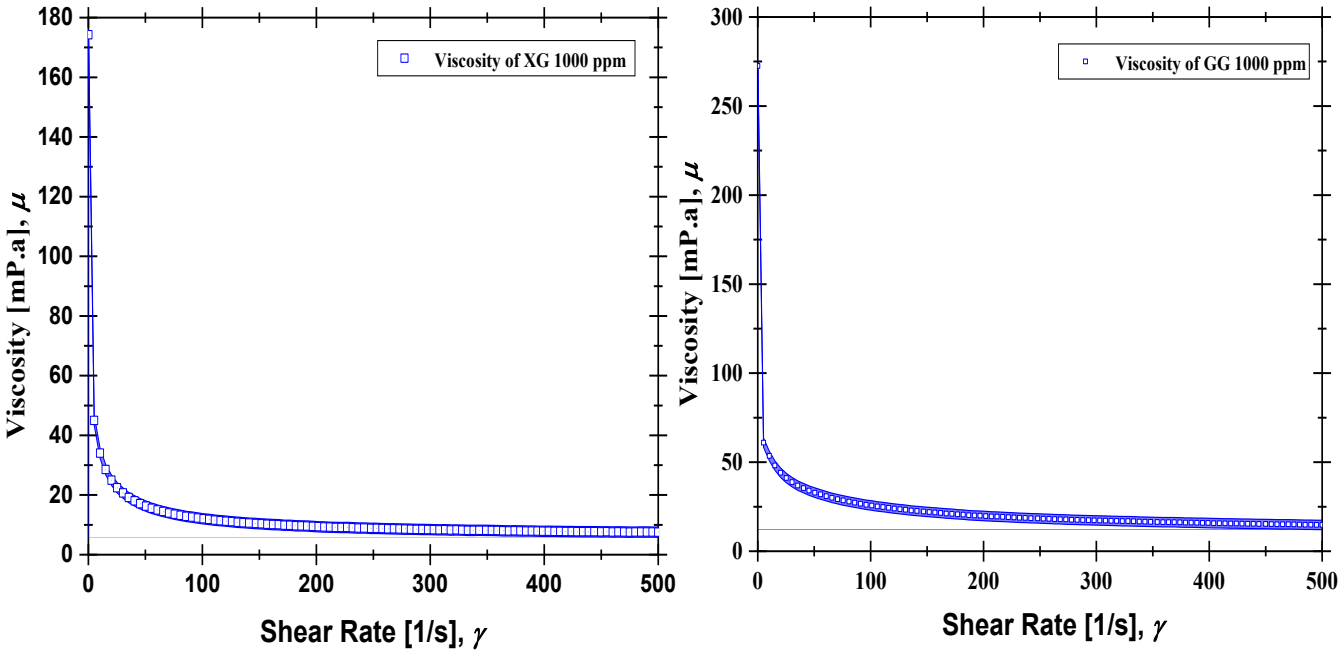

Figure A2. The viscosity curves of concentrated XG And GG solutions (1000 ppm) with standard error shown as shadow zones.

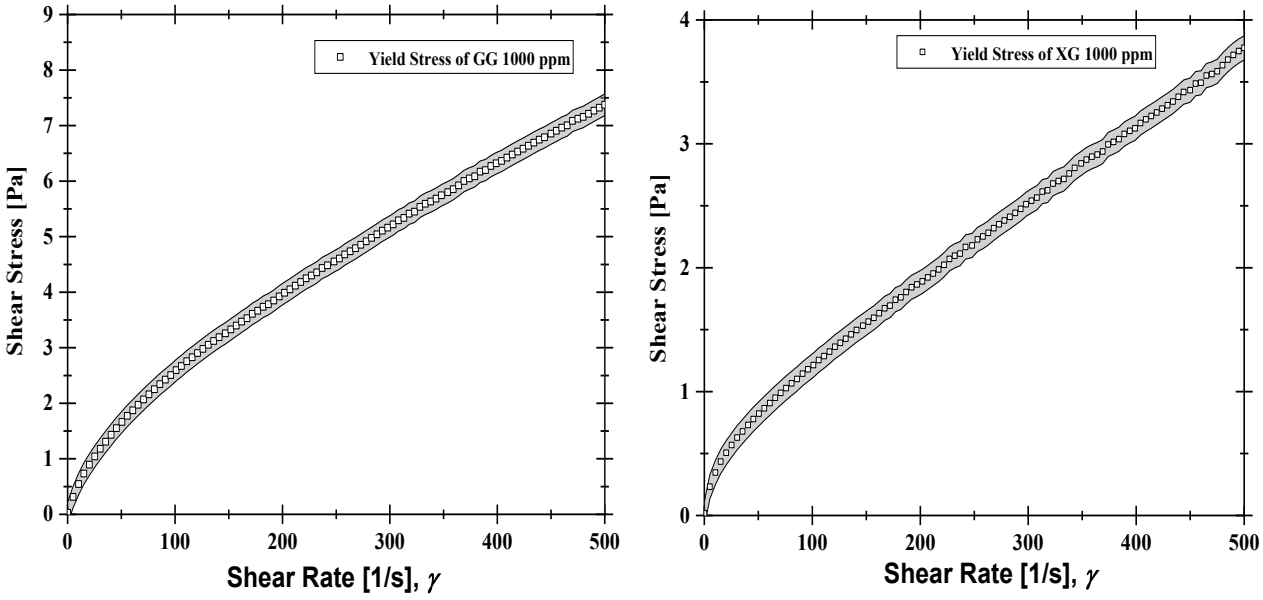

Figure A3. The shear stress curves of concentrated XG And GG solutions (1000 ppm) with standard error shown as shadow zones.

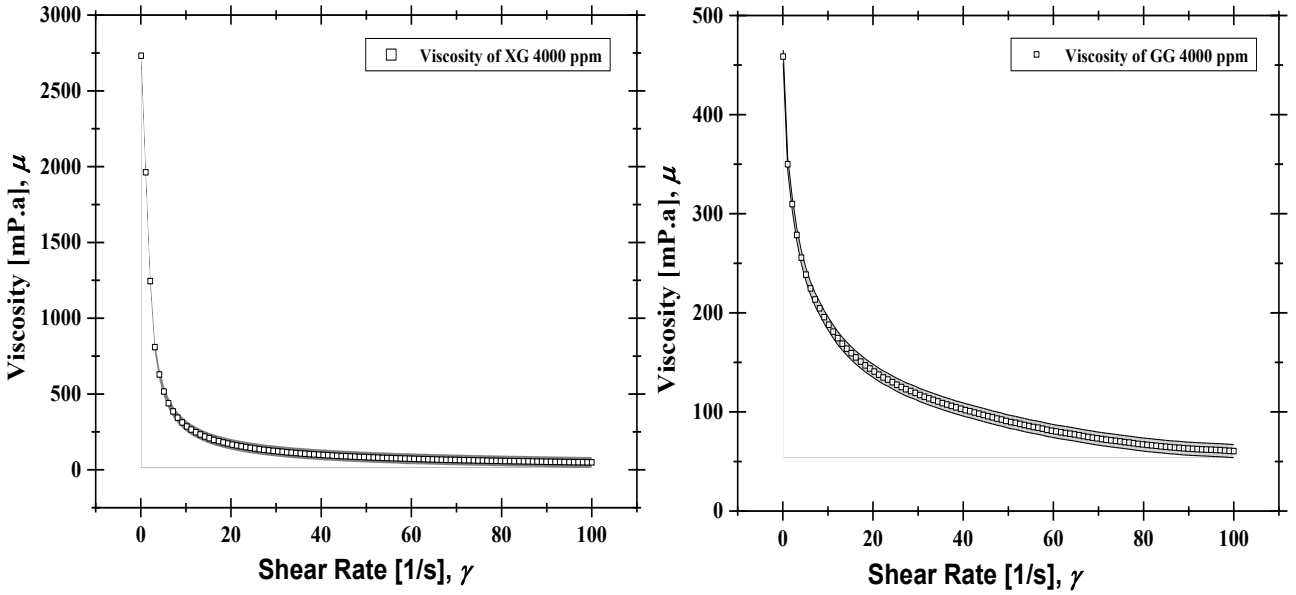

Figure A4. The viscosity curves of concentrated XG And GG solutions (4000 ppm) with standard error shown as shadow zones.

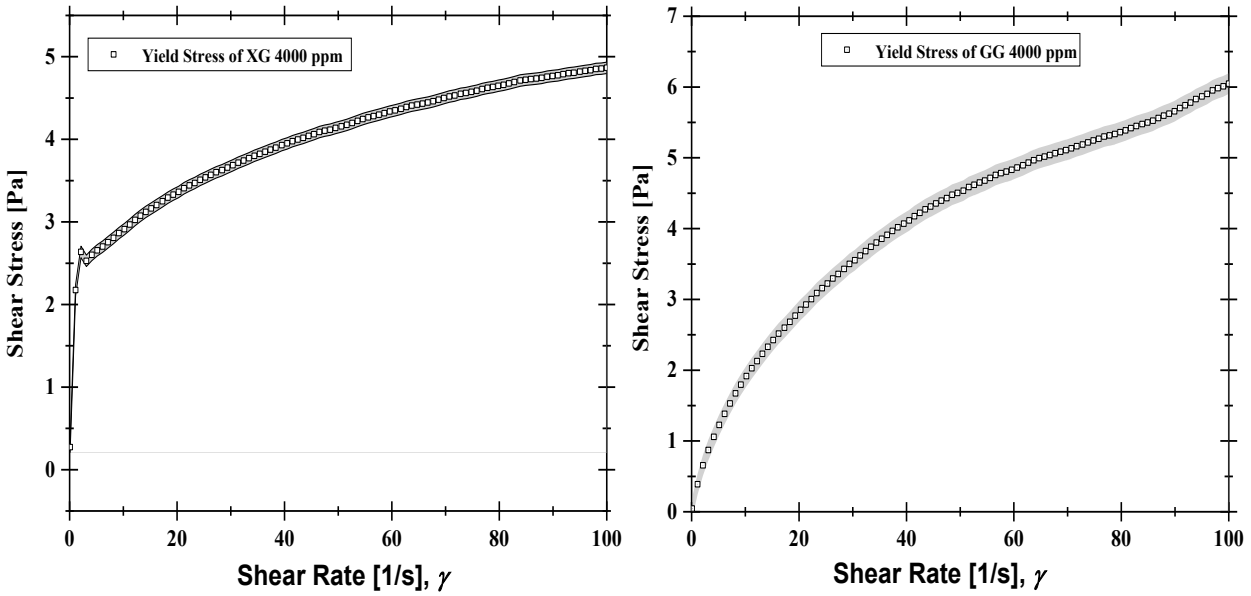

Figure A5. The shear stress curves of concentrated XG And GG solutions (4000 ppm) with standard error shown as shadow zones.

	XG		GG	
	1000 ppm	Yield Point 1000 ppm	4000 ppm	Yield Point 4000 ppm
Standard Deviation	17.23	0.98	66.18	1.46
Square Errors	11.18	11.18	11.18	11.18
Standard Errors	1.72	0.10	6.62	0.15

Table A2. The uncertainty analysis of the viscosity curves of XG and GG solutions

A.3) Replications curves:

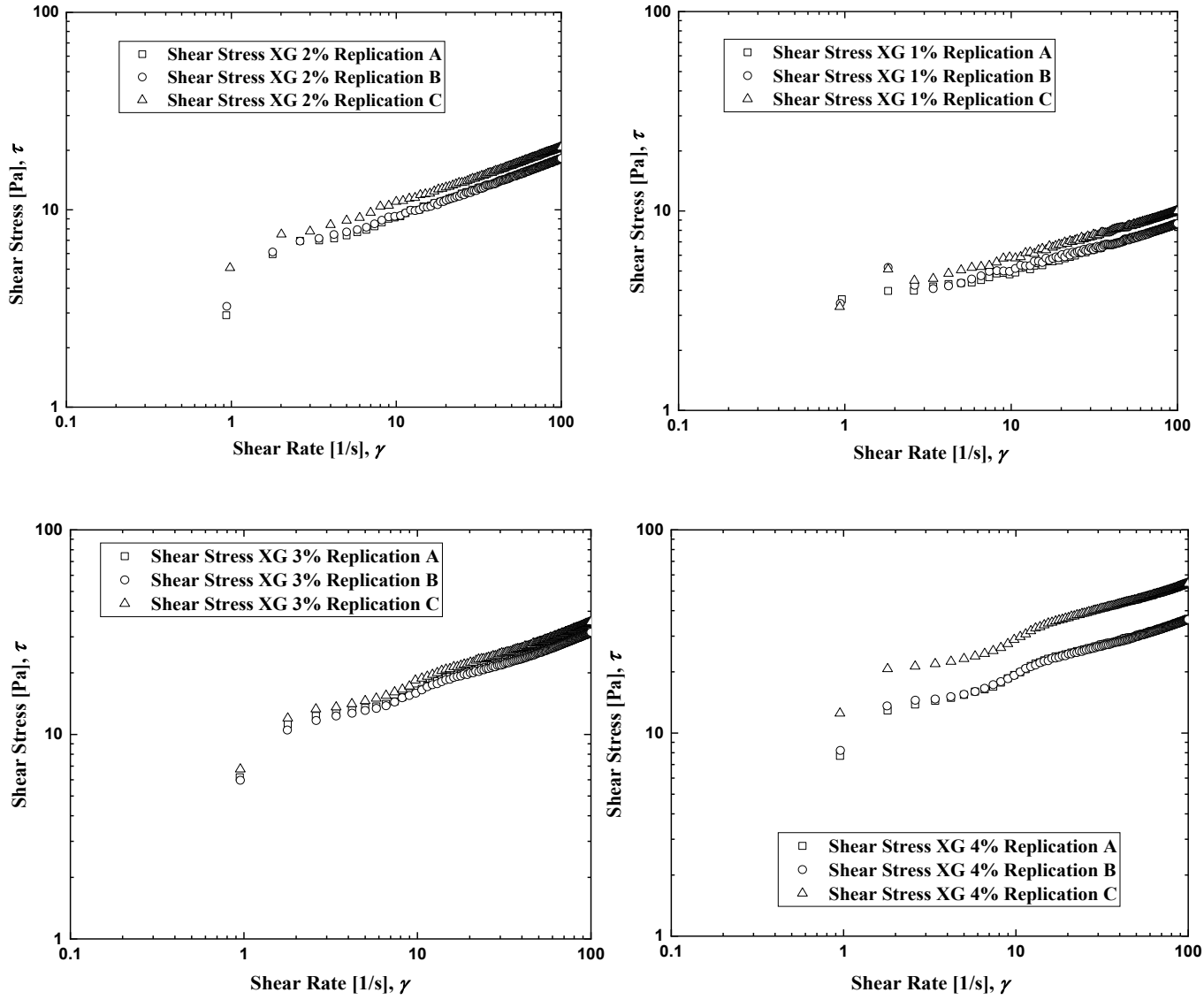

Figure A6. The yield stress replications curves of the Xanthan solutions for all concentrations from 1%wt to 4%wt.

A.4) Convergence of Viscosities Values with the Effect of Storage and Agitation Time Period:

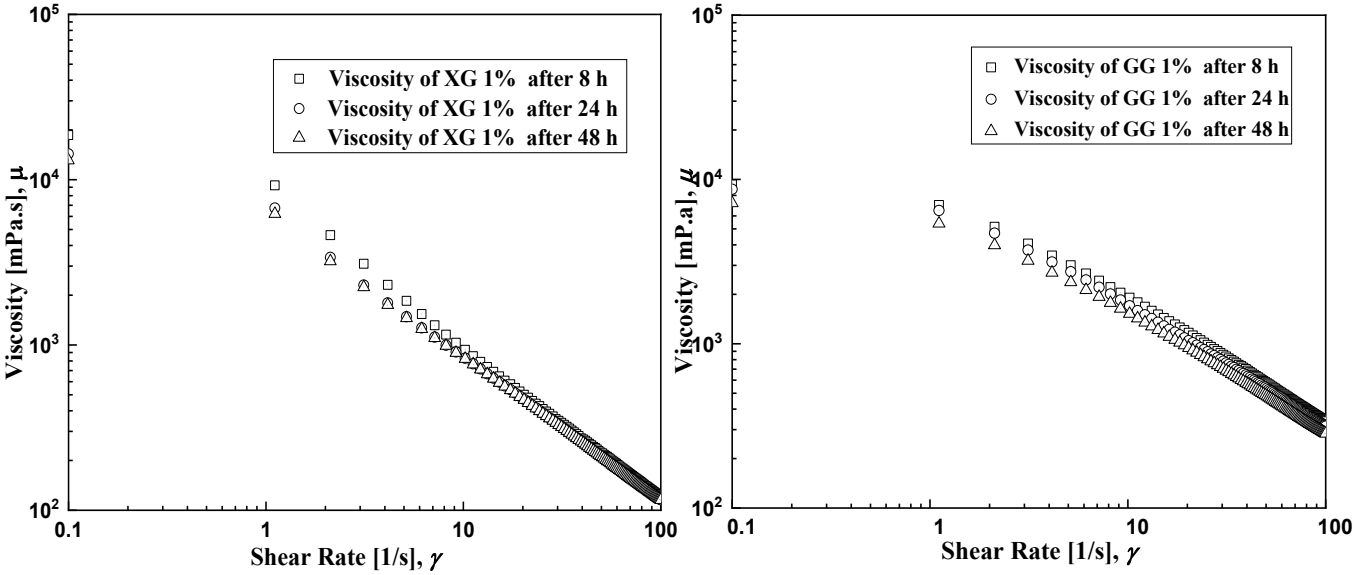

Figure A7. XG And GG solutions' viscosities behavior after the extra agitation time tests.

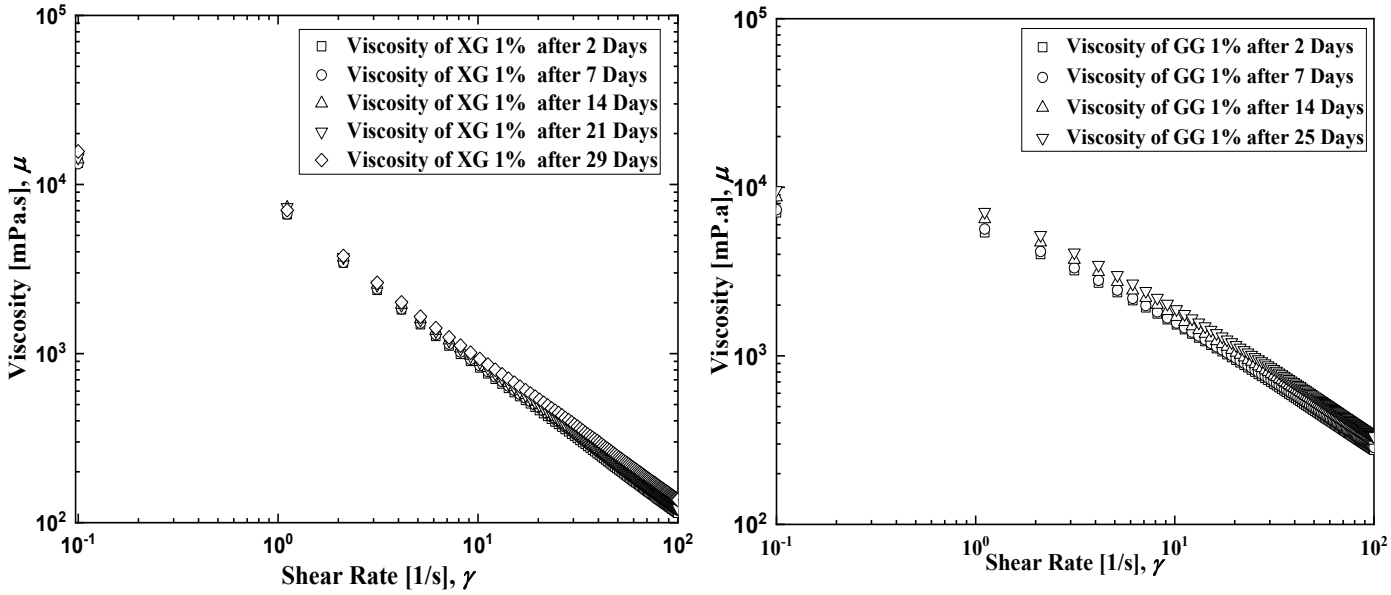

Figure A8. XG And GG solutions' viscosities behavior after the storage time tests.

List of Reference

[1] Rochefort WE, Middleman S. Rheology of xanthan gum: salt, temperature, and strain effects in oscillatory and steady shear experiments. Journal of Rheology. 1987 May;31(4):337-69.

[2] Muller G, Aurhourrache M, Lecourtier J, Chauveteau G. Salt dependence of the conformation of a single-stranded xanthan. International Journal of Biological Macromolecules. 1986 Jun 1;8(3):167-72.

[3] Garcıa-Ochoa F, Santos VE, Casas JA, Gómez E. Xanthan gum: production, recovery, and properties. Biotechnology advances. 2000 Nov 1;18(7):549-79.

[4] Kang KS, Pettitt DJ. Xanthan, gellan, welan, and rhamsan. InIndustrial gums 1993 Jan 1 (pp. 341-397). Academic Press.

[5] Song KW, Kim YS, Chang GS. Rheology of concentrated xanthan gum solutions: Steady shear flow behavior. Fibers and Polymers. 2006 Jun;7(2):129-38.

[6] Gallino G, Migliori M, de Cindio B. A rheological approach to drill-in fluids optimization. Rheologica acta. 2001 Mar;40(2):196-203.

[7] Xia S, Zhang L, Davletshin A, Li Z, You J, Tan S. Application of polysaccharide biopolymer in petroleum recovery. Polymers. 2020 Aug 19;12(9):1860.

[8] Navickis LL, Bagley EB. Yield stresses in concentrated dispersions of closely packed, deformable gel particles. Journal of Rheology. 1983 Dec;27(6):519-36.

[9] Barnes HA, Hutton JF, Walters K. An introduction to rheology. Elsevier; 1989 Jun 15..

[10] Yao ML, Patel JC. Rheological characterization of body lotions. Applied Rheology. 2001 Apr 1;11(2):83-8.

[11] Whittingstall P, Shah R. Yield stress studies on greases. NLGI spokesman. 1998;62(3):8-22.

[12] Dardir MM, Ibrahime S, Soliman M, Desouky SD, Hafiz AA. Preparation and evaluation of some esteramides as synthetic based drilling fluids. Egyptian Journal of Petroleum. 2014 Mar 1;23(1):35-43.

[13] Coussot P, Bertrand F, Herzhaft B. Rheological behavior of drilling muds, characterization using MRI visualization. Oil & gas science and technology. 2004 Jan 1;59(1):23-9.

[14] Adewale FJ, Lucky AP, Oluwabunmi AP, Boluwaji EF. Selecting the most appropriate model for rheological characterization of synthetic based drilling mud. Int. J. Appl. Eng. Res. 2017;12:7614-29.

[15] Fiveland A. *Effect of Nano silica and Salts on Xanthan gum polymer-Bentonite solution* (Master's thesis, University of Stavanger, Norway).

[16] Margaritis A, Zajic JE. Mixing, mass transfer, and scale-up of polysaccharide fermentations. Biotechnology and bioengineering. 1978 Jul;20(7):939-1001.

[17] Rosalam S, England R. Review of xanthan gum production from unmodified starches by Xanthomonas comprestris sp. Enzyme and Microbial Technology. 2006 Jun 26;39(2):197-207.

[18] Lopes L, Andrade CT, Milas M, Rinaudo M. Role of conformation and acetylation of xanthan on xanthan-guar interaction. Carbohydrate Polymers. 1992 Jan 1;17(2):121-6.

[19] Khouryieh HA. Rheological characterization of Xanthan-guar mixtures in dilute solutions. Kansas State University; 2006.

[20] Morris ER, Foster TJ. Role of conformation in synergistic interactions of xanthan. Carbohydrate Polymers. 1994 Jan 1;23(2):133-5.

[21] Chudzikowski RJ. Guar gum and its applications. J Soc Cosmet Chem. 1971 Jan 1;22(1):43.

[22] DES. Directorate of economics and statistics, ministry of agriculture and farmers welfare, government of India.

[23] Parija S, Misra M, Mohanty AK. Studies of natural gum adhesive extracts: an overview. Journal of Macromolecular Science, Part C: Polymer Reviews. 2001 Jul 31;41(3):175-97.

[24] Wise LE. The Chemistry of Plant Gums and Mucilages and Some Related Polysaccharides. ACS Monograph No. 141. Journal of the American Chemical Society. 1960 Jun;82(12):3232-.

[25] Zhang XZ, Yang YY, Chung TS. The influence of cold treatment on properties of temperature-sensitive poly (N-isopropylacrylamide) hydrogels. Journal of colloid and interface science. 2002 Feb 1;246(1):105-11.

[26] Rao MA. Rheology of liquid foods-a review 1. Journal of Texture Studies. 1977 Jun;8(2):135-68.

[27] Chen T. Rheological techniques for yield stress analysis. TA Instruments: New Castle, DE, USA. 2000.

[28] Braun DB, Rosen MR. Preface. In rheology modifiers handbook− Practical use and application.

[29] Steffe JF. Rheological methods in food process engineering. Freeman press; 1996.

[30] Donnelly RJ. Taylor–Couette flow: the early days. Phys. Today. 1991 Nov 1;44(11):32-9.

[31] Stokes GG. Mathematical and physical papers. 1901.

[32] Margules M. Über die Bestimmung des Reibungs-und Gleitungscoëfficienten aus ebenen Bewegungen einer Flüssigkeit. Aus der kk Hof-und Staatsdruckerei in Wien; 1881.

[33] Lillie HR. The Margules method of measuring viscosities modified to give absolute values. Physical Review. 1930 Jul 15;36(2):347.

[34] Mallock A. IV. Determination of the viscosity of water. Proceedings of the Royal Society of London. 1889 Dec 31;45(273-279):126-32.

[35] Rayleigh L. LXII. Further remarks on the stability of viscous fluid motion. The London, Edinburgh, and Dublin Philosophical Magazine and Journal of Science. 1914 Oct 1;28(166):609-19.

[36] Howard LN. Hydrodynamic and Hydromagnetic Stability. By S. CHANDRASEKHAR. Clarendon

Press: Oxford University Press, 1961. 652 pp.£ 5. 5s. Journal of Fluid Mechanics. 1962 May;13(1):158-60.

[37] Couette M. Études sur le frottement des liquides, par M. Maurice Couette. Gauthier-Villars et fils; 1890.

[38] Couette M. Studies relating to the friction of liquids. Ann. Chim. Phys. 1890;21(6):433-510.

[39] Taylor GI. VIII. Stability of a viscous liquid contained between two rotating cylinders. Philosophical Transactions of the Royal Society of London. Series A, Containing Papers of a Mathematical or Physical Character. 1923 Jan 1;223(605-615):289-343..

[40] Andereck CD, Liu SS, Swinney HL. Flow regimes in a circular Couette system with independently rotating cylinders. Journal of fluid mechanics. 1986 Mar;164:155-83.

[41] Liao CB, Jane SJ, Young DL. Numerical simulation of three-dimensional Couette–Taylor flows. International Journal for Numerical Methods in Fluids. 1999 Apr 15;29(7):827-47.

[42] Davey A, Di Prima RC, Stuart JT. On the instability of Taylor vortices. Journal of Fluid Mechanics. 1968 Jan;31(1):17-52.

[43] Wereley ST, Lueptow RM. Spatio-temporal character of non-wavy and wavy Taylor–Couette flow. Journal of Fluid Mechanics. 1998 Jun;364:59-80.

[44] Wereley ST, Lueptow RM. Velocity field for Taylor–Couette flow with an axial flow. Physics of Fluids. 1999 Dec;11(12):3637-49.

[45] Henderson KL, Gwynllyw DR. Limiting behaviour of particles in Taylor–Couette flow. Journal of Engineering Mathematics. 2010 Jun;67(1):85-94.

[46] Burkhalter JE, Koschmieder EL. Steady supercritical Taylor vortex flow. Journal of Fluid Mechanics. 1973 May;58(3):547-60.

[47] Coles D. Transition in circular Couette flow. Journal of Fluid Mechanics. 1965 Mar;21(3):385-425.

[48] Lueptow RM, Docter A, Min K. Stability of axial flow in an annulus with a rotating inner cylinder. Physics of Fluids A: Fluid Dynamics. 1992 Nov;4(11):2446-55.

[49] Elçiçek H, Güzel B. Effect of shear-thinning behavior on flow regimes in Taylor–Couette flows. Journal of Non-Newtonian Fluid Mechanics. 2020 May 1;279:104277.

[50] Cagney N, Balabani S. Influence of Shear-Thinning Rheology on the Mixing Dynamics in Taylor-Couette Flow. Chemical Engineering & Technology. 2019 Aug;42(8):1680-90.

[51] Alibenyahia B, Lemaitre C, Nouar C, Ait-Messaoudene N. Revisiting the stability of circular Couette flow of shear-thinning fluids. Journal of Non-Newtonian Fluid Mechanics. 2012 Sep 1;183:37-51.

[52] Jeng J, Zhu KQ. Numerical simulation of Taylor Couette flow of Bingham fluids. Journal of non-newtonian fluid mechanics. 2010 Oct 1;165(19-20):1161-70.

[53] Di Prima RC, Swinney HL. Instabilities and transition in flow between concentric rotating cylinders. Hydrodynamic instabilities and the transition to turbulence. 1981:139-80.

[54] DiPrima RC, Eagles PM, Ng BS. The effect of radius ratio on the stability of Couette flow and Taylor vortex flow. The Physics of fluids. 1984 Oct;27(10):2403-11.

[55] Murai Y, Tasaka Y, Oishi Y, Takeda Y. Modal switching of bubbly Taylor–Couette flow investigated by particle tracking velocimetry. Experiments in Fluids. 2018 Nov;59(11):1-8.

[56] Peng J, Zhu KQ. Linear stability of Bingham fluids in spiral Couette flow. Journal of Fluid Mechanics. 2004 Aug;512:21-45.

[57] Landry MP, Frigaard IA, Martinez DM. Stability and instability of Taylor–Couette flows of a Bingham fluid. Journal of Fluid Mechanics. 2006 Aug;560:321-53.

[58] Snyder HA. Wave-number selection at finite amplitude in rotating Couette flow. Journal of Fluid Mechanics. 1969 Jan;35(2):273-98.

[59] Barcilon AJ, Brindley J, Lessen M, Mobbs FR. Marginal instability in Taylor–Couette flows at a very high Taylor number. Journal of Fluid Mechanics. 1979 Oct;94(3):453-63.

[60] Koschmieder EL. Turbulent Taylor vortex flow. Journal of Fluid Mechanics. 1979 Aug;93(3):515-27.

[61] Mullin T, Brooke Benjamin T. Transition to oscillatory motion in the Taylor experiment. Nature. 1980 Dec;288(5791):567-9.

[62] Noui-Mehidi MN, Amanullah M. Effect of Borehole Inclination, Annular Clearance, on the Hole Cleaning Efficiency for Water Based Drilling Muds. InSPE/DGS Saudi Arabia Section Technical Symposium and Exhibition 2010 Apr 4. OnePetro.

[63] Bhambri PA, Fleck BR. Drag Reduction using high molecular weight polymers in Taylor-Couette Flow. Int. J. Mech. Prod. Eng. Res. Dev. 2016;6:59-72.

[64] Bhambri P, Narain R, Fleck B. Drag reduction using polysaccharides in a Taylor–Couette flow. Polymers. 2017 Dec 7;9(12):683.

[65] P Bhambri P. Drag reduction using additives in a Taylor-Couette Flow.

[66] Latrache N, Crumeyrolle O, Mutabazi I. Transition to turbulence in a flow of a shear-thinning viscoelastic solution in a Taylor-Couette cell. Physical Review E. 2012 Nov 12;86(5):056305.

[67] Philip Z, Sharma MM, Chenevert ME. The role of Taylor vortices in the transport of drill cuttings. InSPE India Oil and Gas Conference and Exhibition 1998 Feb 17. OnePetro.

[68] Arias BM. *Torque measurement in turbulent Couette-Taylor flows* (Doctoral dissertation, Université du Havre).

[69] Cengel YA. Cimbala, Fluid mechanics: Fundamentals and applications,(Chap. 8).

[70] Norton IT, Goodall DM, Frangou SA, Morris ER, Rees DA. Mechanism and dynamics of

conformational ordering in xanthan polysaccharide. Journal of Molecular Biology. 1984 May 25;175(3):371-94.

[71] Whitcomb PJ, Macosko CW. Rheology of xanthan gum. Journal of Rheology. 1978 Oct;22(5):493-505.

[72] Thurston GB, Pope GA. Shear rate dependence of the viscoelasticity of polymer solutions.: II. xanthan gum. Journal of Non-Newtonian Fluid Mechanics. 1981 Jan 1;9(1-2):69-78.

[73] Rochefort WE, Middleman S. Rheology of xanthan gum: salt, temperature, and strain effects in oscillatory and steady shear experiments. Journal of Rheology. 1987 May;31(4):337-69.

[74] Tam KC, Tiu C. Steady and dynamic shear properties of aqueous polymer solutions. Journal of Rheology. 1989 Feb;33(2):257-80.

[75] Tam KC, Tiu C. Improved correlation for shear-dependent viscosity of polyelectrolyte solutions. Journal of non-newtonian fluid mechanics. 1993 Apr 1;46(2-3):275-88.

[76] Podolsak AK, Tiu C, Saeki T, Usui H. Rheological properties and some applications for rhamsan and xanthan gum solutions. Polymer international. 1996 Jul;40(3):155-67.

[77] Marcotte M, Hoshahili AR, Ramaswamy HS. Rheological properties of selected hydrocolloids as a function of concentration and temperature. Food Research International. 2001 Jan 1;34(8):695-703.

[78] Lee JS, Kim YS, Song KW. Transient rheological behavior of natural polysaccharide xanthan gum solutions in start-up shear flow fields: An experimental study using a strain-controlled rheometer. Korea-Australia Rheology Journal. 2015 Aug;27(3):227-39.

[79] Iseki T, Takahashi M, Hattori H, Hatakeyama T, Hatakeyama H. Viscoelastic properties of xanthan gum hydrogels annealed in the sol state. Food Hydrocolloids. 2001 Jul 11;15(4-6):503-6.

[80] Ross-Murphy SB, Morris VJ, Morris ER. Molecular viscoelasticity of xanthan polysaccharide. InFaraday Symposia of the Chemical Society 1983 (Vol. 18, pp. 115-129). Royal Society of Chemistry.

[81] Picout DR, Ross-Murphy SB. Rheology of biopolymer solutions and gels. TheScientificWorldJOURNAL. 2003 Mar 24;3:105-21.

[82] G Cuvelier G, Launay B. Concentration regimes in xanthan gum solutions deduced from flow and viscoelastic properties. Carbohydrate Polymers. 1986 Jan 1;6(5):321-33.

[83] Bejenariu A, Popa M, Picton L, Le Cerf D. Effect of concentration, pH and temperature on xanthan conformation: A preliminary study before crosslinking. Revue Roumaine de Chimie. 2010 Feb 1;55(2):147-52.

[84] Pelletier E, Viebke C, Meadows J, Williams PA. A rheological study of the order–disorder conformational transition of xanthan gum. Biopolymers: Original Research on Biomolecules. 2001 Oct 15;59(5):339-46.

[85] Ma L, Barbosa-Canovas GV. Viscoelastic properties of xanthan gels interacting with cations. Journal of Food Science. 1997 Nov;62(6):1124-8.

[86] M. Ochoa, *Analysis of drilling fluid rheology and tool joint effect to reduce errors in hydraulics calculations*. 2006.

[87] Piroozian A, Ismail I, Yaacob Z, Babakhani P, Ismail AS. Impact of drilling fluid viscosity, velocity and hole inclination on cuttings transport in horizontal and highly deviated wells. Journal of Petroleum Exploration and Production Technology. 2012 Sep;2(3):149-56.

[88] Picout DR, Ross-Murphy SB. Rheology of biopolymer solutions and gels. TheScientificWorldJOURNAL. 2003 Mar 24;3:105-21.

[89] Marcotte M, Hoshahili AR, Ramaswamy HS. Rheological properties of selected hydrocolloids as a function of concentration and temperature. Food Research International. 2001 Jan 1;34(8):695-703.

[90] Ahmed J, Ramaswamy HS. Effect of high-hydrostatic pressure and concentration on rheological characteristics of xanthan gum. Food Hydrocolloids. 2004 May 1;18(3):367-73.

[91] Lee JS, Kim YS, Song KW. Transient rheological behavior of natural polysaccharide xanthan gum solutions in start-up shear flow fields: An experimental study using a strain-controlled rheometer. Korea-Australia Rheology Journal. 2015 Aug;27(3):227-39.

[92] J Tatham JP, Carrington S, Odell JA, Gamboa AC, Müller AJ, Saez AE. Extensional behavior of hydroxypropyl guar solutions: optical rheometry in opposed jets and flow through porous media. Journal of Rheology. 1995 Sep;39(5):961-86.

[93] Ross-Murphy SB. Structure–property relationships in food biopolymer gels and solutions. Journal of Rheology. 1995 Nov;39(6):1451-63.

[94] Bourbon AI, Pinheiro AC, Ribeiro C, Miranda C, Maia JM, Teixeira JA, Vicente AA. Characterization of galactomannans extracted from seeds of Gleditsia triacanthos and Sophora japonica through shear and extensional rheology: Comparison with guar gum and locust bean gum. Food Hydrocolloids. 2010 Mar 1;24(2-3):184-92.

[95] Torres MD, Hallmark B, Wilson DI. Effect of concentration on shear and extensional rheology of guar gum solutions. Food Hydrocolloids. 2014 Oct 1;40:85-95.

[96] Richardson RK, Ross-Murphy SB. Non-linear viscoelasticity of polysaccharide solutions. 1: Guar galactomannan solutions. International Journal of Biological Macromolecules. 1987 Oct 1;9(5):250-6.

[97] Robinson G, Ross-Murphy SB, Morris ER. Viscosity-molecular weight relationships, intrinsic chain flexibility, and dynamic solution properties of guar galactomannan. Carbohydrate Research. 1982 Sep 1;107(1):17-32.

[98] Wientjes RH, Duits MH, Jongschaap RJ, Mellema J. Linear rheology of guar gum solutions.

Macromolecules. 2000 Dec 26;33(26):9594-605.

[99] GIBOREAU A, CUVELIER G, LAUNAY B. Rheological behaviour of three biopolymer/water systems, with emphasis on yield stress and viscoelastic properties. Journal of Texture Studies. 1994 Jun;25(2):119-38.

[100] Stuart JT. On the non-linear mechanics of hydrodynamic stability. Journal of Fluid Mechanics. 1958 May;4(1):1-21.

[101] Gollub JP, Swinney HL. Onset of turbulence in a rotating fluid. Physical Review Letters. 1975 Oct 6;35(14):927.

[102] Benjamin TB, Mullin T. Notes on the multiplicity of flows in the Taylor experiment. Journal of Fluid Mechanics. 1982 Aug;121:219-30.

[103] Bahrani SA, Nouar C, Neveu A, Becker S. Transition to chaotic Taylor-Couette flow in shear-thinning fluids. In22ème Congrès français de mécanique 2015 Aug 24.

[104] Cagney N, Balabani S. Taylor-Couette flow of shear-thinning fluids. Physics of Fluids. 2019 May 29;31(5):053102.

[105] Lockett TJ, Richardson SM, Worraker WJ. The stability of inelastic non-Newtonian fluids in Couette flow between concentric cylinders: a finite-element study. Journal of non-newtonian fluid mechanics. 1992 Jul 1;43(2-3):165-77.

[106] M. P. Escudier, I. W. Gouldson, and D. M. Jones, "Taylor vortices in Newtonian and shear-thinning liquids," *Proc. - R. Soc. London, A*, vol. 449, no. 1935, pp. 155–176, 1995, doi: 10.1098/RSPA.1995.0037.

[107] Yi MK, Kim C. Experimental studies on the Taylor instability of dilute polymer solutions. Journal of non-newtonian fluid mechanics. 1997 Oct 1;72(2-3):113-39..

[108] Caton F. Linear stability of circular Couette flow of inelastic viscoplastic fluids. Journal of non-newtonian fluid mechanics. 2006 Mar 10;134(1-3):148-54.

[109] Moazzen M, Lacassagne T, Thomy V, Bahrani SA. Torque scaling at primary and secondary bifurcations in a Taylor–Couette flow of suspensions. Journal of Fluid Mechanics. 2022 Apr;937.

[110] Bahrani SA, Nouar C, Neveu A, Becker S. Transition to chaotic Taylor-Couette flow in shear-thinning fluids. In22ème Congrès français de mécanique 2015 Aug 24.

[111] Cagney N, Balabani S. Taylor-Couette flow of shear-thinning fluids. Physics of Fluids. 2019 May 29;31(5):053102.

[112] Majji MV, Banerjee S, Morris JF. Inertial flow transitions of a suspension in Taylor–Couette geometry. Journal of Fluid Mechanics. 2018 Jan;835:936-69.

[113] Borrero-Echeverry D, Crowley CJ, Riddick TP. Rheoscopic fluids in a post-Kalliroscope world. Physics of Fluids. 2018 Aug 23;30(8):087103.